ABSTRACT

Title of Document: INKJET PRINTED PAPER SURFACE ENHANCED RAMAN SPECTROSCOPY DEVICES FOR TRACE CHEMICAL ANALYSIS

Wei Wen Yu, Doctor of Philosophy, 2013

Directed By: Professor Ian M. White, Fischell Department of Bioengineering

The needs of an ever growing human population are fueling demands for better and cheaper sensors for the early detection of harmful chemicals, pathogens and diseases markers from a variety of sources such as food, water, bodily fluids and contaminated surfaces. To address this, recent innovations utilize Microelectromechanical Systems (MEMS) technology to integrate multiple laboratory functions onto millimeter-sized chips to form Micro Total Analysis Systems (μTAS) or Lab-on-chip (LOC) devices. While sophisticated and powerful, the use of these devices for chemical and biological sensing is limited by complicated fabrication processes, high cost and robustness of the sensors.

In this work we have developed a simple and inexpensive but exceptionally sensitive portable chemical and biological sensing platform through the innovative use of paper combined with Surface Enhanced Raman spectroscopy (SERS). Paper is functionalized with plasmonic nanostructures to transform it into a SERS substrate,

while the natural properties of paper are leveraged for sample collection, cleanup, and analyte concentration in user-friendly formats such as wipes, dipsticks, and filters. The use of simple deposition methods such as inkjet printing for sensor fabrication combined with paper as the construction material means that sensors can be made at a very low cost. Additionally, the ability to be printed on demand eliminates issues with sensor shelf-life, while the absence of mechanical components makes these paper sensors much more robust than conventional sensors. In this work, practical applications of paper SERS sensors for the detection of food contaminants, narcotics, pesticides and other chemicals at trace levels are presented. Paper SERS sensors, by virtue of their low cost, simplicity of fabrication, high sensitivity and ease of use, promises to make chemical and biological sensing more accessible to the common user.

INKJET PRINTED PAPER SURFACE ENHANCED RAMAN SPECTROSCOPY DEVICES FOR TRACE CHEMICAL ANALYSIS

By

Wei Wen Yu

Dissertation submitted to the Faculty of the Graduate School of the
University of Maryland, College Park, in partial fulfillment
of the requirements for the degree of
Doctor of Philosophy
2013

Advisory Committee:
Professor Ian White, Chair
Professor Peter Kofinas
Professor Yu Chen
Professor Don DeVoe
Professor Mario Dagenais

Dedication

I dedicate this dissertation to my parents.

Acknowledgments

To Dr. Ian White - Thank you for your mentorship and support. It has been a pleasure to work with you and I have learned a lot from you during these five years.

To my dissertation committee - Thank you for your insightful suggestions and kind advice.

To current and former members of the Photonics Biosensing Lab - It has been fun working alongside you. Thank you for all your help.

To my friends at Maryland – I am grateful for your friendship. We have had great times during these five years; I will always treasure the memories.

Finally, to my family - You have always stood by me in all my endeavors. Thank you for all your support and encouragement. You have made this possible.

Table of Contents

List of Tables

List of Figures

Chapter 1 : A New Approach to Chemical and Biomolecular Sensing

1.1 Need for a new sensing platform

With the human population at over 7 billion, there is an unprecedented need for clean air, water, food, security and health care. Chemical and biological sensors play a tremendous role in the assurance of the quality of food we consume, the safety of the environment we live in and the well-being of our health. The current gold standards for trace detection utilize techniques such as High Performance Liquid Chromatography (HPLC) and Mass Spectrometry (MS) for chemicals, and bioassays such ELISA and Western blot for biological agents. While sensitive, these tests are often time consuming, expensive and require skilled technicians. Recent advances in sensing such as Micro Total Analysis Systems (μTAS) and Lab-on-chip (LOC) technology (see Figure 1.1), have focused on addressing the time and labor aspects of the problem without addressing the issue of cost, in the hope that cost is reduced when the technology gains traction. At present, these μTAS are fairly complex and expensive to fabricate. In addition, they are also not commonly accepted and are difficult to use by an untrained person. Since its introduction in the 1970s, μTAS and LOC devices have largely remained confined to the research laboratory as proof of concept systems and have yet to see wide usage in everyday applications.[1,2]

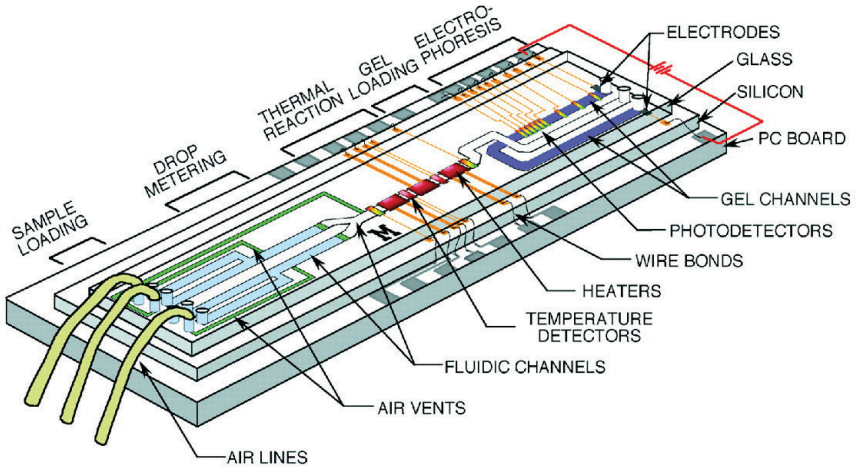

Figure 1.1 Example of a LOC device - an integrated nanoliter DNA analysis device from Burns et al.[3] Reproduced with permission from AAAS.

In this work we introduce paper sensors based on surface enhanced Raman spectroscopy. Paper SERS sensing is a simple and inexpensive yet highly sensitive portable sensing platform which addresses the issues of time, cost and labor simultaneously. This is accomplished through the innovative use of a combination of old and new technologies, namely: paper, inkjet printing, nanotechnology, and SERS. These paper SERS sensors are designed to be capable of detecting trace levels of a target even if it is within a complex sample. Paper SERS has the potential to enable highly sensitive chemical and biological analysis for portable, point-of-sample types of applications.

1.2 Paper based sensing

The use of paper for sensing has numerous advantages. Paper is widely available, inexpensive and a renewable resource. Devices made of paper inherently support sample handling capabilities such as analyte separation and concentration

through fluidic flow, but here instead of fluid flowing along a channel as in conventional microfluidic devices, the flow is driven by capillary wicking of the underlying cellulose. Flow control can be achieved by modification of the substrate properties instead of the use of mechanical components such as syringe pumps and valves, resulting in much simpler devices. Paper can easily be modified to have varying degrees of hydrophilicity, strength and other physical properties by coating or impregnating with other materials. Cellulose as a biological material is intrinsically biocompatible; this enables the storage of chemical and biological species within the cellulose matrix for subsequent release on demand. These capabilities, *which are absent from glass, silicon, plastic and elastomers*, provide a unique "world-to-chip" interface that facilitates sample acquisition from a wide variety of surfaces and complex liquid samples. While these paper sensors are not designed to be reusable, this is compensated for by their low cost and ease of fabrication. They can also be disposed easily (e.g. by burning) after use to eliminate the risks of contamination.

Paper based sensing has long existed in the embodiment of simple litmus strips for pH measurements, but has recently been reintroduced for more complex analytes. Currently there exists a wide range of research on the fabrication of various sensors involving paper. Whitesides et al.[4–6] (re)pioneered the field of paper-based sensing by introducing microfluidic paper-based analytical devices or μPADs (see Figure 1.2). These μPADs were patterned with photoresist to form fluidic channels, along which sample is wicked by the cellulose to analytical regions. The detection mechanism is colorimetric and relies on enzymes and small dye molecules to react with targets to produce a color change. Quantification is achieved by using a scanner

to measure the intensity of the color change. Yager et al.[7–10] explored the movement of fluid on these paper sensors, as well as avenues in using these sensors to achieve functionalities of conventional microfluidic devices (see Figure 1.3). Dungchai et al.[11,12] have explored a different approach to paper sensing by screen printing silver and carbon electrodes on paper to form electrochemical sensors. These electrochemical sensors were used to detect simple metabolites such as glucose, lactate and uric acid. While most of the initial reports on paper analytical devices were for heavy metals detection or simple chemical detection, recent reports have demonstrated assays for proteins and DNA with great potential for disease diagnosis. Shen et al.[13,14], Abe et al.[15,16] and Hossain et al.[17,18] have taken an alternate approach to sensor fabrication by inkjet printing. Abe et al. in particular have developed a colorimetric ELISA-based immunosensor by printing gold labeled antibodies onto paper. Ali et al. created paper strips for the detection of DNA using an isothermal DNA amplification technique called Rolling Circle Amplification (RCA).[19] While implementing ELISA and RCA on paper represent significant advancements, it is well known that immunoreactions and nucleic amplification techniques require numerous laborious wash and rinse steps; thus the creation of a single-step lateral flow assay would be much more advantageous. Furthermore, in these cases, only monoplex detection has been reported because the detection techniques are based on fluorescence or color change.

Paper SERS sensing shares a common thread with the above research in the utilization of paper for simple and inexpensive sensor fabrication, but differs radically through the innovative deployment of SERS as the detection mechanism. SERS has

been demonstrated to be capable of achieving single molecule detection sensitivity, [20,21] and can offer better sensitivity compared to colorimetric and electrochemical modes of transduction. In addition, SERS is capable of multiplexed detection using a single low power laser source.[22,23] These advantages make SERS well suited as a detection modality. The power of SERS comes from the synergy of two optical phenomena – the collective oscillation of electrons on a metal nanoparticle surface known as localized surface plasmon resonance (LSPR), and Raman scattering, the inelastic scattering of light by a molecule which allows it to be uniquely identified. A more in depth study of the interaction of LSPR and Raman Scattering to produce the SERS effect will be discussed in the next chapter.

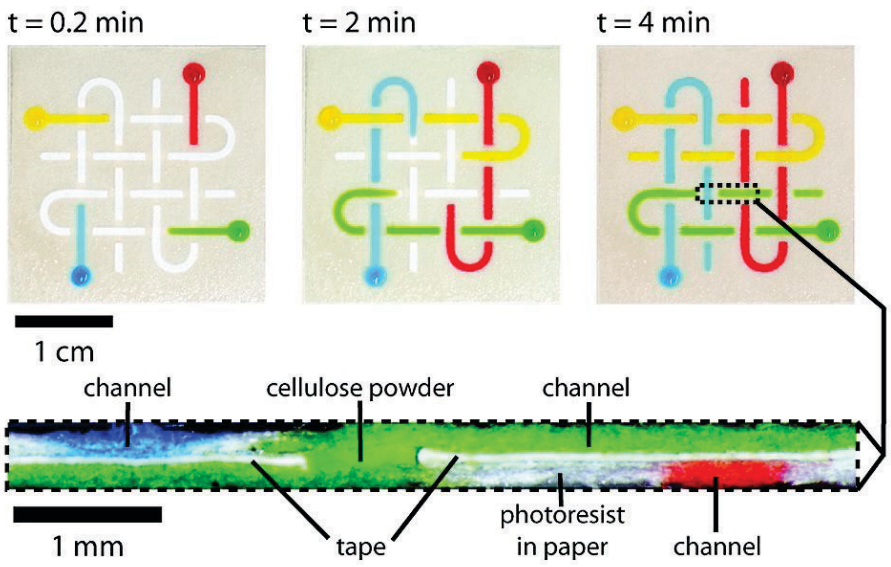

Figure 1.2 Microfluidic paper-based analytical devices (μPADs) made of paper and tape. Photoresist and tape are used to define fluidic channels through which reagents can flow. Reproduced with permission from Whitesides et al.[5] Copyright (2009) American Chemical Society.

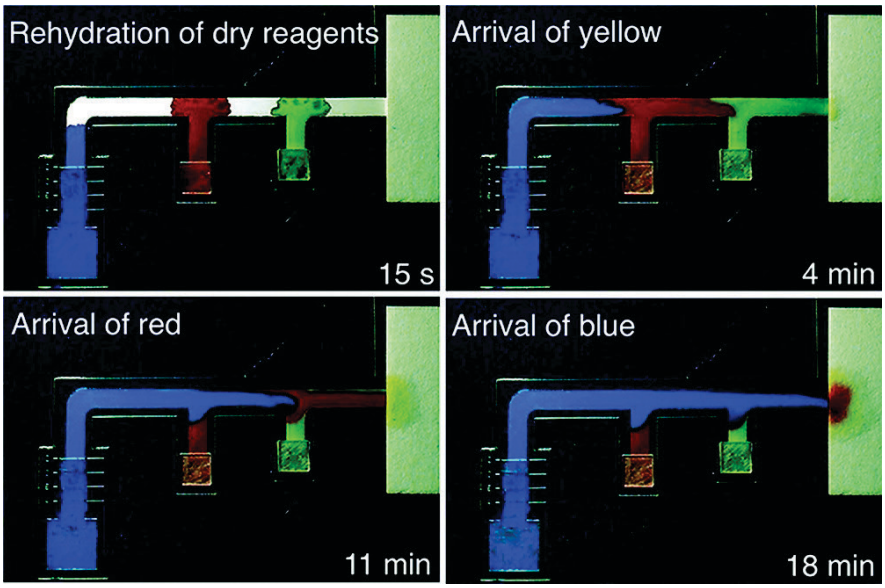

Figure 1.3 Visualization of multiple flows in a Two-Dimensional Paper Network (2DPN). Image series at different time points showing various stages of sequential delivery of the three fluids. Reproduced with permission from Yager et al.[10] Copyright (2012), American Chemical Society.

1.3 Motivation

This work is motivated by the desire to make highly sensitive sensors inexpensive and accessible. From the discussion in the previous section, two key points need to be reemphasized. Firstly, microfluidic lab-on-a-chip devices, while promising, have largely remained confined to the laboratory due to the high costs of fabrication and complexity. Secondly, the emerging technology of paper sensing, while inexpensive and user-friendly, is hampered by the relatively insensitive colorimetric and electrochemical transduction mechanisms. SERS can offer orders of magnitude better detection sensitivity compared to colorimetric and electrochemical sensing, but has rarely been employed in real-world application due to the high cost of existing solid state SERS substrates. In addition, these solid state substrates lack

the flexibility and user-friendly features paper devices offer, and they do not possess the fluidic handling capabilities which are useful for sample processing.

Taking into account all of these aspects, this work proposes to create a new sensing platform that synergistically integrates the positive aspects of each technology – the inexpensive nature of paper sensing, the fluidic capabilities of paper for sample processing and the high sensitivity of SERS detection. It is driven by the following question:

Is it possible to make an inexpensive SERS sensing platform on paper and porous membranes by deposition of plasmonic nanostructures and make use of the fluid handling properties of paper and membranes for sample collection and processing?

In order to answer this question, the results from this dissertation have been organized in the following manner – We first provide in Chapter 2 a brief overview of the theory of Raman scattering, plasmonics and SERS. In Chapter 3, we report the properties of paper loaded with silver nanoparticles by inkjet printing, while in Chapter 4, the SERS properties of silver-loaded filter membranes are examined. In Chapters 5 and 6, we explore the application of paper SERS devices in the forms of wipes, dipsticks and chromatography devices for the detection and analysis of trace chemical analytes from a variety of sources. Finally, in Chapter 7, we present an outlook of the impact of paper SERS devices for chemical and biological sensing.

Chapter 2 : Raman Scattering, Plasmonics and SERS

"I propose this evening to speak to you on a new kind of radiation or light emission from atoms and molecules." - C. V. Raman (1928)

To appreciate how the use of SERS can provide better detection sensitivity for paper sensors over existing colorimetric and electrochemical transduction modalities, an understanding of Raman scattering – which forms the basis of SERS, is necessary. In this chapter, the plasmonic properties of certain coinage metal nanostructures such as gold and silver nanoparticles which play a crucial role in the enhancement of the Raman spectrum will be examined. We also provide a brief overview of the existing types of SERS active substrates and discuss the SERS characteristics of the proposed inkjet printed SERS substrates on paper.

2.1 Raman scattering

When a stream of photons impinges on a molecule, the photons are scattered in all directions from the molecule. Most of the photons are scattered elastically without any change to its energy or frequency through a process called *Rayleigh scattering*, which was explained by Lord Rayleigh in 1871. However, some of the scattered photons were observed to have a higher or lower energy than the incident photons. This was the new kind of radiation light emission from atoms and molecules announced by the physicist Dr. C. V. Raman in 1928, now commonly known as the *Raman effect* or *Raman scattering*.

Classically, the elastic and inelastic scattering processes can be thought of as the radiation from an oscillating molecular dipole induced through the interaction of incident electromagnetic waves with the molecule,[24] however the scattering processes can be explained more simply using a quantum approach: energy from an incident photon excites the molecule from a vibrational state to a higher virtual energy state as shown in Figure 2.1. This energy state is "virtual" because the change in energy level is an intermediary quantum process and is not associated with any transitions in electronic levels. When the molecule relaxes, a photon is re-emitted. If the molecule relaxes to its original state, the emitted photon has the same energy as the incident photon, resulting in Rayleigh scattering. If the molecule relaxes to a different vibrational energy state than it originally started with, the result is Raman scattering. Raman scattering can be further classified as Stokes or anti-Stokes depending on whether the final state is higher or lower in energy than the initial state respectively. By Boltzmann statistics, the molecule is more likely to be in the ground state than in an excited state at thermodynamic equilibrium, hence Stokes Raman is more prevalent and more likely to be observed than anti-Stokes Raman.

Raman scattering is able to reveal information about the unique vibrational structure of the molecule, just like IR spectroscopy. However, unlike IR absorption, in which the excitation energy must match that of the vibrational energy states, there is no such restriction on the incident photons in Raman scattering. This allows a wide range of laser wavelengths to be used for Raman spectroscopy, ranging from UV to Infrared. This flexibility means that light sources can be custom selected for the desired application. In general, shorter wavelength such as UV, results in stronger

Raman scattering intensity, but can excite fluorescence transitions. Infrared sources are widely available and relatively cheaper, but result in weaker Raman intensity at the same laser power.

Raman scattering is a relatively fast event, occurring on the scale of picoseconds, compared to fluorescence emission which occurs on the nanosecond scale. This temporal difference is due to the non-radiative transfer processes that fluorescent molecules undergo after an electronic transition, which does not occur in Raman scattering. In addition, fluorescence also results in much larger line widths, typically in the range of a few hundred cm^{-1}, compared to Raman scattering which has a line width of 2-10 cm^{-1}.

The Raman effect can be intensified if the laser wavelength is chosen such that it can excite an electronic transition in the molecule. In this case, it is known as resonant Raman scattering. Resonant Raman scattering is usually observed with dye molecules due to the possibility to excite the ground state to a higher electronic state with commonly available visible and IR light sources.

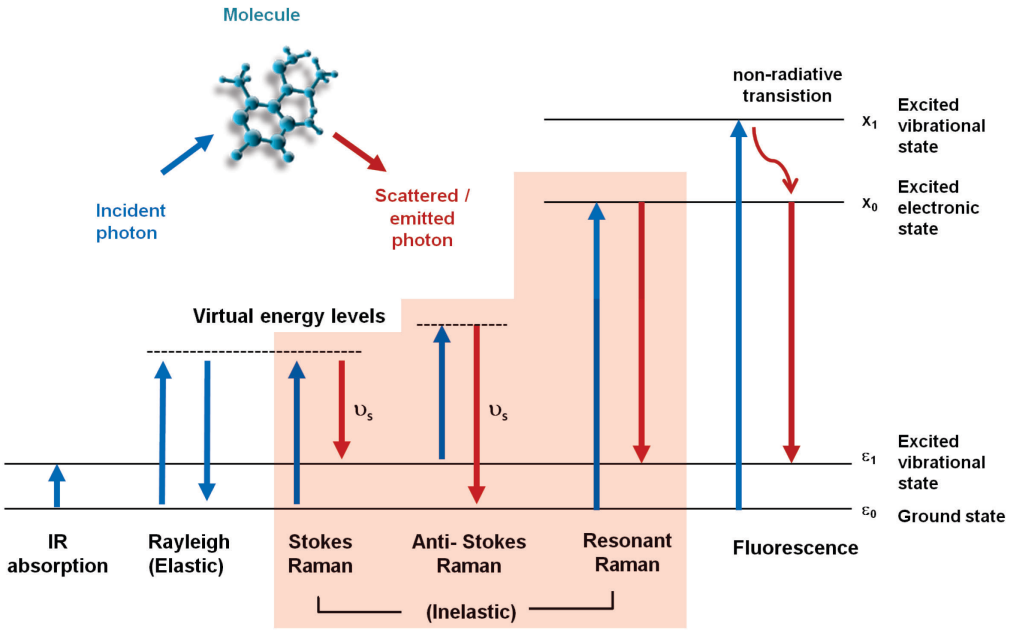

Figure 2.1 Jablonski diagram illustrating the processes of IR absorption, scattering and fluorescence emission from a molecule. The highlighted area indicates the different types of Raman scattering.

The change in the vibrational energy of the molecule due to the Raman effect is:

$$\begin{aligned} \Delta\varepsilon &= \varepsilon_f - \varepsilon_i \\ &= h(\Delta\upsilon) \\ &= h\upsilon - h\upsilon_s \\ &= hc(1/\lambda - 1/\lambda_s) \end{aligned}$$

where ε_i and ε_f are the initial and final vibrational energy, h is the Planck constant, c is the speed of light, υ and λ are the frequency and wavelength of the incident photon, υ_s and λ_s are the frequency and wavelength of the scattered photon respectively. The term $(1/\lambda - 1/\lambda_s)$ is the difference in wave number of the incident and scattered light (expressed in unit of cm^{-1}) and is known as the Raman shift. The Raman shift is

dependent only on the initial and final vibrational energy states of the molecule and is independent of energy of the incident photon, hence the Raman shift measured by a spectrometer is the same regardless of the wavelength of the laser used to excite the molecule.

For a nonlinear molecule composed of N atoms, there exist a maximum of 3N-6 internal normal modes of vibration, after subtracting 3 degrees of freedom for translation and 3 for rotation. Some of the possible vibrational modes that a molecule can have are illustrated in Figure 2.2. Each normal vibrational mode has its own excitation energy, giving each molecule a unique set of Raman shifts or its characteristic Raman spectrum. By analyzing the spectrum of scattered light for its characteristic shifts (or peaks in the spectrum), it is possible to identify the scattering molecule. The Raman spectrum measured from a bulk material is the sum of Raman scattered photons from all molecules present, therefore the intensity of the Raman peaks corresponds directly to its concentration, enabling the quantification of the scattering molecules.

Although useful, Raman scattering is an extremely inefficient process as a result of the very small fraction of the incident light being inelastically scattered. From an optical efficiency standpoint, the Raman scattering cross sections is generally at least 3 orders of magnitude smaller compared to Rayleigh scattering, and about 10 orders of magnitude smaller compared to fluorescence.[25] For example, the Raman scattering cross section of a Rhodamine 6G (R6G) dye molecule is estimated only to be at 10^{-27} cm^2, which is several orders of magnitude smaller compared to its fluorescence cross section of 10^{-16} cm^2.[20,26] Hence Raman scattering is only

noticeable when a large concentration of the scattering molecule is present, and even then, a diffraction grating or optical filter must be used to remove the much stronger Rayleigh scattering.

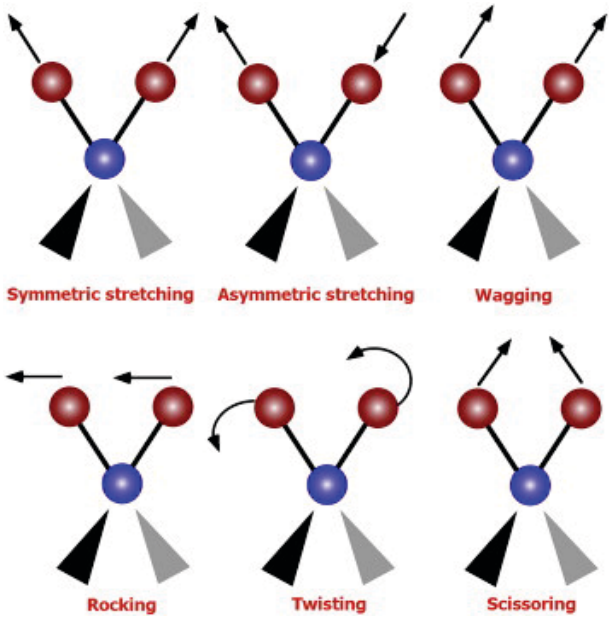

Figure 2.2 The different vibrational modes associated with a molecule. Reproduced from Marcelli et al.[27] with permission from Elsevier.

2.2 Surface enhanced Raman spectroscopy

An enhancement to the Raman effect was first observed in 1974 by Fleischman et al.[28] using pyridine molecules adsorbed on electrochemically roughened silver. However, they incorrectly attributed the enhancement to the increase in surface area as a result of the roughening. It was not until 1977 that Jeanmaire and Van Duyne[29], and Albrecht and Creighton[30] independently demonstrated conclusively that the increase in surface area was not the cause for the

enhancement and that alternative mechanisms must be responsible. Subsequently, they and other early pioneers in the field such as Otto, Moskovits and others established that the increase in electromagnetic field at the surface of the roughened nanostructures coupled with the charge transfer between the adsorbate and the surface were responsible for the enhanced Raman scattering, hence the name - surface enhanced Raman spectroscopy.[31–33] With SERS, improvement of up to 11 orders of magnitude to the Raman scattering efficiency is possible, allowing for the detection of single molecules as first reported by Nie and Emory,[20] and Kneipp et al. in 1997.[21] (See footnote[1])

With this discovery, interest in SERS and its applications has soared. In addition to its high sensitivity and specificity, other advantages that distinguish SERS from other commonly used analytical techniques are high throughput, capability for multiplex detection, and relatively simple setup (a single excitation source and detector). SERS has now been demonstrated for a variety of applications - It has been used for the detection and identification of trace chemicals, such as pesticides,[34–36] explosives,[37] and drugs.[38] Others have utilized SERS for the detection of more complex targets such as metabolites,[39] proteins,[40–43] DNA,[44–47] viruses and bacteria[48]. It has been used for monitoring chemical processes and in the study of intracellular activity[49]. In addition, researchers have applied SERS towards medical imaging and medical diagnosis.[50,51]

[1] Initial reports by Nie and Emory, and Kneipp et al. estimated that the enhancement was up to 14 orders of magnitude. Subsequent analysis by Le Ru and Etchegoin[26,158] revealed that the estimations of the non-SERS cross sections were off by factor of ~10^3, hence the maximum enhancement observed in these single molecule detection studies have been revised to 10^{11}.

Without a doubt, the discovery that noble metal nanostructures can lead to an enhancement to the Raman signal is a major milestone. To understand how nanostructures can give rise to such a dramatic improvement to the scattering intensity, we must first examine the optical properties of nanoparticles, specifically, that of gold and silver nanostructures.

2.2.1 Nanostructures and plasmonics

Le Ru and Etchegoin define plasmons as quantum quasi-particles which represent the modes of oscillations of a charge density in plasma, and are "simply to the plasma charge density what photons are to the electromagnetic field".[26] The collective oscillations of electrons localized on a metal nanoparticle surface are referred to as localized surface plasmons (LSP). When the LSP of nanoparticles are resonant with the frequency of incident light, a strong enhancement of electromagnetic field occurs close to the surface of the nanostructure. Figure 2.3 illustrates the excitation of LSP on the surface of spherical nanoparticles. For molecules adsorbed onto the metal surface, this strongly enhanced electromagnetic field leads to a significant enhancement to the scattering of the electromagnetic radiation,[52] giving rise to SERS. In addition, for certain charged molecules, there is a contribution from the charge transfer between the adsorbed molecular species and the nanoparticle. It is widely accepted that the coupling to the LSP is the dominant force, accounting for up to a factor of 10^9-10^{10} in the enhancement, while the chemical enhancement only accounts for a factor of 10^2.[53] SERS is a distance dependent effect, in order for SERS to occur, the molecule must interact with the enhanced electromagnetic field, and since this enhancement is only located near the surface of

the nanostructure, the molecules must also be close to the surface. For a nanoparticle of radius of curvature a and a molecule at distance d from the surface, the SERS enhancement shows $(1/(a+d))^{12}$ dependence. Therefore maximum SERS is observed when $d = 0$ and falls off rapidly with distance.[26,53–57]

The frequency at which the LSP is resonant with the incident electromagnetic wave is dependent on several factors. The first and foremost is the composition of the nanostructures. The most prominent materials are gold and silver, which display resonance in the visible to near infrared frequencies and are thus easily accessible due to the wide availability of lasers at these frequencies (wavelengths). Also available are platinum, copper and aluminum,[26,58–62] but the enhancement from these metals are generally several orders of magnitude lower compared to gold and silver. In addition, it is possible to create nanoparticles composed of a mixture of gold and silver, such as Janus particles, or composite with other materials such as silica to create core-shell nanoparticles which can also display LSPR.

Other factors which can influence the LSPR are the size and shape of the nanostructures. Generally, the sizes of gold and silver nanoparticles which display LSPR are in the range of 10 – 200 nm, with a red shift in the resonance peak as size increases. The ability to tune the size and shape of the nanoparticles is an extremely useful feature, as it allows the optimization of the LSPR to the available laser wavelengths (see Figure 2.4). In some cases, it can even be tuned to match the wavelengths at which the analyte exhibits resonant Raman activity.

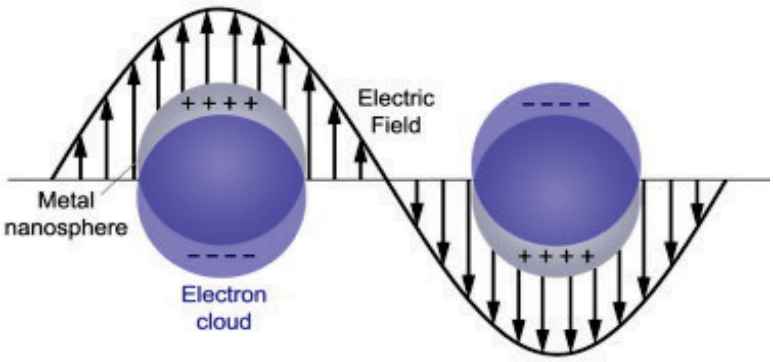

Figure 2.3 Schematic illustration of localized surface plasmon resonance (LSPR) showing the oscillation of delocalized electrons in the presence of an electromagnetic wave. Reproduced from Cobley and Xia[63] with permission from Elsevier.

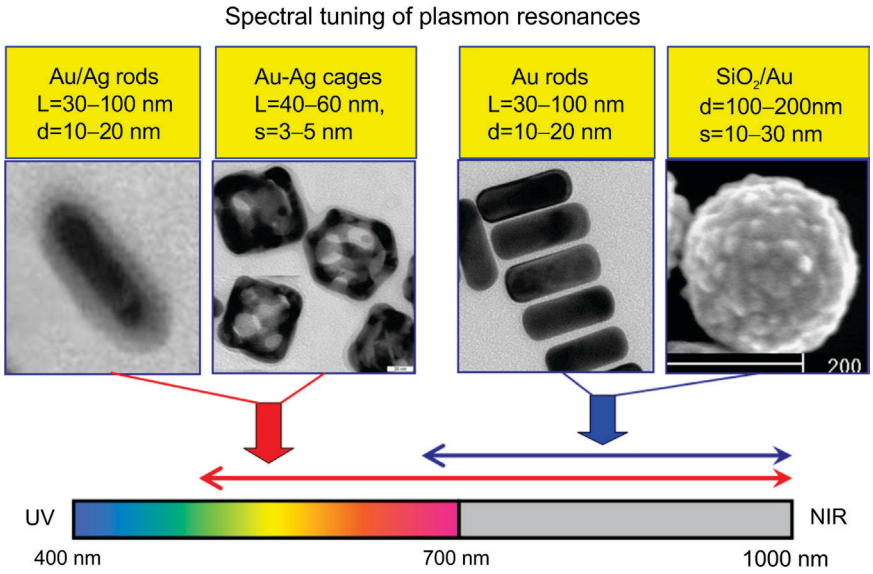

Figure 2.4 Spectral tuning of gold nanorods with silver coatings and Au–Ag nanocages across vis–NIR spectral bands and of gold nanorods and SiO2/Au nanoshells across red-NIR spectral bands. On the top of the TEM images, the typical geometrical parameters of nanoparticles are indicated: nanorod diameter (d) and length (L), nanocage edge length (L) and wall thickness (s), nanoshell outer diameter (d) and gold shell thickness (s). Reproduced from Khlebtsov[64] with permission from Elsevier.

2.2.2 'Hotspots' and 'Lightning rods'

Apart from the material composition, size and shape, the proximity of the nanostructures can also affect the LSPR. This is due to the coupling of plasmons of closely packed nanoparticles. For this coupling effect to occur, the nanostructures must be within ~2 nanometers of each other.[26,65] The coupling increases with decreasing distance, creating so called 'hotspots' at which the electromagnetic enhancement is extremely high and results in particularly large enhancements to the SERS signal. Hotspots can be created in periodic nanostructures with predetermined gap sizes using nanofabrication processes such as E-beam lithography, or through random processes such as nanoparticle aggregation. With periodic nanostructures, hotspots can be generated reliably and demonstrate very good SERS enhancement, but they do not show the highest SERS enhancement factor possible due to the difficulty in attaining the narrowest gap distances. For random processes, extremely narrow gaps are possible, but the uniformity of the hotspots is difficult to control. As an example, in the nanoparticle aggregation approach to hotspot generation, various salts such as chlorides, iodides, and nitrates are added to colloidal solutions to induce aggregation of nanoparticles, while capping agents may also be added to stabilize the nanoparticle clusters.[44,66,67] The enhancement capability of these hotspots are strongly dependent on the gap distances between nanoparticles (see Figure 2.5); the result is that the mixture of aggregating agent, nanoparticles and capping agents is a delicate balance for optimal hotspot generation.

In addition to hotspots, another approach to attaining regions of extremely large electric field enhancement is by designing nanostructure having sharp features,

such as tips, corners and edges. This enhancement arises naturally as a result of geometry of the nanoparticles and is commonly known as the 'lightning rod effect',[68] in reference to the electrostatics phenomenon whereby high electric fields are found at sharp corners or points. Substrates displaying the lightning rod effect typically possess rough surfaces - such as in electrochemically or mechanically roughened electrodes, or sharp points and corners – such as in nanostars, nanocubes and nanorods.

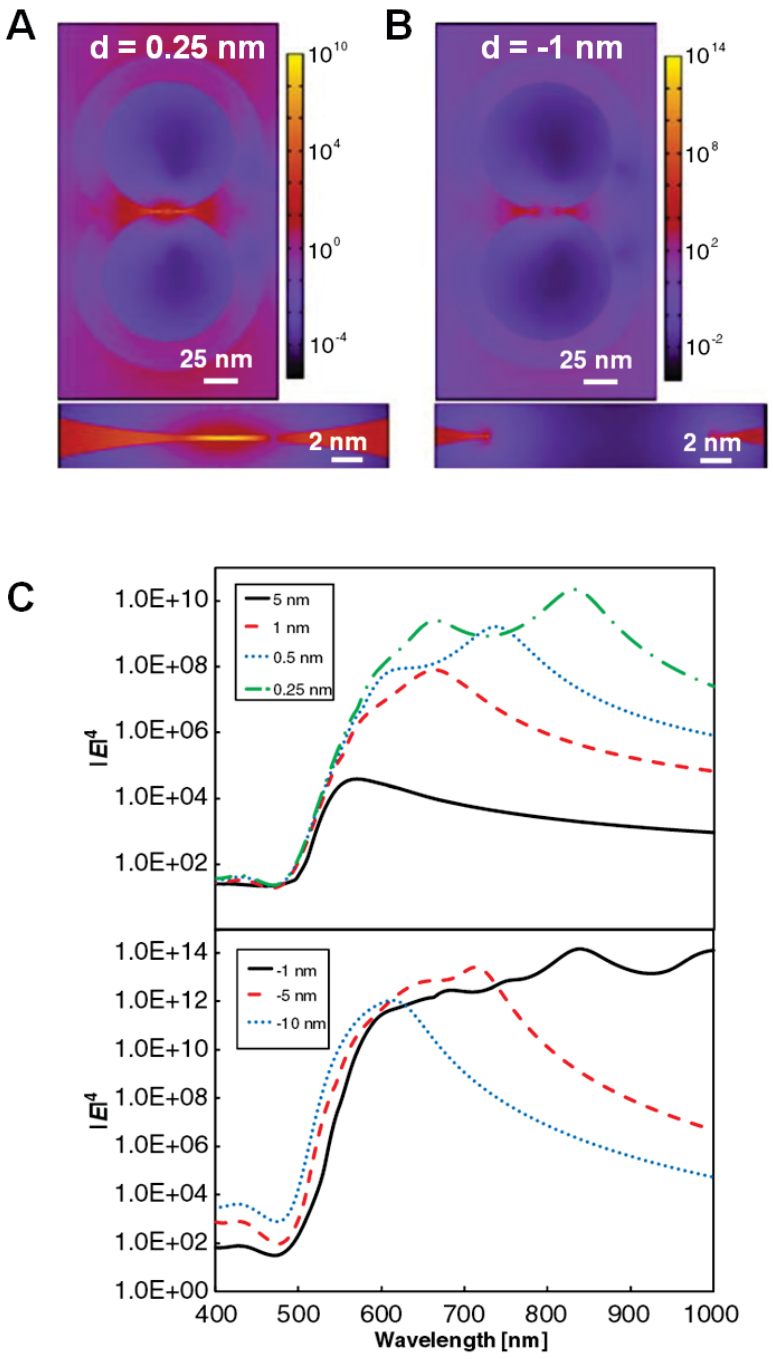

Figure 2.5 Modeling of Electromagnetic (EM) enhancement ($|E|^4$) using finite element method calculations at λ=785 nm for gold nanoparticle dimers with separations of (A) d=0.25 and (B) d=−1 nm. (C) Maximum EM enhancements ($|E|^4$) for gold nanoparticle dimers with separations of d=5 to d=−10 nm at different wavelengths. Reproduced with permission from McMahon et al.[69] Copyright (2009) Springer-Verlag.

2.3 SERS substrates[2]

The discovery that the plasmonic properties of gold and silver nanostructures can be tune by controlling the size, shape, composition and aggregation state has led to the synthesis of a wide variety of nanostructures or substrates that exhibit large SERS enhancements. Substrates can be broadly classified according to the synthesis approach. In the top-down strategy, nanoscale features are obtained by etching away material from the bulk. E-beam lithography is a classic example of the top-down approach. The converse is the bottom-up process, where smaller building blocks are pieced together to generate SERS active features. Nanoparticle self-assembly is a good example of the bottom-up approach. An alternative classification scheme is according to whether the SERS hotspots and lightning rods are generated randomly or by design (i.e. by having periodic arrays of closely packed nanostructures). Substrates with random hotspots and lightning rods are capable of generating some of the largest enhancements attainable in SERS, but unfortunately they can also exhibit great variability in the enhancement factors. Random substrates include roughened electrodes, galvanic displacement substrates and aggregated nanoparticles. In general, random substrates are relatively easy to fabricate. Periodic substrates on the other hand, are much more laborious and expensive to synthesize, but yield more reproducible hotspots. Periodic substrates are composed of arrays of nanostructures obtained typically through lithography, or by self-assembly and directed-assembly

[2] Section 2.3 has been adapted from: Jordan Betz, Wei Yu, Yi Cheng, Ian White, and Gary Rubloff, *Simple SERS substrates: Powerful, Portable, and Full of Potential.* (in preparation)

processes. We will highlight some of the most common SERS substrates in this section.

2.3.1 Electrochemically roughed electrodes

The very first 'substrates' for SERS, although they were not identified as such initially, were electrochemically roughened electrodes. Very simply, the silver or gold electrode to be roughened and a counter electrode are dipped inside an electrolyte bath and connect to a source of electrical potential where it is subjected to oxidation-reduction cycles (ORC). The cycling potential causes a redox reaction to occur at the electrode whereby the metal dissolves and is re-deposited to form nanoscale features on the electrode. Depending on the ORC rate and duration, and electrolytic bath, the size of nanoscale features can be controlled (See Figure 2.6A).[70,71]

To utilize these nano-roughened electrodes, SERS measurements are performed simply by either depositing analyte onto the electrodes or by dipping electrodes into the sample and then allowing them to dry.[72] In certain cases, *in situ* ORC roughening of electrodes with the target molecule in the electrolyte bath can promote the adsorption of analyte to the surface, and/or the formation of surface complexes between the metal surface and oxidized/reduced target, leading to improvements in the SERS signal.[73,74]

2.3.2 Galvanic displacement

When a metal is placed inside an ionic solution containing a metal of a higher reduction potential, a spontaneous electrochemical process known as galvanic displacement occurs in which the ions in solution are reduced and become deposited, whereas the metal becomes oxidized and dissolves into the solution. By controlling

parameter such as concentration and volume of the reactants, the reduced ions can be made to grow into nanostructures of various shapes and sizes such as core-shell nanoparticles,[75] nanorattles,[76] nanopea pods,[77] and dendritic nanostructures (see Figure 2.6B).[78,79] To demonstrate the simplicity of SERS substrate fabrication by galvanic displacement, Betz et al. employed this technique to create dendritic silver nanostructure on a copper penny. The Ag^{+} ions from the precursor solution oxidized Cu atoms on the penny to form Cu^{2+} ions, resulting in the formation of nanostructures with many sharp branches that are highly SERS active. These silver dendrites were utilized as inexpensive SERS substrates for the detection of melamine in infant formula.[78]

2.3.3 Colloidal nanoparticles

Colloidal solutions of noble metals such as gold and silver have been demonstrated to be highly SERS active and useful in many applications.[80] Metal salts of gold and silver, such as chloroauric acid ($HAuCl_4$) and silver nitrate ($AgNO_3$) are reduced to form nanoparticles through wet-chemistry. The size of nanoparticles can be tuned very simply by changing the strength of the reducing agent, time length of the reaction, and reagent concentration. In addition, nanoparticles of various geometries such as spheres,[80] rods,[81,82] stars,[83] cubes,[84] and other exotic shapes can be formed, usually by employing a surfactant in the reaction mixture to control the growth of the nanoparticles in a desired crystal plane (see Figure 2.6C).[85] The charge on the resulting nanoparticles can also be customized through the choice of surfactants, or the choice of reducing agents. As an example, for Ag and Au nanoparticles synthesized through the popular method of Lee and Meisel, the use of

trisodium citrate as the reducing agent imparts a negative charge to the resulting nanoparticles due to the citrate ions. The addition of CTAB in the synthesis of Ag and Au nanorods by the method of Jana et al.[81,82,86] results in positively charge Ag and Au nanorods due to the capping of the nanoparticles by the positively charged CTAB. In addition to imparting charge to the nanoparticles, the capping of the nanoparticles stabilizes the colloid, preventing the nanoparticles from aggregating and falling out of solution. The presence of the type and concentration of these capping agents have a important effect on their application for SERS, as they either can help facilitate the adsorption of analyte to the surface, or prevent their adsorption altogether.

Once synthesized, performing SERS analysis using colloidal solutions is relatively straight forward; the sample is mixed with the colloid solution to allow the analyte to interact with the nanoparticles. To further increase the SERS signal intensity, the mixture is often dried to form a thin film in order to promote adsorption of the analyte to the nanoparticle surface, as well as increasing the concentration of the analyte.

In addition to taking advantage of the lightning effect by creating nanostructures with sharp corners or edges, further enhancement can be obtained by inducing the formation of hotspots with the addition of salts such as NaCl, KNO_3 and other aggregating agents to the analyte-colloid mixture as noted in Section 2.2.2. The resulting hotspots create extremely high SERS enhancement, enabling the detection of trace analytes. In fact, the first demonstrations of single molecule detection were done through salt induced hotspot formation in Ag colloids.

2.3.4 Nanoparticle coated substrates

Real-world samples are not always water soluble and may not be miscible with colloidal solutions. In addition, handling colloid solutions and waiting for the sample-colloid mixture to form a dry film can be inconvenient. This led to the introduction of nanoparticle coated substrates. This is achieved by employing various approaches of depositing nanoparticles onto surfaces. These deposition approaches include micropipetting,[87] soaking,[88,89] screen-printing,[90] filtration[91], inkjet printing,[92–94] and vapor deposition.[95,96] However, in these deposition processes, it can be difficult to control the assembly of nanoparticles reliably, resulting in randomly distributed hotspots and substrate variability. Although these issues can be problematic, they can be overcome through averaging methods such as rastering, wide area illumination and sampling from many regions on the substrates. These techniques will be discussed in detail later in Section 2.6.

In order to obtain more consistent hotspots from nanoparticles, researchers have explored both self-assembly and directed-assembly techniques,[87] such as the Langmuir-Blodgett assembly,[97] to create regular arrays of nanoparticles. However, these techniques also introduce more complexity to the fabrication process as compared to simple deposition processes mentioned previously.

2.3.5 Periodic SERS substrates

The randomness of hotspot generation arising from the aggregation of nanoparticles spurred the pursuit of SERS substrates having regular, uniform features. In addition to the assembly of nanoparticles into regular arrays by directed and self-assembly techniques mentioned previously, widely used semiconductor industry

nanofabrication processes such etching, electron beam lithography (EBL) and atomic layer deposition (ALD) processes have been adapted to create nanostructures that have high SERS activity (see Figure 2.6D). These nanofabrication techniques offer unprecedented control over structure size, shape, and spacing of the nanofeatures.[98] Periodic substrates generally display lower enhancement factors than random nanoparticle aggregates, but this is compensated by the ability to attain better SERS reproducibility.

Due to the high cost of traditional lithography processes, researchers have introduced non-conventional lithography techniques such as nanoimprint lithography (NIL),[99–105] and nanosphere lithography (NSL)[106–111] for fabricating periodic substrates. In NIL, a template is created by EBL or photolithography on a stiff material. This template is then used to imprint the pattern onto the substrate, followed by vapor deposition of the desired metal onto the pattern. In NSL, the template is created by the self-assembly of nanospheres into a regular array. Gold or silver is then vapor deposited onto the template. After the removal of the nanosphere template, regular triangular nanostructures are obtained from the metal deposited through the gaps created by the close packing of the nanospheres (see Figure 2.6E).

2.3.6 Substrates with a mix of periodic and random features

Substrates that are purely random or pure periodic represent the opposite ends of the spectrum of SERS substrates that have been invented. Several groups have introduced novel fabrication methods for SERS substrate that possess a mix of random and periodic features. One of the techniques of note is metal film on nanospheres (MFONs) by Van Duyne et al.[106] MFONs is a closely related technique

to nanosphere lithography, but instead of removing the nanosphere template after metal deposition, it is left in place. The resulting metal film on the nanopsheres shows nanoscale roughness, which is responsible for the SERS enhancement.

Zhao et al. fabricated arrays of aligned silver nanorods by oblique angle deposition (OAD) (see Figure 2.6F). In OAD, a glass substrate is mounted on a stepper motor and rotated while silver is vaporized by an electron-beam/sputtering evaporation system and is deposited onto the glass substrate in the shape of nanorods. Growth of the nanorods is controlled by shadowing effect and surface diffusion. The resulting nanorods were demonstrated to have good SERS activity and reproducibility.[95]

As research on the fabrication of novel SERS substrate is an extremely active field, an exhaustive discussion on all the types of SERS substrates is not possible. Instead, Table 2.1 summarizes some of the substrates in existence and provides a comparison in terms of enhancement, cost of fabrication, complexity of fabrication and the approximate gap sizes. More comprehensive discussions of hotspots and different types of SERS substrates can be found in the reviews by Kleinman et al.,[112] Banholzer et al.,[113] Fan et al.,[114] and Lin et al.[115]

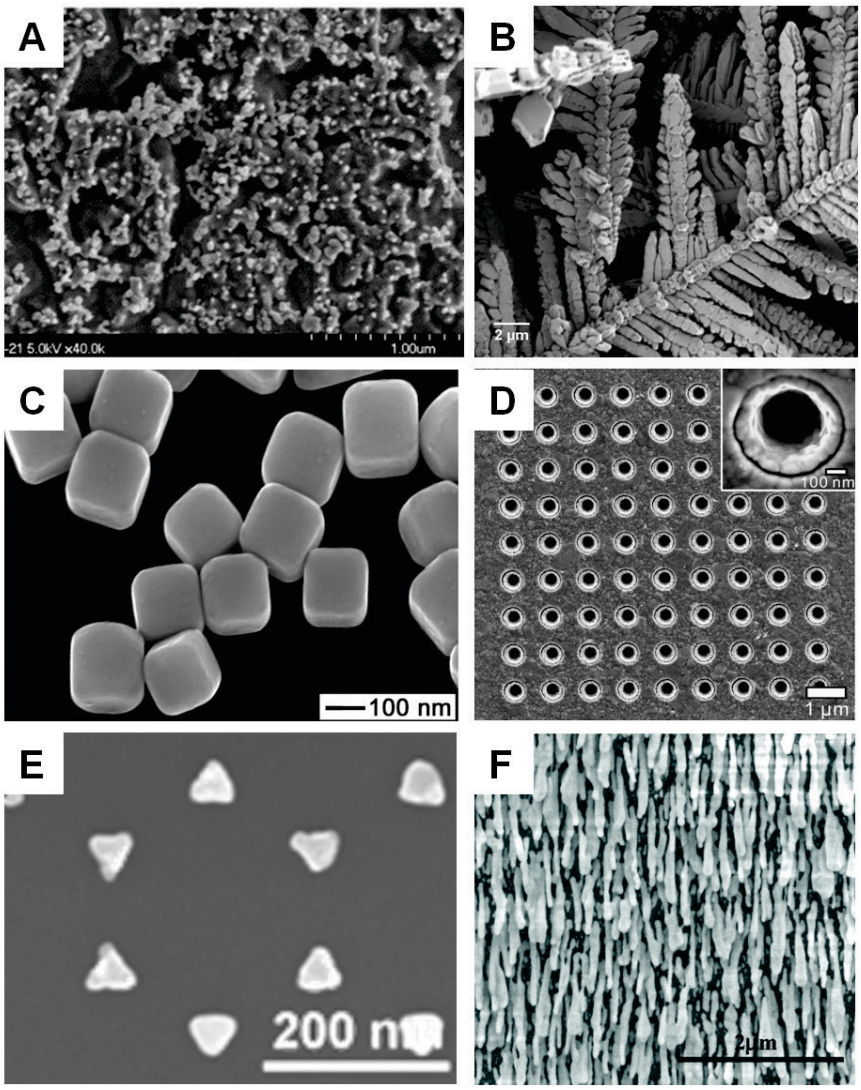

Figure 2.6 Different types of SERS substrates – (A) Electrochemically roughened gold substrate, adapted from Liu et al.[72] with permission from Elsevier. (B) Silver dendrites by galvanic displacement, adapted with permission from Gutes et al.[79], Copyright (2010) American Chemical Society. (C) Silver nanocubes, adapted from Sun and Xia[84], with permission from AAAS. (D) Nanogap arrays prepared by lithography and ALD, adapted with permission from Im et al.[98], Copyright (2010) American Chemical Society. (E) Nanotriangle arrays fabricated by NSL, adapted with permission from Whitney el al[116], Copyright (2005) American Chemical Society. (F) Silver nanorod arrays by OAD, adapted with permission from Zhao et al.[117] Copyright (2005), American Chemical Society.

Table 2.1 Comparison of some of the different types of SERS substrates in existence. Some entries in this table have been adapted from Kleinman et al.[112]

(Note: E.F = Enhancement factor, $ = low cost, $$ = moderate cost, $$$ = high cost, NS = not specified, NR = not relevant)

Substrate type	E.F	Gap distances (nm)	Cost	Comments	References
Substrates with sharp features					
Individual nanoparticles (nanorods, nanocubes, nanowires, etc.)	10^3-10^8	NR	$	- Nanoparticles of different shapes and sizes can be controlled through chemical precursors - Shapes with sharp features, which result in large electromagnetic field enhancements are desirable - Mainly for solution-based SERS measurements - Relatively low-cost, wet-chemistry based synthesis	118–123
Electrochemically roughened electrodes	10^6	NR	$	- Roughness of the surface features can be controlled by reduction-oxidation cycles	32,70–74
Island films	10^8	NR	$$	- Surface roughness is controlled by metal deposition conditions	124–130
Galvanic displacement	10^6	NR	$	- A wide variety of shapes and sizes are possible - Features are controlled by displacement reaction conditions (e.g. concentration, volume, duration)	78,79,131,132

Substrate type	E.F	Gap distances (nm)	Cost	Comments	References
Random substrates					
Aggregated nanoparticles	10^5-10^{11}	0-10	$	- Extent of aggregation is controlled by the additions of salts and capping agents - Extremely narrow gaps are possible, but exhibit large variability - Single molecule detection have been demonstrated with aggregated nanoparticles	20,21,133,134
Nanoparticle coated substrates (screen printing, soaking, inkjet printing, filtration, etc.)	10^5 - 10^7	NS	$	- Adhesion of nanoparticles onto support via chemical or electrostatic attraction - Various types of supports have been used (e.g. plastics, glass, paper) - Differs from direct or self-assembly methods in that nanoparticles cluster randomly	88,90,92,94,135
Periodic substrates					
E-Beam lithography (EBL) substrates	10^3-10^5	1-100	$$$	- Relatively expensive and laborious fabrication technique - Highly periodic and reproducible arrays can be obtained	136–141
Nanoimprint lithography	10^8	NS	$$	- Differ from EBL in that a mold is first created, which is then used to imprint features onto a substrate	99–105

Nanosphere lithography	10^8	100-500	$$	- Gap size controlled by size of nanospheres and amount of metal deposited - Highly periodic and reproducible arrays can be obtained	106–111
Self-assembly and directed-assembly	10^4-10^9	5-100	$$	- Organization of nanoparticles into periodic structures based on effects such as charge, hydrophobicity, capillary forces, etc.	87,97,142,143
Substrates with a mix of random and periodic features					
MFONS	10^3-10^{11}	NR	$$	- Enhancement arises from nanoscale roughness of deposited metal film	107,144–147
Nanorod arrays by oblique angle deposition	10^8	NR	$$	- Dimensions of nanorods are dependent on the conditions of the deposition process - Resulting nanorods show quasi-regular features	95,148–151
Nanofingers	10^{10}-10^{11}	1-10	$$$	- Nanopillars are formed by nanoimprint lithography - Pillars aggregate/close upon sample evaporation to generate hotspots	152,153

2.4 SERS substrate enhancement factor

Owing to the wide variety of SERS substrates at one's disposal and many more being continually developed, there is a need for a commonly accepted way to gauge their effectiveness. One of the key parameters of evaluating and comparing the wide variety of substrates is the enhancement factor. Conceptually, the enhancement factor (EF) of a SERS substrate is the measure of the enhancement in the SERS signal resulting from the presence of the nanofeatures compared to the pure Raman spectrum. Experimentally, the enhancement factor of a substrate can be calculated by:[88,111,154–157]

$$EF = \left(\frac{I_{SERS}}{I_{Raman}} \right) \times \left(\frac{N_{Raman}}{N_{SERS}} \right) \qquad \text{(Equation 2.1)}$$

where I_{SERS} and I_{Raman} are the SERS and Raman intensities at a selected peak and N_{SERS} and N_{Raman} represents the total number analyte molecules responsible for generating the corresponding SERS and Raman intensities.

While the intensities I_{SERS} and I_{Raman} can be obtained in a straightforward manner from the output of the spectrometer, the total number of analyte molecules N_{SERS} is much more difficult to calculate. In determining N_{SERS}, one must be careful to count only those molecules which are adsorbed onto the nanostructures and hence are responsible for the SERS, and not those molecules which are adsorbed onto the support material or are in solution. In particular, the concentration of analyte used should be such that the surface coverage is significantly smaller than one monolayer. As SERS is highly distance dependent, the existence of more than a single monolayer

when performing SERS means that the scattering intensity is no longer proportional to the number of molecules. Moreover, the enhancement factor is dependent on the analyte used for testing. Two unrelated chemical species used even with the same substrate can yield disparate enhancement factors, owing to the difference in adsorption of the molecules onto the nanostructured surface. Therefore, comparisons of EF between different substrates are only valid if similar analyte-nanostructure interaction can be achieved in the experimental conditions. This is generally very difficult to do.

Nevertheless, when computed appropriately, the EF is a useful parameter for evaluating how 'good' a SERS substrate is. Normally, a good substrate will have an EF of 10^5 - 10^6, while an excellent substrate can have EF of over 10^{10}. A comparison of the types of SERS substrates and their EF is presented in Table 2.1.

More in depth derivation and discussion of the computation of SERS substrate enhancement factors can be found in the works of Le Ru and Etchegoin.[26,158] In addition to the enhancement factor for SERS substrates, they also consider the SERS enhancement factors under different conditions, such as the Single Molecule EF - for evaluating EF in single molecule detection cases, the Analytical EF - for evaluating EF in practical analytical chemistry applications, the total SERS substrate EF - for evaluating the EF over the entire substrate, as well as calculating the EF by comparing the Raman and SERS cross sections of analyte molecules.

2.5 Simple SERS substrates[3]

While making SERS substrates with large EF is an important goal, other aspects of the process must also be taken into account. Due to the nanoscale features of the SERS substrates, they are prone to oxidation, resulting in limited shelf-life. Hence factors such as the complexity of the synthesis process, expense, and expertise required are also important considerations, as are variability and reproducibility of the fabrication processes. The major limiting factors to SERS being widely adopted as a analytical technique despite its proven high sensitivity are the high cost associated with producing these SERS active nano-featured substrates, as well as the short shelf life of these nanostructures.[159,160] Currently, commercially available SERS substrates are typically created through nanofabrication techniques such as e-beam lithography, which are expensive, time consuming and have very low throughput. To this end, research into simple and inexpensive approaches for fabricating SERS substrates is an important goal. Betz et al.[161] identified four characteristics of simple SERS substrates.

1. Fabricated using equipment and reagents that can be commonly found in chemistry laboratories. Moreover, the use of 'green' nontoxic reagents is a plus.
2. Minimal training or experience required for fabrication.
3. Easily transported to or fabricated at the point of sampling.
4. Easily integrable into simple analytical systems and procedures.

[3] Section 2.5 has been adapted from: Jordan Betz, Wei Yu, Yi Cheng, Ian White, and Gary Rubloff, *Simple SERS substrates: Powerful, Portable, and Full of Potential.* (in preparation)

SERS substrates satisfying the above requirements will dramatically reduce the cost of performing SERS, and can make SERS analysis more accessible.

2.5.1 Inkjet printing as a simple SERS substrate fabrication method

In this work, we explore the use of a commercial inkjet printer for simple and inexpensive SERS substrate fabrication. The innovative use of inkjet printing eliminates the need for any complicated fabrication techniques; sensor fabrication can be as simple as printing out a document. Inkjet-printing requires the formulation of a nanoparticle ink in an appropriate liquid carrier for proper viscosity and surface tension. Since volumes as small as a picoliter can be ejected, ink wastage is reduced and the nanoparticles can be delivered very precisely to a predefined region. Inkjet printing is computer controlled, thus avoiding complicated handling procedures, and complex geometries can be designed very easily. The simplicity of the process also addresses other short-comings of established sensing techniques - the life span of the nanostructures and biorecognition elements is not a problem because they are printed on demand. Since inkjet printers are designed to print several different colors, it is conceivable that additional functionalization of SERS-active nanoparticles and substrate surface can be achieved by printing of different reagents simultaneously using the additional channels. Inkjet printing is a well-established technology; this makes it a very attractive tool for SERS sensor fabrication.

2.5.2 Paper and other porous materials for substrate fabrication

While inkjet printing is an extremely useful technique for inexpensive substrate fabrication, astute selection of the surface onto which the nanoparticles are deposited can impart an additional functionality to the substrate. Surfaces such as

glass, silicon and polymers have been used for substrate fabrication because they do not retain liquid from the sample, which can help to ensure that most of the analyte adheres to the nanoparticles. However, these solid surfaces are rigid and inflexible and thus are only convenient in situations where the sample can be applied to it. In contrast, paper is extremely useful as a vehicle for supporting nanostructures for SERS applications. Its hydrophilicity can be leveraged for analyte separation and concentration. Its porosity can be used to filter out analytes of interest. The natural wicking ability of cellulose can be utilized to soak up the sample, or drive the flow of samples without relying on any mechanical components. The physical properties of paper, such as porosity, hydrophilicity and strength can be easily modified by the composition of underlying cellulose fibers, or by coating and impregnating with other materials. As a renewable resource, paper is also widely available and relatively inexpensive compared to aforementioned solid substrates. For these reasons, paper is increasingly being explored for a variety of sensing applications.

In addition to paper, other porous materials such as modified cellulose products (e.g. nitrocellulose, cellulose acetate), nylon and PVDF can also be used for SERS substrate fabrication. In particular, membranes made of nitrocellulose, nylon and PVDF have been used extensively for protein blotting assays due to their high nonspecific binding affinity towards proteins. In certain situations, such as for sample clean up of highly proteinaceous samples, it may be advantageous to use membranes rather than paper. We will demonstrate this application in chapter 6.

Taking advantage of these special properties of paper and other porous materials, we explore the application of inkjet printed SERS substrates in the form of

sensor arrays, swabs, dipsticks and filters. In addition, analyte separation by paper chromatography, as well as analyte concentration, achieved by a lateral flow concentration assay will be studied. With these considerations in mind, inkjet printed SERS substrates made of paper and other porous materials are not just mere substrates, they can become highly sensitive detection platforms that can rival traditional trace analysis techniques such as HPLC-MS. Compared to other emerging optofluidic SERS techniques which aim to integrate SERS detection with lab-on-a-chip microfluidic devices, inkjet printed SERS sensor made of paper and other porous materials are much simpler and less expensive to fabricate. They are also easier and more intuitive to use.

2.6 The random nature of simple SERS substrates

With SERS substrate fabrication by electrochemical roughening, galvanic displacement and deposition, the formation of SERS hotspots is a random process; as a result, these SERS substrates can have much higher point-to-point variability than specially designed, highly regular substrates. This applies to inkjet printed SERS substrates as well. However, techniques to mitigate this problem have been demonstrated in Raman spectroscopy and in SERS. One of the simplest options is wide area illumination (WAI): the use of a laser spot that is relatively large compared to nanoparticle size (> 10^3 times). In this case, thousands of nanoscale hotspots exist within the region illuminated by the laser, thus variations from hotspot to hotspot are averaged out.[162] Another technique to average the SERS spectra is by collected signal from many different locations on a sample.[163] Finally, constantly moving the laser spot relative to the SERS substrate, a technique called rastering, allows the laser to

sample different regions of the substrate, thus in effect averaging the SERS signal. This has also been demonstrated to be effective.[164,165] These approaches are summarized in Figure 2.7.

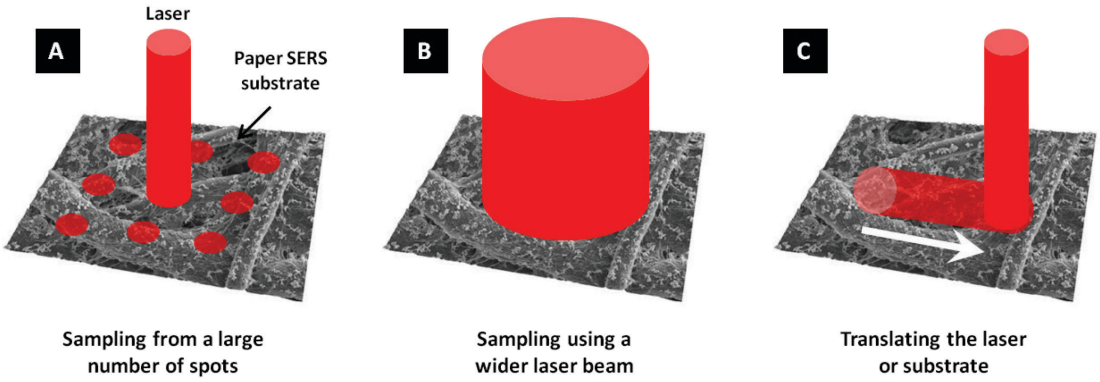

Figure 2.7 Techniques for improving SERS signal variability. (a) Averaging of Raman spectra collected from several regions on the substrate, (b) Sampling using a wider laser beam, and (c) Rastering of the laser or sample during spectral collection.

2.7 Summary

In our proposed work of paper SERS sensing, Raman scattering provides the basis for analyte identification through the unique spectrum associated with each molecular species. Quantification is made possible through the analysis of characteristic peak heights. Without the additions of plasmonic nanostructures in the matrix of the paper, paper sensing has limited sensitivity. The aggregation of nanoparticles on the paper creates hotspots which can enhance the Raman signatures dramatically, enabling the detection of trace analytes. Compared to SERS substrates created through expensive nanofabrication processes, inkjet paper SERS substrates

may show higher variability due to the random nature of the aggregation process, but the use of averaging techniques can help to reduce its impact. Equipped with this knowledge, we will study the characteristics of inkjet printed SERS substrates on paper and other porous materials, and explore the ways they may be applied in real-world scenarios in the subsequent chapters.

Chapter 3 : Inkjet Printed SERS Arrays on Cellulose Paper[4]

3.1 Introduction

Surface-enhanced Raman spectroscopy (SERS) has excellent potential to be a rapid, portable and highly sensitive analytical technique, but is currently limited to research laboratories due to the high cost and short shelf-life of SERS-active substrates. A new paradigm to enable simple and low-cost fabrication of disposable SERS devices is needed.

In this work, we extend the newly emerging field of paper-based molecular analysis devices to include SERS. To our knowledge, we are reporting on the first highly sensitive SERS substrate to be fabricated on paper by inkjet printing, at a total material cost of a few cents per device. A few reports of SERS using silver coated paper were presented decades ago.[166–169] However, in this work; silver nanoparticles are embedded into the paper with any desired pattern at micro-scale precision using an inexpensive ($60) consumer inkjet printer. In addition, the inkjet printer is used to create a hydrophobic surface in the sensing region, which prevents the sample from spreading and thus concentrates the analyte molecules in the small sensing area. SERS measurements are acquired after a sample droplet is placed onto the SERS-active printed region. Using this silver nanoparticle substrate, we show the ability to identify the fingerprint signal of Rhodamine 6G (R6G), even when only 10 attomoles of analyte are applied to the paper-based SERS substrate. In addition, we show the

[4] This chapter is adapted from: Wei W. Yu and Ian M. White, *Inkjet Printed Surface Enhanced Raman Spectroscopy Array on Cellulose Paper*, Analytical Chemistry 82, 9626-9630, 2010. Copyright (2010) American Chemical Society.

reproducibility of the signal across multiple printed spots of the sensing region and at different locations within each printed spot.

3.2 Methods

3.2.1 Materials

Fisher chromatography paper, 0.19 mm in thickness, was used for the substrate; hexadecenyl succinic anhydride (ASA) from Thermo-Fisher Scientific was used to create a hydrophobic surface on the paper. Silver nitrate, chloroauric acid, sodium citrate, glycerol and hexanol were obtained from Sigma-Aldrich. Rhodamine 590 chloride, also known as Rhodamine 6G (R6G), was purchased from Exciton. All chemicals were used as received. Safety precautions were taken in the handling of all chemicals according to their respective MSDS. Refillable ink cartridges were purchased from Alpha D Development Inc. and used without modification.

3.2.2 Hydrophobic treatment

Prior to the printing of silver nanoparticles onto paper, the substrate was made hydrophobic using ASA, a common paper sizing agent. Hydrophobization was achieved by inkjet printing a 10% ASA solution in hexanol onto the entire surface of the paper, followed by curing at 175° C on a laboratory hotplate for 5 minutes. The paper surface is rendered hydrophobic through the reaction of ASA with the cellulose molecules.[170,171] The succinic anhydride group on the ASA reacts with the hydroxyl groups on the cellulose to form a chemical bond as illustrated in Figure 3.1(A), the hydrocarbon tail of the hexadecenyl group on the ASA molecule repels water from

the surface of the paper. ASA treated chromatography paper is shown in Figure 3.1(B).

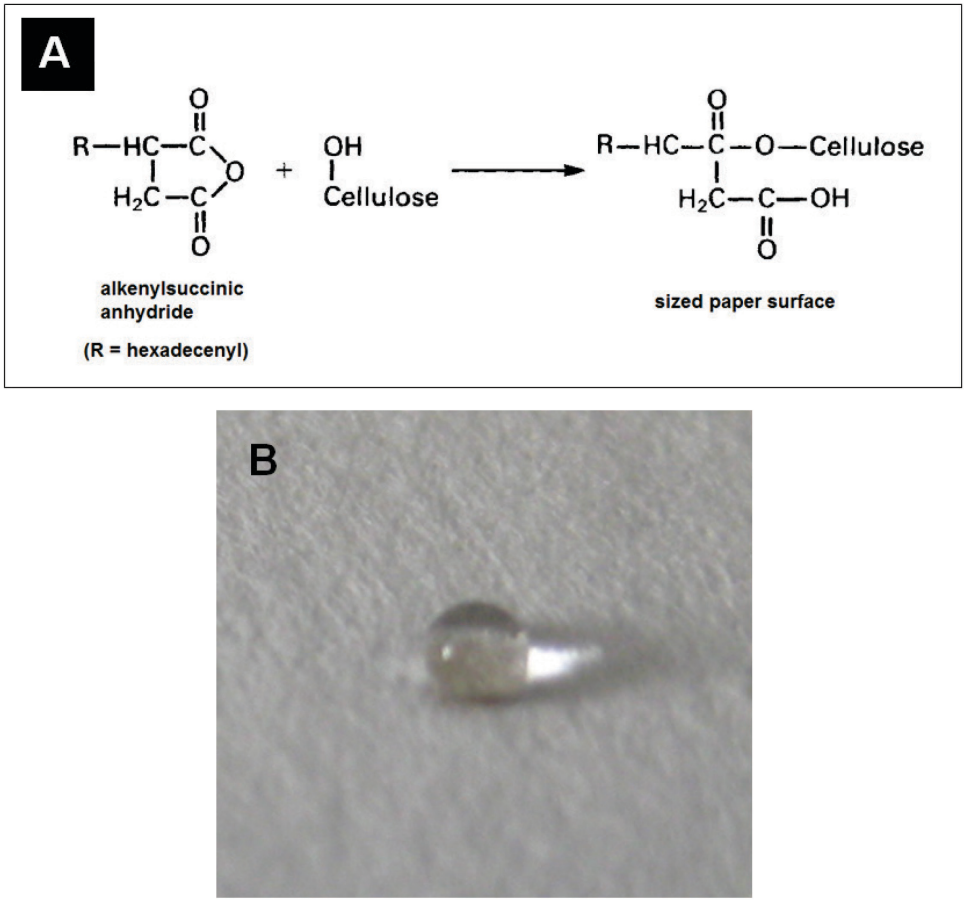

Figure 3.1 (A) Paper sizing using ASA.[170] (B) A water droplet on chromatography paper treated with ASA beads up on the paper surface, indicating it has become hydrophobic.

3.2.3 Nanoparticle synthesis

Silver nanoparticles were synthesized by reduction of silver nitrate using trisodium citrate as the reducing agent by the method of Lee and Meisel.[80] Briefly, 90 mg silver nitrate was added to 500 mL of ultrapure water (18.2 MΩ), which was then brought to a boil in a flask under vigorous stirring. 100 mg of sodium citrate was added and the solution was left to boil for an additional 10 minutes. After the solution

turned greenish brown, which indicated the formation of silver colloid, it was then removed from heat. According to NMR studies of the reaction solution by Munro et al.,[172] the reaction which occurs in the boiling mixture is:

$$Ag^{+} + \text{citrate ion} \rightarrow Ag^{0} + \text{acetoacetic acid} + \text{formate}$$

with acetonedicarboxylic acid as the intermediary product. As the reaction progresses, excess Ag nucleates and grows into spheroidal nanoparticles. In addition it was noted that the excess citrate ions becomes adsorbed onto the surface of the resultant nanoparticles, but neither acetoacetic acid nor formate were detected as being adsorbed at the surface. Gold nanoparticles were prepared in a similar manner using chloroauric acid ($HAuCl_4$) as the precursor instead of silver nitrate.

The as-synthesized silver colloid was brown in color, with peak absorption of 400 nm as measured by a UV-Vis spectrophotometer, while the gold colloid was reddish-purple in color, with peak absorption of 520 nm as shown in Figure 3.2.

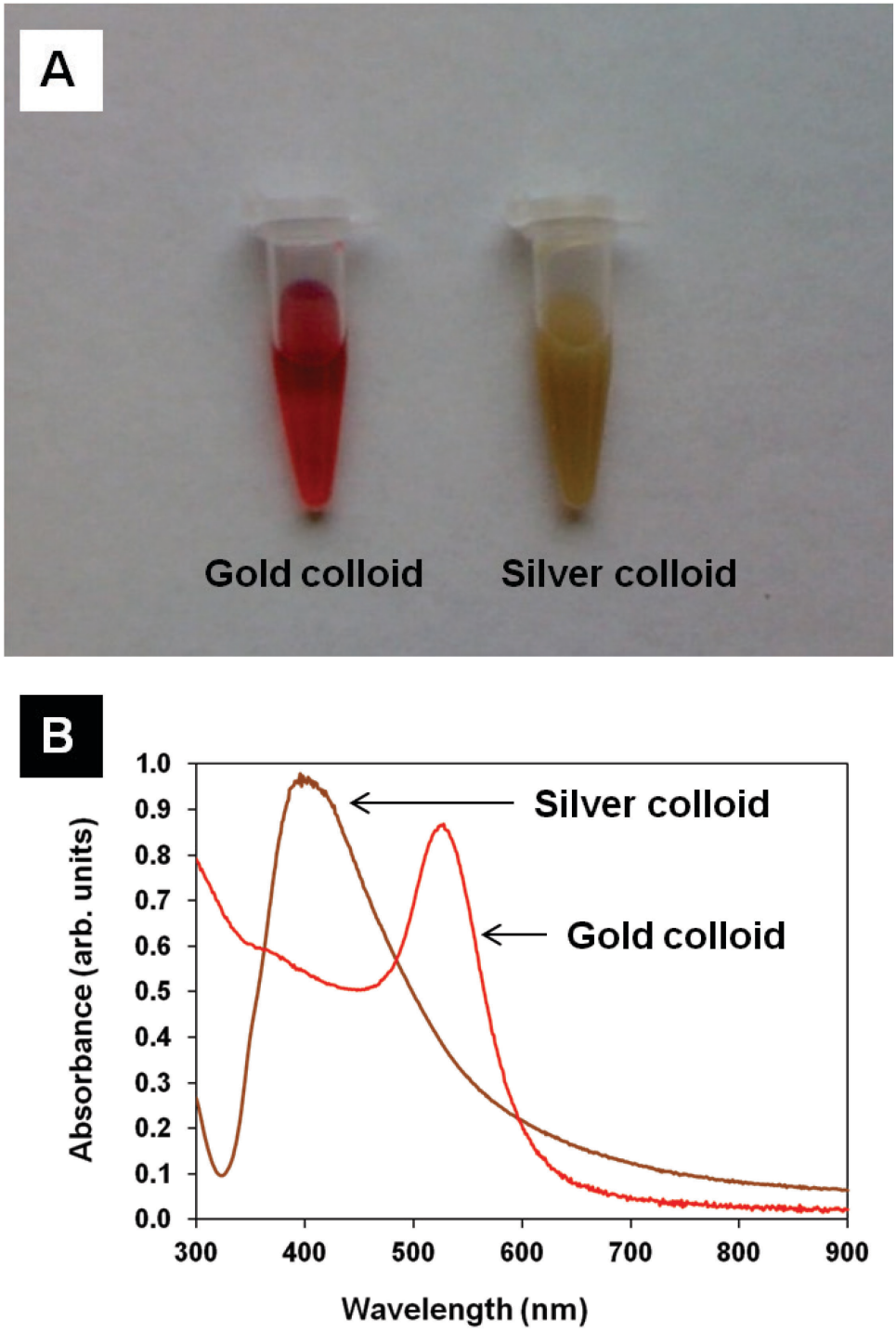

Figure 3.2 (A) Gold and silver nanoparticles prepared by reduction of chloroauric acid and silver nitrate using sodium citrate. (B) UV-Vis spectra of gold and silver colloids.

3.2.4 Printing

An Epson Workforce 30 inkjet printer (Figure 3.3) was chosen to generate the SERS-active substrates because Epson's Micro Piezo technology uses piezo elements to propel ink onto the substrate. Piezo elements are much more amenable to the different kinds of solvents used for printing compared to bubble jet printers. To form the silver ink, nanoparticle colloids were centrifuged at 10,000*g* to concentrate the nanoparticles; 98% of the supernatant was removed, and glycerol in a volume ratio of 2:5 (glycerol: colloid solution) was added to the remaining solution to adjust the viscosity and surface tension of the ink for optimal printing. To prevent clogging of the print head, the nanoparticle ink was filtered using a 0.2 micron Millipore PTFE membrane filter to remove any large particles from the ink solution.

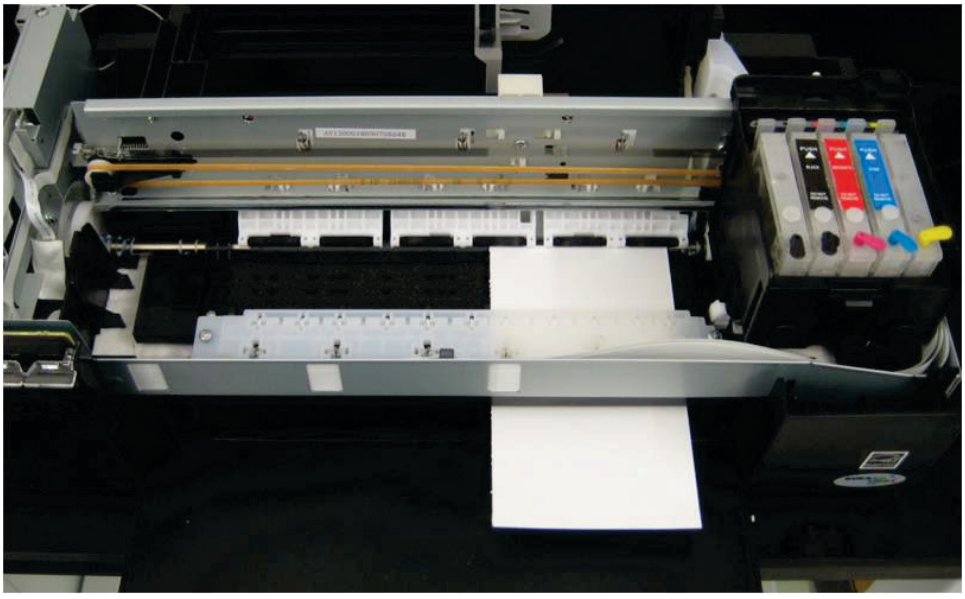

Figure 3.3 Epson Workforce 30 Inkjet printer used for printing gold and silver nanoparticles on filter paper.

The ink was then injected into refillable printing cartridges. An open source vector graphics editor, Inkscape, was used to define the shapes to print using colors that correspond to unique cartridges. Silver nanoparticles were printed in circles of 1 mm diameter. To increase the nanoparticle concentration in the paper, the printing of sensors was repeated multiple times.

3.2.5 SERS measurements

Measurements were acquired within 3 hours of printing the substrates. SERS was performed using a Horiba Jobin-Yvon LabRAM HR-VIS Raman microscope using 632.8 nm HeNe laser excitation with less than 15 mW output. A 10X objective was used for focusing the excitation light onto the substrate and for collecting the scattered photons. The paper containing an array of printed SERS active regions was taped onto a glass slide, which was then placed on the microscope stage. Using a micropipette, a 1 μL droplet of sample analyte was placed onto the printed circle of silver nanoparticles. SERS measurements were acquired after the droplet dried. Concentrations of 1 nM, 10 nM, 100 nM and 1 μM R6G in water were tested on 3 spots each. Measurements were acquired at three different locations within each printed circle, giving a total of nine SERS measurements for each R6G concentration. For 1 nM and 10 nM concentrations, a 5 second CCD exposure was used; for 100 nM R6G, a 2 second exposure was used, and for 1 μM, a 2 second exposure and an optical density 1 (OD1) filter on the laser were used. To determine the SERS enhancement factor of the inkjet-printed substrates, a 1 μL droplet of 2 mM R6G was spotted onto the paper coated with ASA. The resulting signal was compared with the measurements recorded with printed silver spots.

3.3 Results and Discussion

3.3.1 Types of paper and fluorescence

When using an organic material as a substrate for SERS, a major concern is that the scattered light from the substrate could overwhelm the signal from the analyte. In fact, we measured the scattered light from 21 different types of paper in order to select the material with the least background signal. These materials included printer paper, 100% cotton fiber paper, coffee filter paper, a napkin, and many others. The Raman microscope was used to measure the scattered light detected within the spectrum of interest for SERS detection (500 cm^{-1} – 2000 cm^{-1}). The signal from many of the papers saturated the CCD of the spectrometer after only a few seconds of integration time, making them absolutely impossible to use for paper-based SERS. This is likely due to the chemical treatments that many paper products undergo.[173] The papers with the lowest background were filter paper and chromatography paper, which contain essentially nothing other than cellulose. In this work and all subsequent works presented, chromatography paper was used for all of the SERS measurements.

3.3.2 Effect of print cycles and nanoparticle clustering

Figure 3.4 shows a photograph of silver nanoparticles printed onto the paper. The circles of printed nanoparticles were designed to be 1 mm in diameter. During printing, the silver nanoparticles appear brown on the paper initially and progressively become darker in color with each consecutive printing. Upon drying, the spots appear grayish due to the formation of silver clusters.

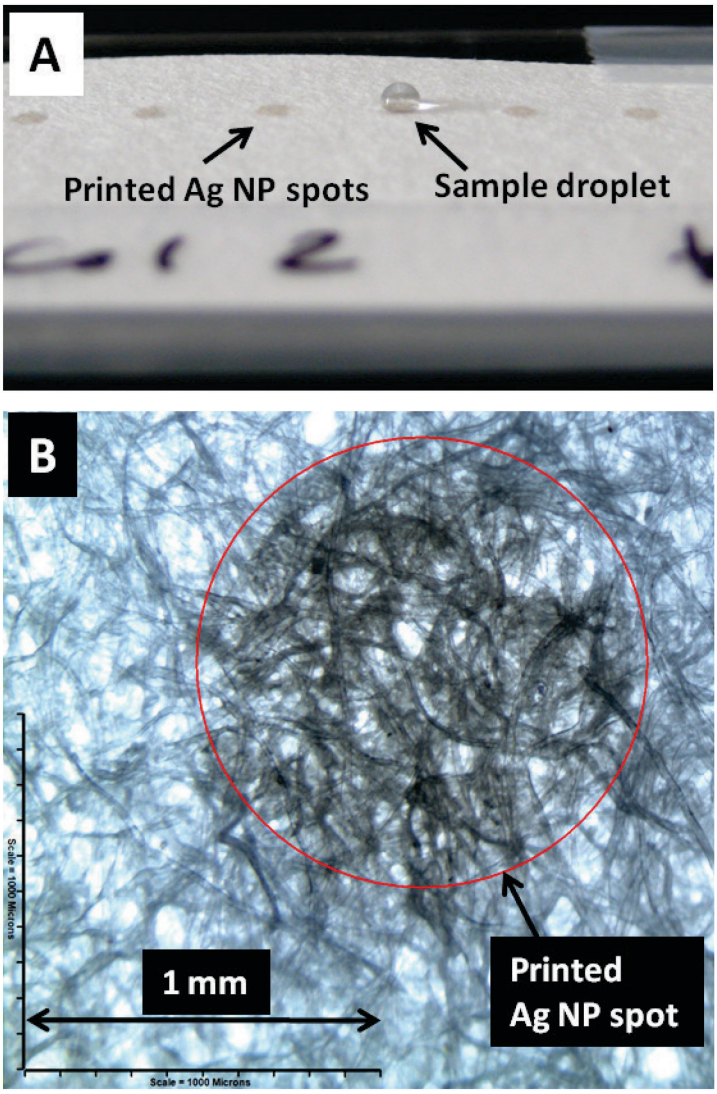

Figure 3.4 (A) Photo of an array of inkjet-printed silver nanoparticle (Ag NP) spots on chromatography paper. A 1 µL aqueous droplet was placed on one Ag NP spot. (B) Micrograph of one printed Ag NP spot on paper in bright-field mode.

A Scanning electron micrograph (SEM) of an inkjet-printed spot revealing the formation of silver nanoparticle clusters on the paper surface is shown in Figure 3.5. The high surface density of silver nanoclusters in Figure 3.5(A) illustrates the promise of this printing technique for generating substrates with high SERS activity. The image also reveals the precision of the inkjet-printing technique. The dashed line shows the discrete border of the printed SERS-active spot. The density of silver nanoclusters below and to the right of the dashed line is similar throughout the entire spot, while it is essentially zero to the upper left of the dashed line. The precision with which we can print the nanoparticles is demonstrated in Figure 3.5(A), which is a magnified image of one of the nanoparticle substrates in Figure 3.4(A). Even after 5 printing cycles, the transition between the silver nanoparticle embedded region and the region without silver is clearly distinguishable. It appears that even with repeated feeds, we can print with a precision better than tens of microns. With better ink formulation, repeated printing could be avoided. We expect that the precision as good as 10 μm and lower can be achieved, making it possible to print SERS microarrays with sub-millimeter sensor sizes.

Figure 3.5(B) shows a few selected silver nanoclusters dried onto the paper fibers. These clusters, which assemble as the silver colloid solution dries, generate hotspots which are advantageous for SERS. It was observed that multiple print cycles resulted in increased SERS activity as compared to a single print cycle; in addition, it was observed that the performance peaks at roughly 12 print cycles (Figure 3.6), after which the SERS activity starts to decline. We hypothesize that the initial increase in the SERS activity results from the increasing number of hotspots being generated.

However, after some point, the addition of more nanoparticles result in the formation of larger clusters, which are no longer resonant at the excitation wavelength used, hence the reduction in SERS.

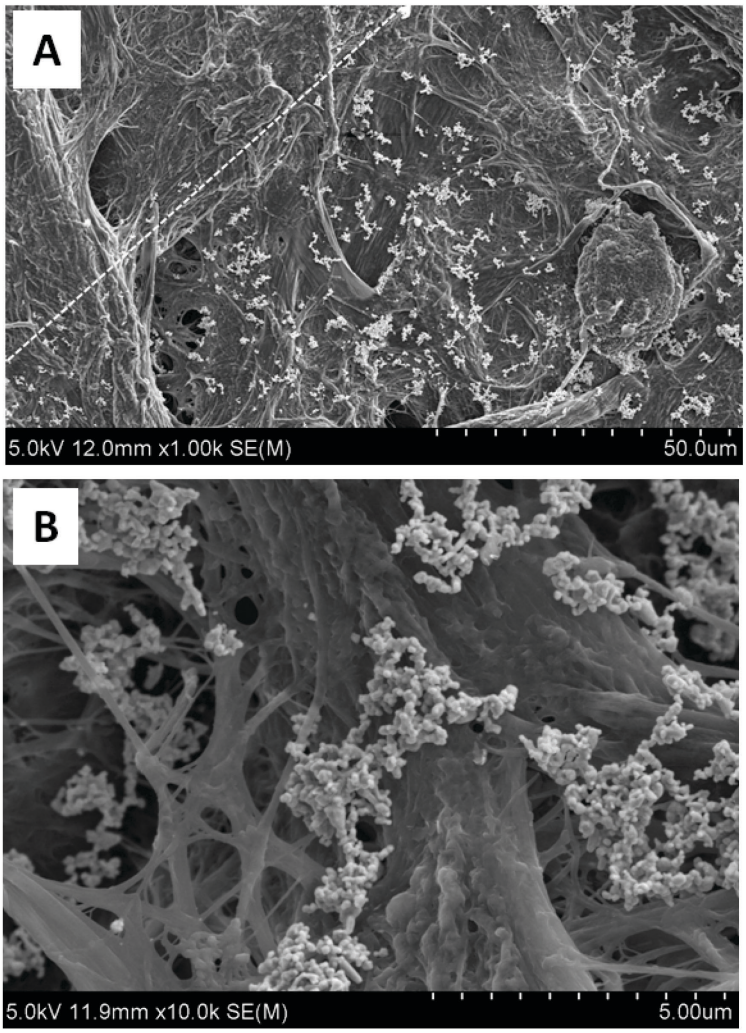

Figure 3.5 (A) Scanning electron micrograph of a printed Ag NP spot. The dashed line shows the boundary of the spot. (B) Ag nanoclusters within the printed spot.

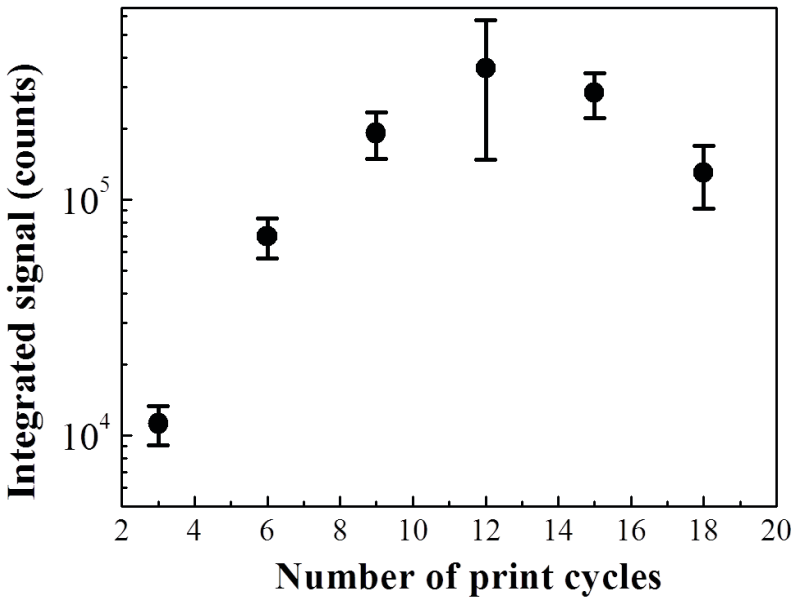

Figure 3.6 Effect of number of print cycles. Maximum SERS activity was observed at 12 print cycles.

3.3.3 Plasmon resonance of nanoparticle colloids and printed SERS substrates

Plain chromatography paper without any loading of nanostructures reflects light almost uniformly in the visible to infrared range. After printing of gold and silver nanoparticles onto the cellulose paper, the paper begins to display similar characteristic reflectances of the gold and silver nanoparticles as shown in Fig 3.7.

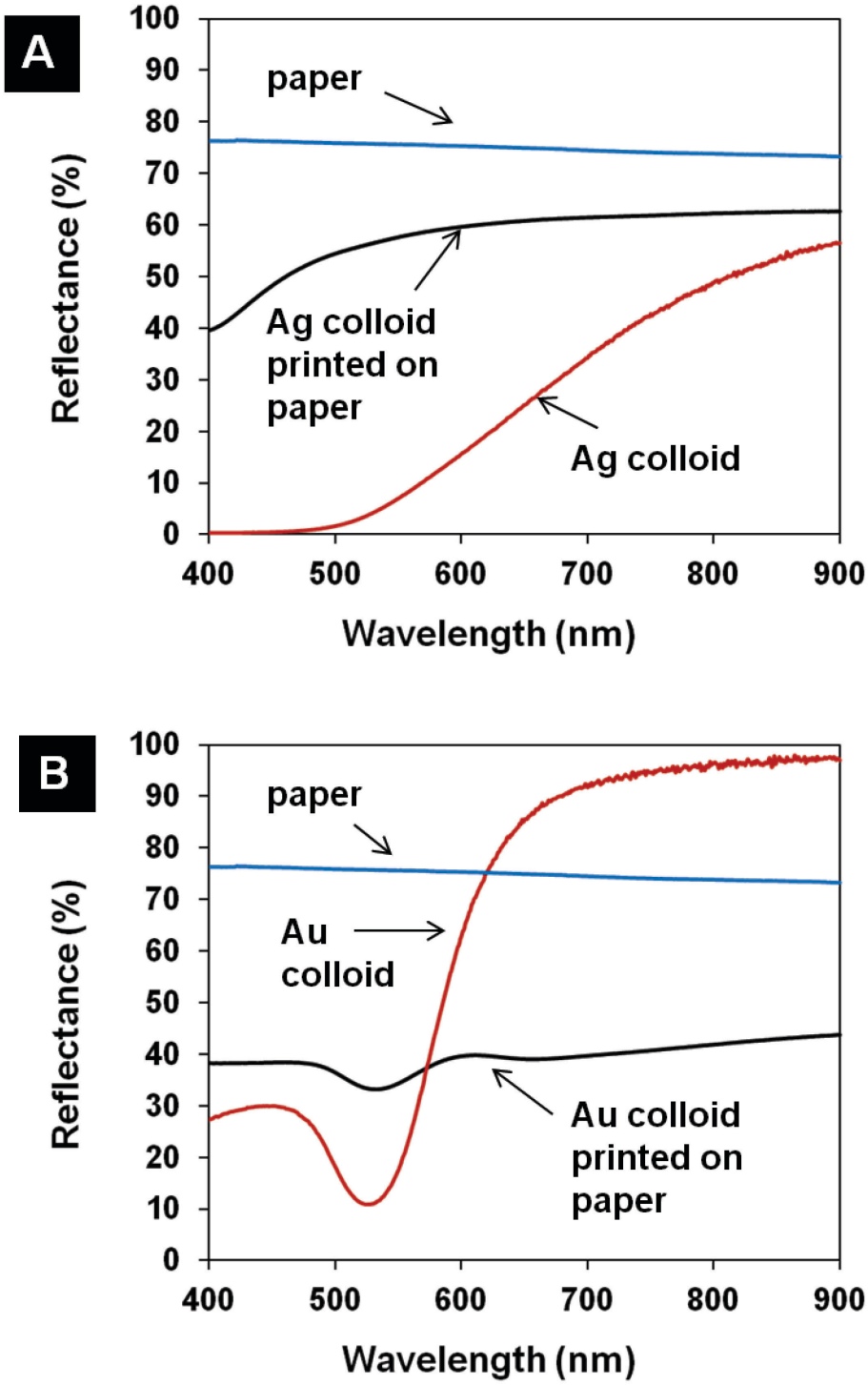

Figure 3.7 Reflectance spectra of inkjet printed SERS substrates on paper with silver (A) and gold (B) compared to silver and gold colloids respectively.

3.3.4 Effect of surface modifications

Printing high-precision small-area SERS-active substrates on paper for the analysis of small samples (microliter-sized samples) is not useful if the sample delivery is not well controlled. We observed that a 1 μL droplet of water applied to plain chromatography paper immediately spreads by approximately 5 mm in diameter, which dilutes the sample across this large area. For SERS, this is problematic, as the laser excitation is delivered only to a sub-millimeter area of the sensor. To control the aqueous sample delivery, we printed ASA, a common paper sizing agent, onto the sensing region of the paper before printing the nanoparticles. As seen in Figure 3.4(A), when a 1 μL droplet of water is applied to the SERS-active spot, the water beads up on top of the sensor, slowly drying in place. This delivers all of the target analyte molecules onto the small-area SERS-active substrate. The simplicity of this inkjet printing hydrophobization technique means that the paper can be treated immediately before use as a sensing substrate. Hydrophobic treatment is demonstrated in this case as a desired option to limit the spreading of analyte over the surface of paper and to concentrate the analyte onto the printed silver area. In later chapters, we demonstrate cases where the hydrophilicity of the cellulose is a desirable property and no such treatment is used.

3.3.5 Enhancement factor

In light of the discussion in Chapter 2.4, for paper SERS, we have decided to adhere to the definition of EF as formulated in Equation 2.1.

$$EF = \left(\frac{I_{SERS}}{I_{Raman}} \right) \times \left(\frac{N_{Raman}}{N_{SERS}} \right)$$

This decision is based on the observation that the underlying paper support already has a high surface area due to the cellulose fibers; the embedding of a relatively low percentage of nanoparticles into the cellulose matrix should not significantly alter the surface area of the substrate. In addition, with the small amount of analyte used for testing, there should not be more than a single monolayer of analyte coverage. This allows us to simply estimate the number of analyte molecules N by $N = CV$ (i.e. concentration of analyte solution (C) multiplied by the volume of analyte used (V)).

The SERS enhancement factor for the inkjet-printed substrate was determined by comparing signals acquired on paper with and without printed silver nanoparticles. For a 1 μL droplet of 2 mM R6G on paper, the acquired SERS signal (N = 3) for the 1508 cm^{-1} was approximately equal to the signal acquired for 10 nM R6G on the printed silver nanoparticles. This implies an enhancement factor of approximately 2 x 10^5 over the entire area covered by the laser spot size. We believe it is possible to further improve this through optimization of the nanoparticle geometry and clustering to match the Raman excitation wavelength.

3.3.6 Detection limit

Typical SERS signals recorded for 10 nM, 100 nM, and 1000 nM R6G concentrations are shown in Figure 3.8. As only 1 μL sample volume is consumed for each measurement, the total number of R6G molecules applied to the sensors is 10, 100, and 1000 femtomoles, respectively. Different CCD exposure times and laser power values were used to record the SERS signals across the concentration range

shown in Figure 3.8; the signals are normalized to 1 second of CCD exposure and to zero optical density filtering of the laser source. Even for the signal acquired from 10 femtomoles of analyte, the characteristic R6G Raman bands at 605 cm^{-1}, 1310 cm^{-1}, 1365 cm^{-1}, and 1508 cm^{-1} have high signal to noise ratio and are easily distinguishable. As a result of the extended exposure time (5 seconds) for this concentration, optical scattering due to the paper is also visible; however, it does not interfere with the ability to identify the R6G Raman signal. In fact, using the same substrates, we were able to detect as low as 10 pM of R6G (10 attomoles total) even when using a 785 nm laser with a portable spectrometer (Ocean Optics QE 65000) as shown in Figure 3.9.

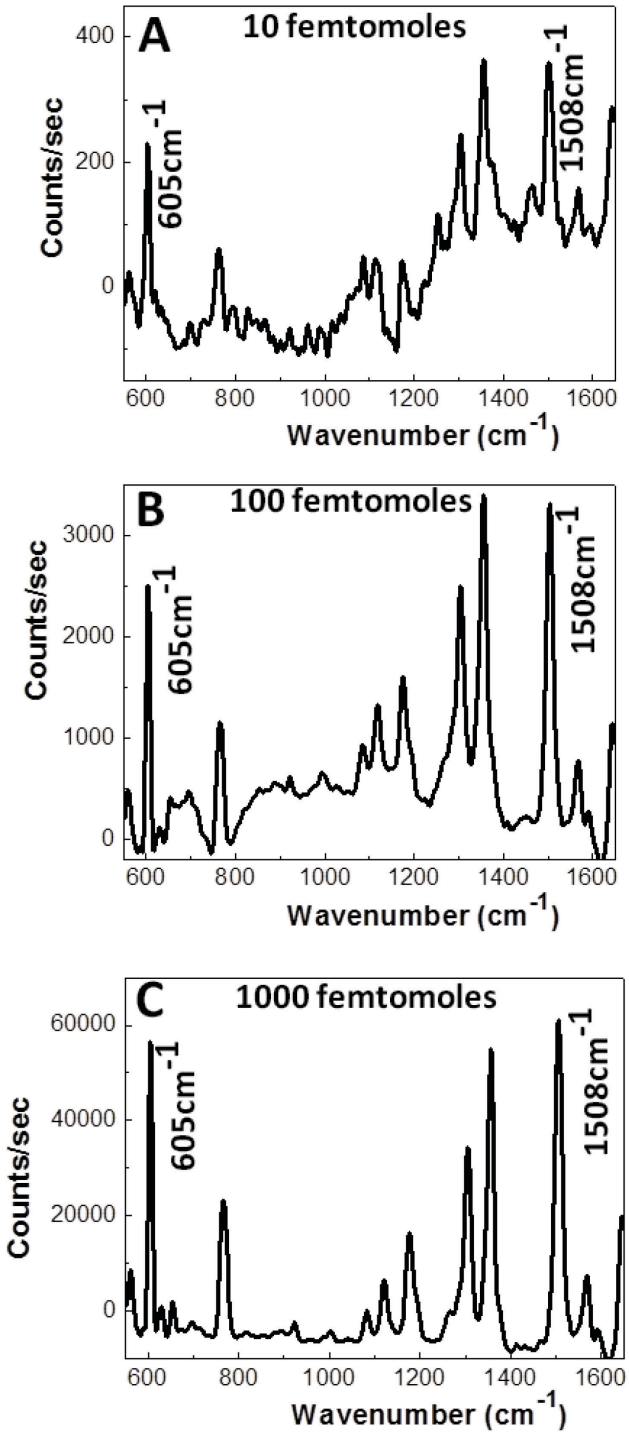

Figure 3.8 Typical Raman spectra of R6G acquired from three spots on the printed array. (A) 10 femtomoles, (B) 100 femtomoles, and (C) 1000 femtomoles R6G in the droplet sample. A 5-point FFT smoothing is used on the data.

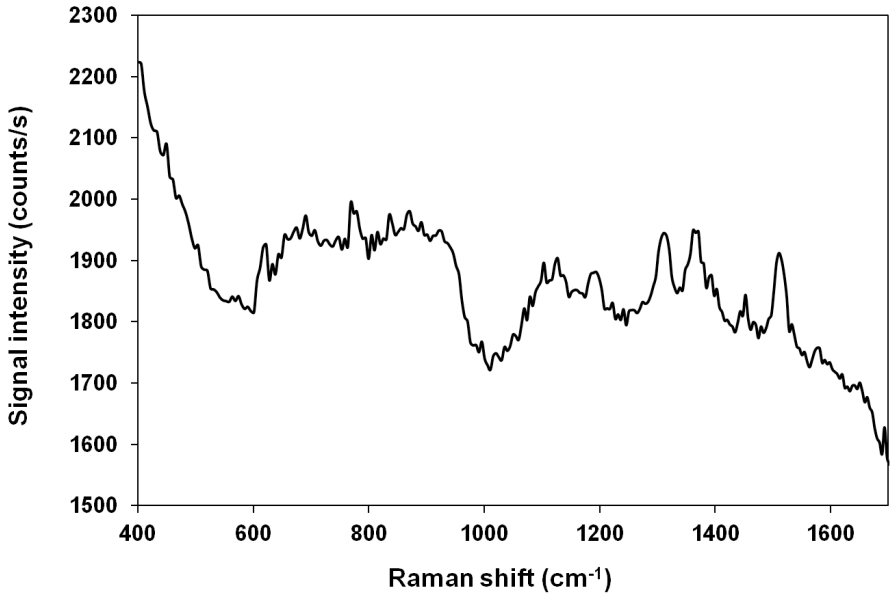

Figure 3.9 SERS signal of 10 pM R6G using a 785 nm laser and a portable spectrometer (Ocean Optics QE65000).

3.3.7 Signal variability

Variation in measured signal intensity across various locations has always been a concern for SERS, especially when the substrate has randomized features. To determine if signal inconsistencies pose problems for our inkjet-printed SERS substrates, we recorded SERS signals from three randomly selected locations within each printed SERS-active spot, separated by a distance greater than 100 μm, and we recorded signals from three printed spots for each concentration of R6G (i.e., nine data sets for each sample concentration). To analyze the collected signals, we calculated the area in the 605 cm^{-1} and the 1508 cm^{-1} R6G Raman bands and then summed the areas for each acquired signal (after normalization). Table 3.1 shows the

mean and standard deviation of the sums within each SERS-active spot in the array. The results indicate that the variation within each spot is small, but variation from spot to spot for the same concentration is relatively higher. We suspect that this resulted from a combination of factors: namely the random clustering of the silver nanoparticles, variations in printing process, and inconsistency in applying the 1 μL sample droplet onto each spot. In addition, large variability due to the uneven drying of analyte onto the substrate is possible. Differences in the evaporation rates across a drying droplet create a capillary flow within the droplet which result in a higher concentration of analytes at the edge, a phenomenon commonly known as the 'coffee-ring effect'.[174] Similar observations of variability due to the coffee ring effect have been made for solid state SERS substrates.[175–178]

Despite the variability that was observed, when the averaged signal for each concentration across the respective three spots was analyzed, a predictable trend in the data emerges. In Figure 3.10, we have plotted the mean and standard deviation across all of the 9 signals acquired for each concentration (3 signals acquired at 3 locations in each of 3 spots). These results illustrate that overall the measurements are repeatable and predictable across the concentration range using an inkjet printed array of SERS-active sensors.

Table 3.1 Mean and standard deviation of sum of the integrals of the 605 cm^{-1} and 1508 cm^{-1} R6G Raman bands within each SERS-active spot in the array.

Concentration of R6G	Spot No.	Mean No. of Counts/s	Standard Deviation	Coefficient of variation (CV)
10 nM	1	1.07×10^4	2.07×10^3	0.19
	2	8.28×10^3	6.36×10^2	0.08
	3	4.04×10^3	5.28×10^2	0.13
100 nM	4	7.47×10^4	9.92×10^3	0.13
	5	3.15×10^4	1.54×10^4	0.49
	6	9.44×10^4	1.90×10^4	0.20
1000 nM	7	2.98×10^6	1.30×10^6	0.43
	8	3.31×10^6	9.62×10^5	0.29
	9	2.38×10^6	2.11×10^6	0.89

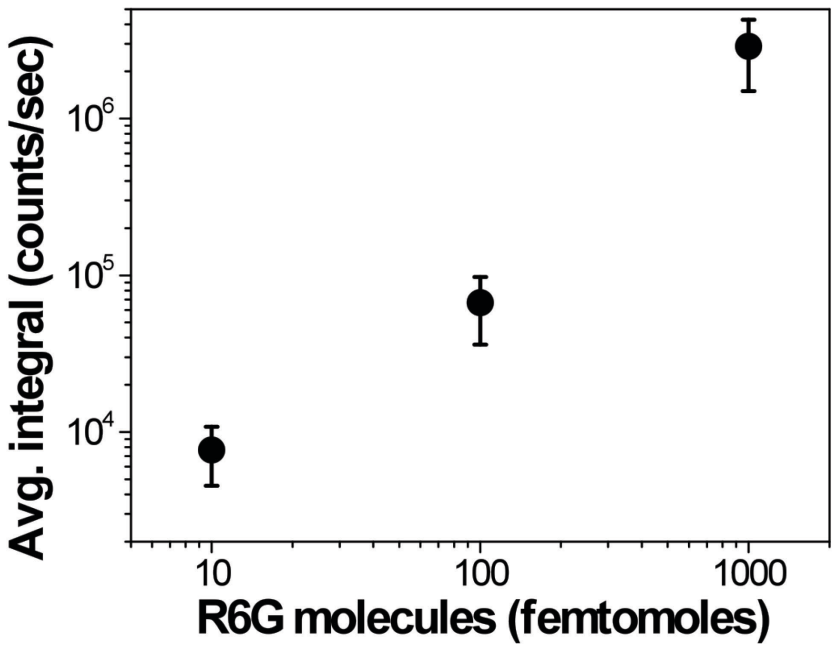

Figure 3.10 Average signal magnitude and standard deviation for each R6G dilution. For each concentration, three signals are acquired from each of three spots. The data points represent the averaged sum of the integrals of the 605 cm^{-1} and 1508 cm^{-1} R6G Raman bands.

3.4 Conclusion

We have demonstrated an ultra-low-cost paper-based SERS substrate using inkjet printing as the fabrication method. A high signal to noise ratio was achieved, even with only 10 attomoles of analyte molecules in the entire sample volume, and using a relatively low power 785 nm laser as the excitation source. In addition to the excellent performance, the substrate does not require any complicated or lengthy micro- or nanofabrication. The SERS substrate can be created in nearly any environment at the moment the user is ready to perform a measurement. Most importantly, this eliminates the problem of the limited shelf life of SERS substrates because the inkjet printed substrates do not need to be acquired in bulk and stored; instead, they can be fabricated with unprecedented simplicity and speed at the time and point of use. The extremely low cost and simplicity of fabrication make the paper-based SERS substrates ideal for a number of applications, including routine lab use, as well as use in the field at the point of sample acquisition. We believe that this technique has the potential to dramatically increase the applicability of SERS-based chemical and biomolecular detection, and as a result, enable much-needed low-cost and rapid sample analysis.

Chapter 4 : A Simple Filter-based Approach to Surface Enhanced Raman Spectroscopy for Trace Chemical Detection[5]

4.1 Introduction

Detection of trace chemicals in liquid samples and on solid surfaces is currently achieved by well-established methods that combine chromatography with mass spectrometry. While sensitive, these approaches are labor intensive, time consuming, and costly. They also require expensive and bulky equipment, and hence are not portable.

SERS offers an attractive alternative for chemical analysis. To make SERS analysis simple and inexpensive, we introduce in this work the development of a new technique for trace chemical detection called filter SERS. Filter SERS completely avoids the high costs of nanofabricated SERS substrates and the complexity associated with conventional microfluidic-based SERS by leveraging the filtration process to create a SERS-active substrate and to concentrate the analyte. The membrane traps nanoparticles from a colloid solution and also serves to extract analytes from a liquid sample. The substrate is fabricated on-demand and so shelf-life is no longer a concern. The technique requires only a filter membrane, a filter holder, and a syringe. There are no complicated fabrication steps and no mechanical or electrical components needed. In addition, filter SERS allows large volumes of trace

[5] This chapter is adapted from: Wei W. Yu and Ian M. White, *A Simple Filter-based Approach to Surface Enhanced Raman Spectroscopy for Trace Chemical Detection*, Analyst, 137, 168-173, 2012. Reproduced by permission of The Royal Society of Chemistry.

analyte samples to be processed very quickly, resulting in orders of magnitude increases in the number of analyte molecules that interact with the SERS-active surface as compared to current techniques of drying a sample onto a substrate or mixing a sample with a silver colloid solution. Consequently, filter SERS is extremely simple and inexpensive, but highly sensitive for trace chemical detection. The simplicity of the technique makes it particularly well suited for low resource, field based applications.

In this work, we demonstrate that the detection performance of the filter SERS technique is at least 1-2 orders of magnitude better than the typical approach of drying a sample in silver colloid onto a surface. We achieved a detection limit of 10 nM for the common model SERS analyte Rhodamine 6G (R6G) using a portable spectrometer and diode laser. Furthermore, we demonstrate the utility of the filter SERS technique for field based applications by detecting parts per billion (ppb) concentrations of melamine, a food contaminant, as well as ppb concentrations of malathion, a widely used pesticide, in aqueous solution. Importantly, our technique shows relatively low variability, and all acquired data sets could be fit well with a Langmuir isotherm. This indicates that our field based technique is not only simple and sensitive, but it can also be quantitative.

4.2 Methods

4.2.1 Materials

Nylon and Millipore PVDF filter membranes, 13 mm diameter, 0.22 μm pore sizes were purchased from Fisher Scientific and used with syringe filter holders from Cole-Palmer for performing the filter SERS assay. Silver nitrate, sodium citrate,

sodium chloride and melamine were obtained from Sigma-Aldrich. R6G was purchased from Exciton. Malathion was purchased from Cerilliant. Chemicals were used as received with safety precautions taken as according to their respective MSDS.

4.2.2 Nanoparticle synthesis

Silver nanoparticles were synthesized by the method of Lee and Meisel[80] as in chapter 3. Briefly, 90 mg of silver nitrate was added to 500 mL of ultrapure water (18.2 MΩ), which was then brought to a boil in a flask under vigorous stirring. Sodium citrate (100 mg) was added, and the solution was left to boil for an additional 10 minutes. After the solution turned greenish brown, which indicated the formation of silver colloid, it was removed from heat.

4.2.3 SERS measurements

To perform the filter SERS assay, the filter membrane is first wetted by dipping in a 50% ethanol-water mixture. The membrane is then placed into the filter holder, which can be attached to a typical syringe. A volume of silver colloid solution pre-aggregated with 5 mM NaCl is loaded into the syringe. The filter holder is then attached to the syringe and silver colloid is passed through the filter membrane (Figure 4.1(A), step 1). The membrane traps the silver nanoparticles, forming a SERS active substrate. The filter holder is removed, and the same syringe is then loaded with the sample. After re-attaching the filter holder, which now contains the nanoparticle-coated membrane, the sample is passed through the syringe (Figure 4.1(A), step 2). Target analyte molecules become adsorbed onto the nanoparticles or to the filter membrane, effectively concentrating the analyte. The membrane is then removed from the holder, dried, and analyzed using a SERS detection setup

consisting of a portable spectrometer (Ocean Optics QE65000), a 785 nm diode laser, and a fiber optic Raman probe. The filter SERS protocol and SERS detection setup is illustrated in Figure 4.1(A). A silver-nanoparticle-coated filter membrane is shown in Figure 4.2(A). It is clearly visible in the SEM images that the silver nanoparticles are trapped within the pores of the filter, yielding clusters of nanoparticles that are highly SERS active. Note: In order to establish the order in which filtration was to be performed, steps 1 and 2 of Figure 4.1(A) were reversed. Initial results indicated that Ag filtration followed by sample filtration yielded better results as shown in Figure 4.1(B). We hypothesize that this is as a consequence of the greater opportunity for interaction between the nanostructures and analyte by having the nanostructures already assembled on the membrane.

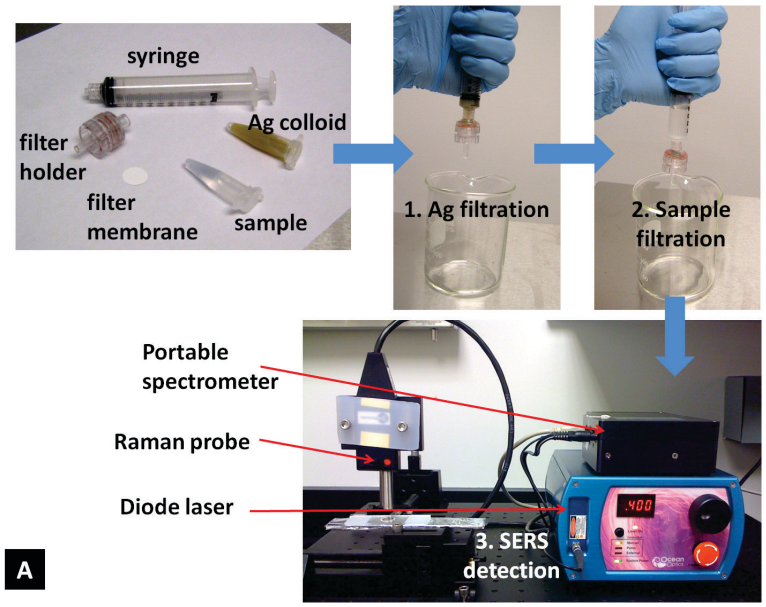

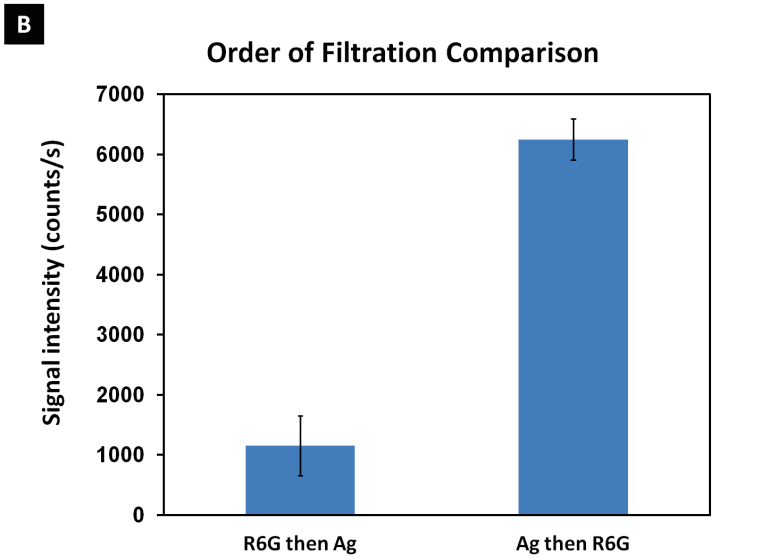

Figure 4.1 (A) SERS-active substrates are created simply by passing a silver colloid solution through a filter membrane using a syringe. Analyte molecules are concentrated into the substrate from a large sample volume. The SERS signal is detected using a small and portable photonic setup. (B) Comparison of the order of filtration on the SERS signal intensity. A much higher SERS intensity (6X) is observed when Ag is filtered first to form a SERS active surface, followed by sample filtration.

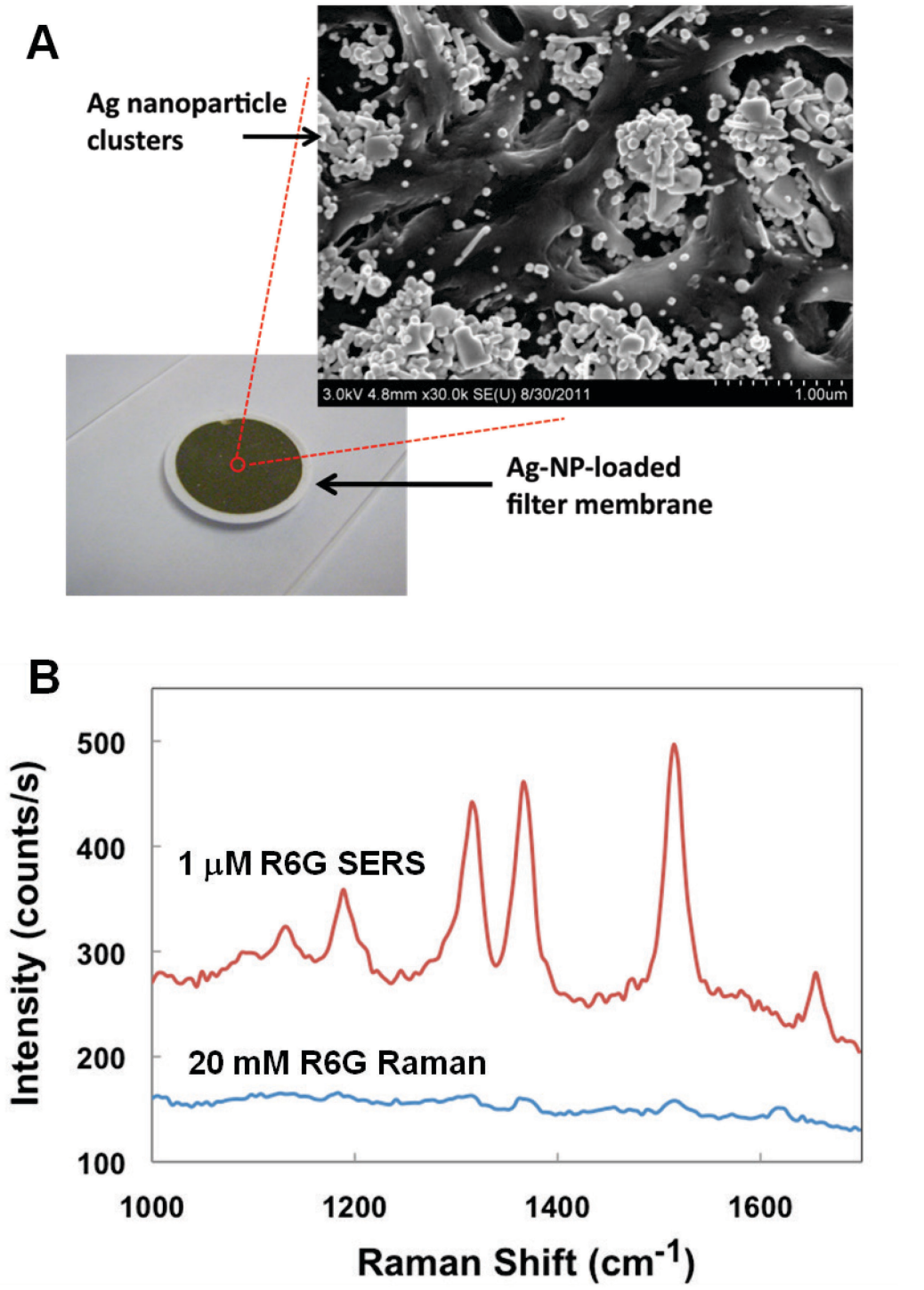

Figure 4.2 (A) Ag-NP-loaded filter membrane (bottom), and SEM image showing the clustering of silver nanoparticles in the pores of the filter membrane. (B) Measured Raman spectra for R6G with and without loading silver colloid through the membrane.

SERS measurements were acquired from three randomly selected locations within each membrane and repeated over three membranes, giving a total of nine SERS measurements for each analyte concentration. The laser power used was 3 mW (for R6G) and 10 mW (for melamine and malathion). A 1-second CCD exposure was used, with averaging of the SERS signal over 5 signal acquisitions. To determine the signal intensity, the height of the most prominent peak from the Raman bands was calculated (1509 cm^{-1} for R6G, 508 cm^{-1} for malathion and 690 cm^{-1} for melamine). Background contributions are accounted for by subtracting the background from the SERS signal. To establish the SERS enhancement factor of the silver nanoparticle coated membranes, a 1 μL droplet of 20 mM R6G was spotted onto a plain filter membrane; the resulting signal was compared with the SERS signal from 1 μL of 1 μM R6G pipetted onto a filter membrane after loading silver nanoclusters.

Three analytes were used for analysis: R6G, melamine, and malathion. R6G and malathion were used in water, while 0.1% HCl was added to the melamine/water sample before loading to protonate the melamine. For all three analytes, the filter SERS technique was compared with a conventional SERS method. For the conventional method, 1 μL of silver colloid and 5 μL of sample analyte were spotted onto an aluminum foil surface. The Raman spectrum was acquired after the droplet dried onto the surface. Finally, to verify that the filter SERS technique generates quantitative data, all concentration curves were fit using the Hill equation with N = 1 (i.e. The Langmuir isotherm) in Origin.

4.3 Results and Discussion

4.3.1 Quantification of the enhancement factor

The SEM image in Figure 4.2(A) indicates that a high density of SERS-active hot spots exist across the membrane, which will enable a large enhancement as compared to conventional Raman spectroscopy. To quantify the enhancement of the silver-nanocluster-treated membrane, we measured the Raman signal for 1 μM R6G dried onto the membrane with silver nanoparticles and for 20 mM R6G dried onto a membrane with no silver. The two Raman signals are presented in Figure 4.2(B). The enhancement factor of the membrane is determined by applying Equation 2.1:

$$EF = \left(\frac{I_{SERS}}{I_{Raman}} \right) \times \left(\frac{N_{Raman}}{N_{SERS}} \right)$$

where the intensities I_{Raman} and I_{SERS} are the heights of the 1509 cm^{-1} R6G Raman and SERS peaks respectively, and N_{Raman} and N_{SERS} represent the total number of R6G molecules deposited onto the plain membrane and the silver-nanocluster-treated membrane respectively. Using the data in Figure 4.2(B), an enhancement factor of 3×10^5 is determined. However, according to SEM images, only approximately 20% of the membrane surface is covered by silver nanoclusters; thus, assuming that the analyte molecules are evenly distributed across the membrane, the enhancement of the silver nanoclusters is approximately 1.5×10^6.

4.3.2 Effect of pre-aggregation using NaCl solution

It is well known that aggregation of nanoparticle colloids by sodium chloride (NaCl) solution can lead to formation of hotspots which are favorable for SERS. We investigated the effect of pre-aggregating the silver colloids solution by using various

concentrations of NaCl on the SERS signal. We observed that pre-aggregating the colloid solution with 5-20 mM of NaCl (final concentration) yields better SERS signal than silver nanoparticles that are not pre-aggregated. However, at higher concentrations of sodium chloride, this improvement is not observed. We suspect that this is a result of over-aggregation of the silver nanoparticles at high salt concentrations.

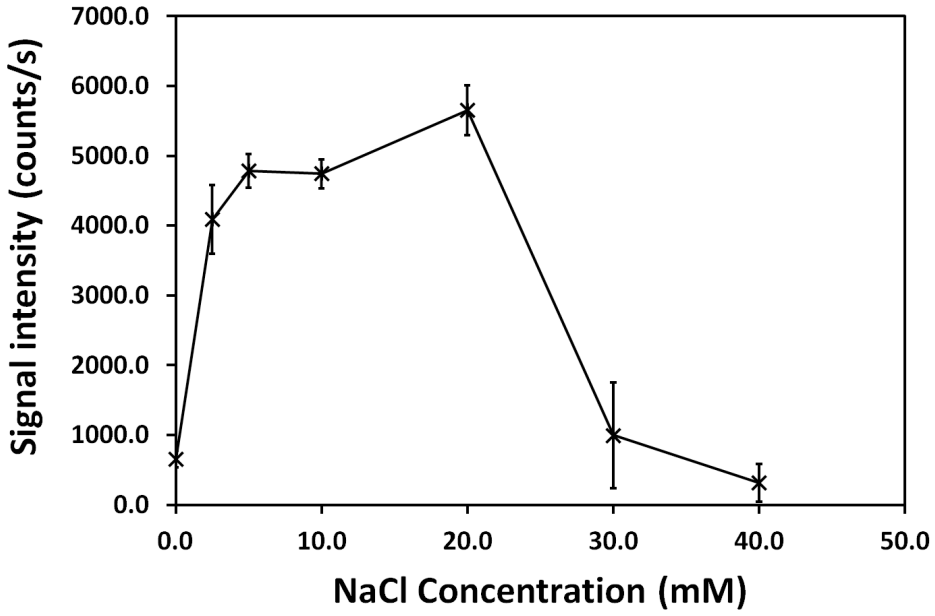

Figure 4.3 Effect of pre-aggregating the colloid solution using different concentrations of sodium chloride on the SERS signal.

4.3.3 Effect of silver colloid loading

Intuitively, the amount of silver colloid passed through the membrane will affect the SERS activity. The aim is to load enough silver nanoclusters to create a high surface density; however, we hypothesize that loading too many silver nanoparticles will cause the membrane to become a relatively thick silver film instead of a plasmonic nanostructured surface. Figure 4.4(A) shows the measured intensity of the 1509 cm^{-1} R6G Raman peak after first loading increasing volumes of silver colloid through the filter and then loading 10 μM R6G. As the data shows, the signal intensity decreases significantly when loading more than 0.5 mL of colloid through the filter. However, the variation in signal intensity is higher for 0.25 ml and 0.5 mL than for larger volumes. Therefore, for all subsequent experiments, as a compromise between signal variability and SERS activity, we load 1 mL of silver colloid through the membrane before loading the sample through the filter.

4.3.4 Effect of sample volume

We also explored the dependence of the Raman scattering intensity upon sample loading. Figure 4.4(B) shows that the signal increased linearly for increasing sample volume when loading between 1 mL and 8 mL of R6G (1 μM). As would be expected, this implies that increasing the number of analyte molecules passed through the filter increases the Raman signal. For the experiments in this work, we limited the sample volume to 5 mL, which is a compromise between signal intensity and sample loading time.

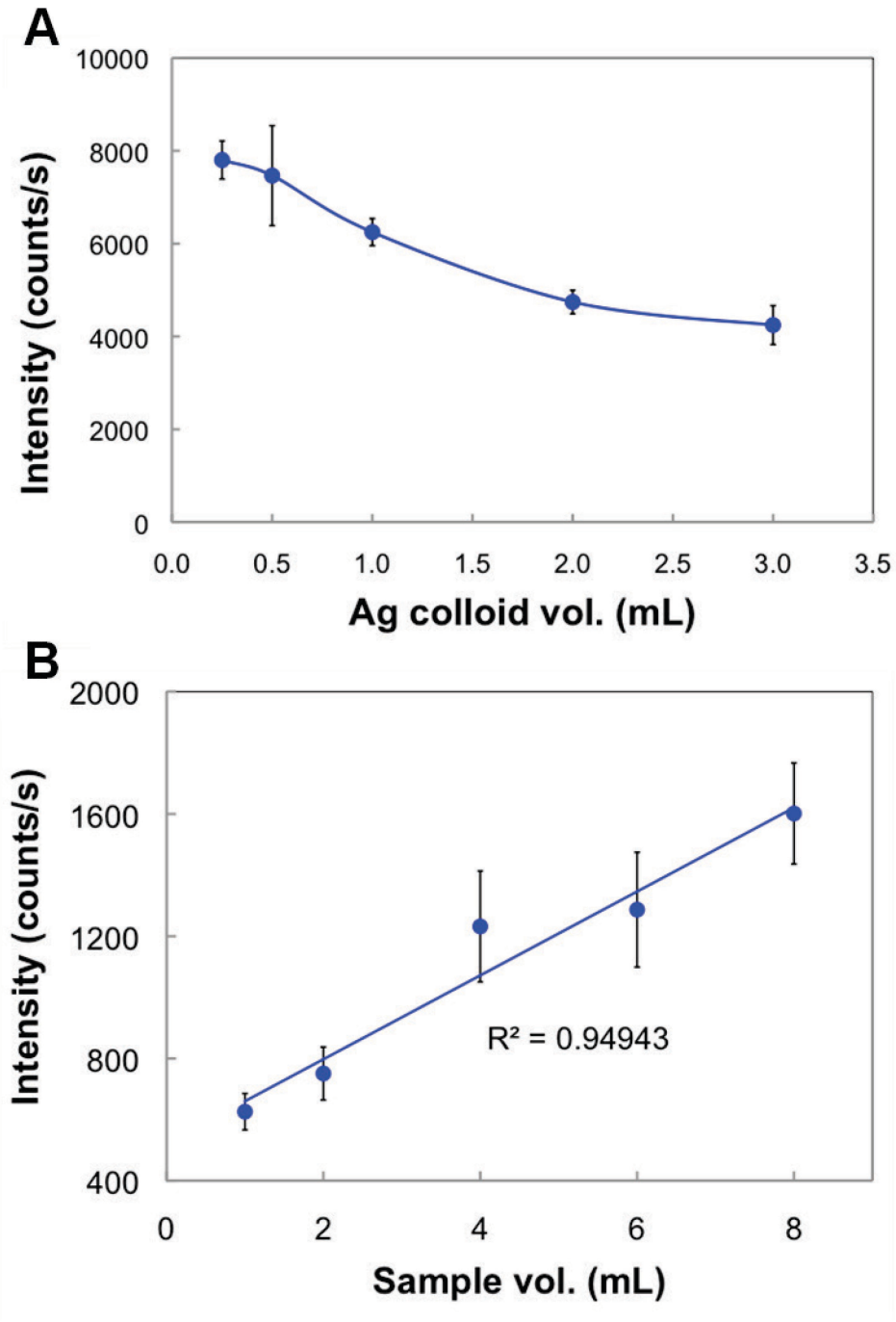

Figure 4.4 Measured intensity of the 1509 cm^{-1} R6G Raman peak for (A) increasing volumes of silver colloid loaded into the membrane filter, and (B) increasing volumes of sample loaded into the membrane filter.

4.3.5 Comparison of detection performance to colloidal SERS

Figure 4.5 presents the detection performance of the filter SERS technique for R6G as the analyte. In Figure 4.5(A), the detection performance of filter SERS is compared with that of a typical SERS measurement, in which the sample of R6G is added to a silver colloid and dried onto a surface. The measured Raman signals in Figure 4.5(A) show that the signal intensity for 1 μM R6G in colloid dried onto a surface is similar to the signal intensity for 100 nM R6G using the filter SERS technique. Thus for R6G, the filter SERS technique enables an order of magnitude improvement in detection performance as compared to typical SERS measurements.

4.3.6 Detection performance

To determine the detection limit for R6G using the filter SERS technique, we prepared dilutions of R6G in water from 100 μM down to 10 nM. Figure 4.5(B) shows recorded Raman spectra for this range of R6G concentrations. Data points representing the peak height of the 1509 cm^{-1} R6G Raman peak are plotted against R6G concentration in Figure 4.5(C). Data for both the nylon and PVDF membranes are plotted and analyzed; very little difference is observed between the two. In the plot, the data points represent the mean value for three separate membranes, and the value associated with each membrane is the mean across three separate spots on the membrane (*i.e.*, nine data points are taken for each concentration). Error bars represent the standard deviation of the mean values for each membrane. Figure 4.6 and Table 4.1 present the variation of the signal intensity in more detail.

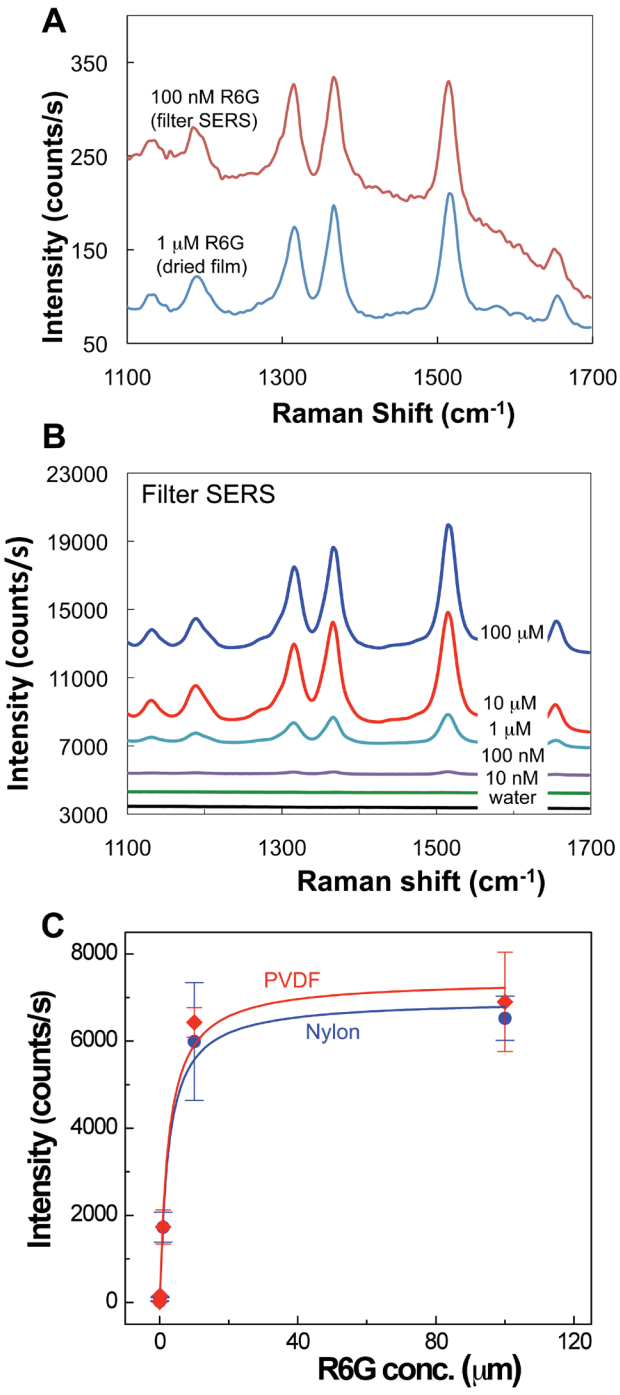

Figure 4.5 (A) Comparison of R6G detection performance of filter SERS with a sample in colloid dried onto a surface. (B) Signals of R6G detected using filter SERS. (C) Plot of the intensity of the 1509 cm^{-1} R6G Raman peak for various R6G concentrations using nylon and PVDF membranes. Each data set is fit with a Langmuir isotherm.

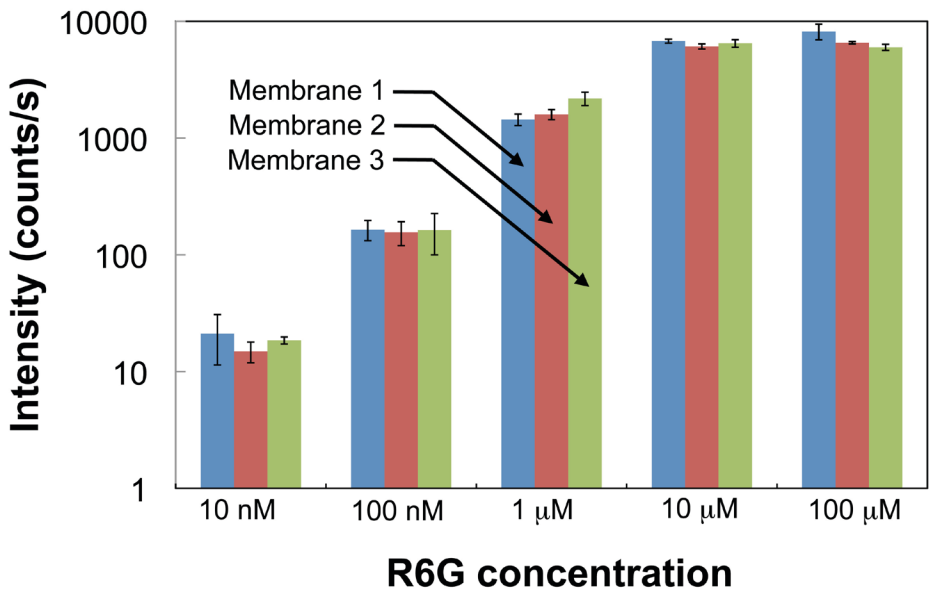

Figure 4.6 Variability of the SERS intensity of the 1509 cm^{-1} R6G Raman peak. Each bar represents the mean intensity from one membrane. The error bars show the standard deviation of the intensity measured at three random spots on the membrane.

Table 4.1 Variability of the average SERS signal intensity over three separate trials at varying concentrations of R6G.

R6G Conc. (μM)	Average SERS signal (3 trials)	Standard Deviation	coefficient of variation (C.V)
0.01	18	3	0.17
0.1	161	4	0.03
1	1738	391	0.22
10	6436	339	0.05
100	6906	1139	0.16

In Figure 4.6, each bar represents the mean for a particular concentration and a particular membrane, while the error bar for each bar is the standard deviation of the signal intensity of three spots measured within the respective membrane.

Two important characteristics can be seen in data plotted in Figure 4.5(C), Figure 4.6 and Table 4.1. First, the data in Figure 4.4(C) was fitted with the Langmuir isotherm; the fit is excellent ($R^2 = 0.989$ for the nylon membrane, $R^2 = 0.985$ for the PVDF membrane). Second, the standard deviation of each data point is relatively low for SERS measurements. These two facts suggest that the filter SERS method is not only simple and practical, but it also has the potential to be a quantitative technique.

4.3.7 Application for food contaminant and pesticide detection

To demonstrate the use of this practical and portable technique for field-based applications, we performed detection of melamine, a toxic food contaminant, and malathion, a commonly used organophosphate pesticide. The detection performance for melamine is presented in Figure 4.7. The signal obtained by filter SERS at 6.3 ppb melamine is compared with the signal measured for 1.26 ppm melamine in silver colloid dried onto a surface in Figure 4.7(A). It is evident that the filter SERS technique boosts the detection performance by a factor of 200 as compared to traditional SERS measurements.

Figure 4.7(B) shows the measured SERS spectra for melamine for a concentration range between 12.6 ppm and 6.3 ppb (50 nM) when using the PVDF filter membrane, which proved to be more effective than nylon for melamine. The intensity of the 690 cm^{-1} Raman peak for melamine is plotted for each concentration in Figure 4.7(C). Similar to the case of R6G, the variability of the intensity values is

relatively low, and the data can be fit well with a Langmuir isotherm. Even though a portable spectrometer is used for the measurements, the detection limit of 6.3 ppb is achieved, which is well below the currently accepted levels of 2.5 ppm for melamine in foods as established by the FDA,[179] making it possible to use filter SERS as a detection method for melamine in foods.

In a similar manner, we analyzed the performance of filter SERS for the detection of the organophosphate malathion in water. As shown in Figure 4.8(A), by drying a sample of malathion in silver colloid onto a surface, only 12.3 ppm malathion could be detected, while the filter SERS technique enabled the detection of 61.5 ppb, an improvement by a factor of 200. In this case, we used a nylon membrane, which proved to be more effective for malathion. The recorded SERS spectra for a malathion concentration range of 12.3 ppm to 61.5 ppb is presented in Figure 4.8(B). As proven in Figure 4.8(C), this data can also be fit well by a Langmuir isotherm, and exhibits low variability, which suggests that quantitative detection of malathion in water can be performed using our low cost portable SERS detection technique.

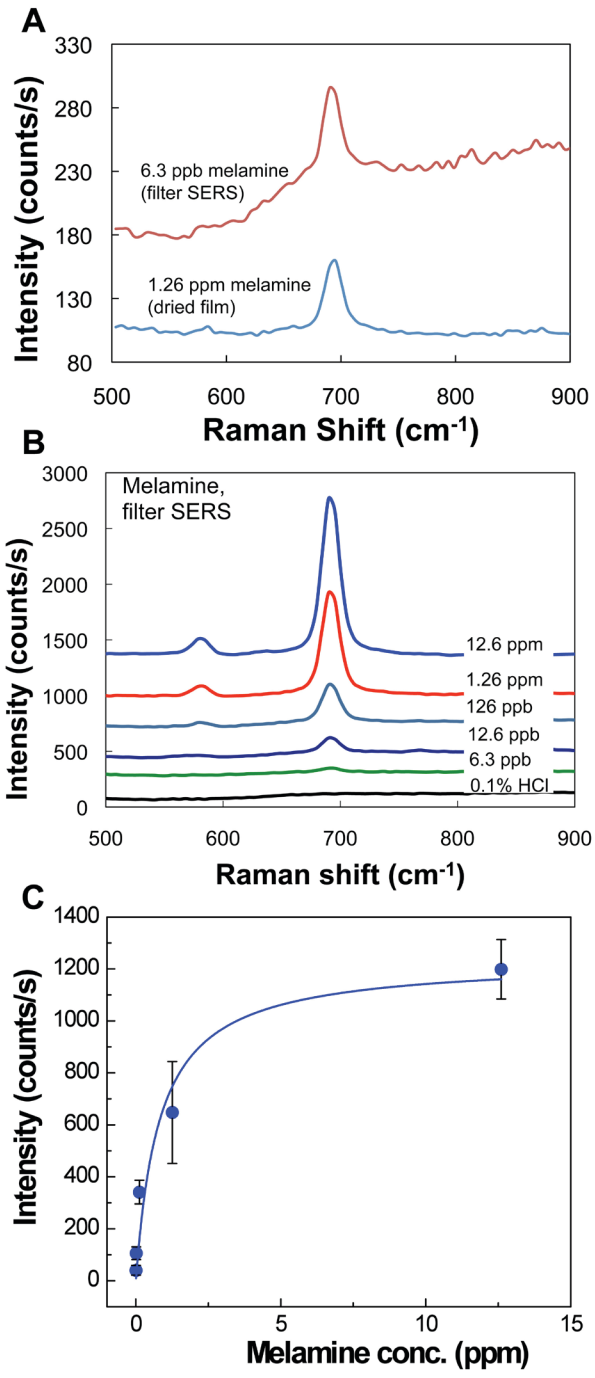

Figure 4.7 (A) Comparison of melamine detection performance of filter SERS with a sample in colloid dried onto a surface. (B) Signals of melamine detected using filter SERS. (C) Plot of the intensity of the 690 cm^{-1} melamine Raman peak for various melamine concentrations. The data is fit with a Langmuir isotherm.

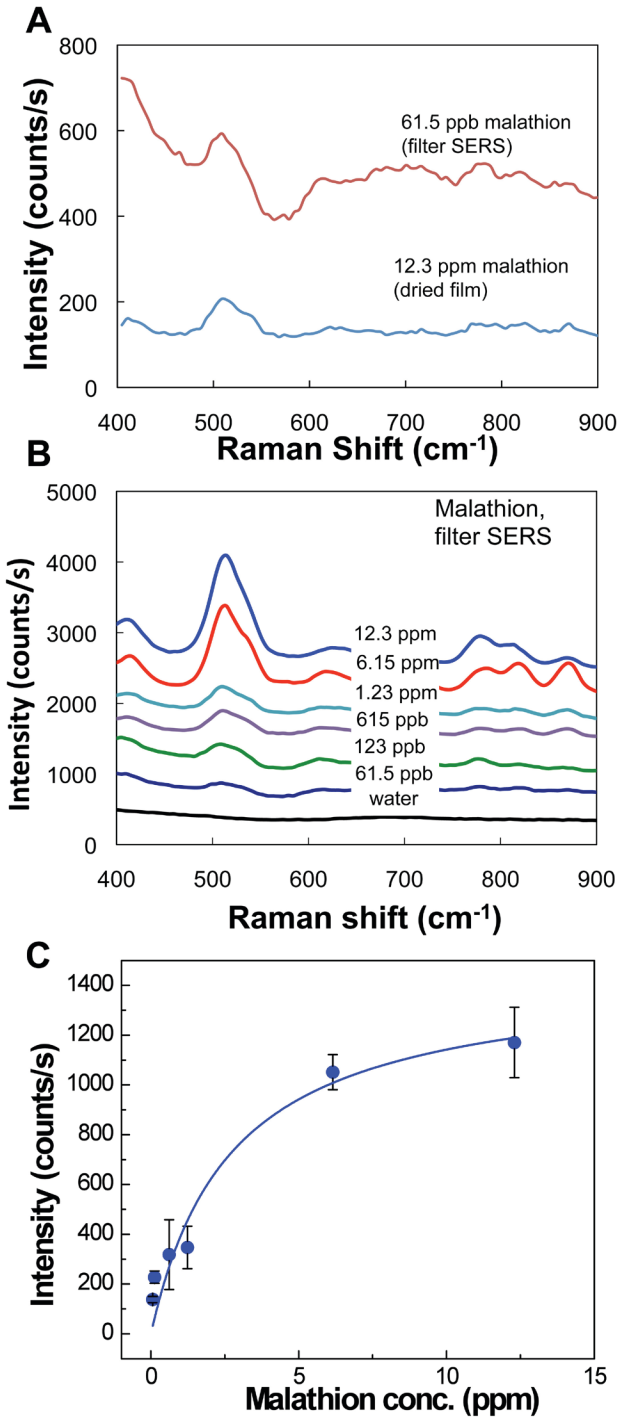

Figure 4.8 (A) Comparison of malathion detection performance of filter SERS with a sample in colloid dried onto a surface. (B) Signals of malathion detected using filter SERS. (C) Plot of the intensity of the 508 cm^{-1} malathion Raman peak for various malathion concentrations. The data is fit with a Langmuir isotherm.

4.4 Conclusion

We have developed an extremely simple and inexpensive, but highly sensitive method of performing SERS by filtration. The filter membranes create a SERS-active surface by trapping and concentrating nanoparticles from a colloid solution. They also concentrate analytes from relatively large sample volumes into the immobilized matrix of nanoparticles. The results presented here prove that the filter SERS technique is more sensitive than the conventional dried film SERS technique and that it can be quantitative. Detection limits of 6.3 ppb for melamine and 61.5 ppb for malathion were achieved with this technique. Furthermore, quantitative performance was verified by Langmuir isotherm line fits. This work demonstrates that filter SERS is well suited for low resource settings, in particular, for on-site environmental monitoring and food analysis.

Chapter 5 : Inkjet-Printed Paper-Based SERS Dipsticks and Swabs for Trace Chemical Detection[6]

5.1 Introduction

An active drive to improve the usability and sensitivity of SERS is the synergistic integration of SERS with microfluidics – also known as optofluidic SERS.[180–183] However, the cost of traditional microfabricated devices based on PDMS, glass, and plastics, is currently impractical to meet the needs for sensitive, ultra-low-cost disposable analytical devices. In chapter 3, we have introduced SERS-active substrates on paper by embedding nanoparticles into the cellulose matrix through the use of a low-cost inkjet printer. These paper SERS substrates demonstrate an enhancement factor of about 10^5 to 10^7, which is on par with many of the SERS substrates fabricated through self assembly and directed assembly.[184–188]

To add to this repertoire of ultra-low-cost and highly sensitive paper-based SERS devices, we demonstrate in this work SERS-active paper dipsticks fabricated by inkjet printing that can be used to collect analyte molecules from a liquid sample by simply dipping the paper into the sample. The capillary action of the cellulose fibers wicks the sample into the paper, including any target analytes present. These paper dipsticks are capable of processing much larger sample volumes than conventional SERS substrates and the previously demonstrated printed silver arrays on paper. Furthermore, no external pumps are necessary to load the sample, in

[6] This chapter is adapted from: Wei W. Yu and Ian M. White, *Inkjet-Printed Paper-Based SERS Dipsticks and Swabs for Trace Chemical Detection*, Analyst, 138, 1020-1025, 2013. Reproduced by permission of The Royal Society of Chemistry.

contrast to microfluidic-based SERS devices. In addition, due to the flexible nature of the paper substrate, these devices can also act as surface swabs to collect trace analytes from a large-area surface. As a result, the SERS substrates can collect analyte molecules directly from a surface, a feature that is impossible with today's rigid SERS substrates and microfluidic-based SERS devices.

In addition to this extraordinary simplicity of sample loading, the paper SERS devices also enable the concentration of analyte molecules into a small detection volume through a simple lateral-flow operation. In this step, the dipstick or swab is placed in a vial containing a volatile solvent, which transports analyte molecules to the tip as it is wicked up the paper. This lateral-flow step helps to improve the SERS signal intensity and uniformity by concentrating the analyte to a very small sensing area.

In this work, we demonstrate a detection limit of 95 femtograms of Rhodamine 6G (R6G) using paper SERS substrates. While far from the single molecule detection as first demonstrated by Kneipp et al. and Nie et al.,[20,21] this detection limit compares well with values reported for silver nanowires,[97] nanoparticles films,[189,190] e-beam fabricated substrates,[191] and self-assembled nanostructures.[192,193] In addition to R6G, we also achieved detection limits of 413 picograms of the organophosphate pesticide malathion, 9 nanograms of heroin, and 15 nanograms of cocaine, by concentrating these analytes into an area on the scale of a few mm^2 utilizing nothing more than the micro-capillary action of the paper. This technique requires no syringe pumps, electric field generation, microfabrication, or external equipment of any kind to load and concentrate analyte molecules, making it a

uniquely simple optofluidic SERS assay. In addition, the technique is demonstrated to be quantitative and has fairly low signal variability across multiple paper SERS devices. This device has obvious applications as a surface swab for detecting narcotics or detecting pesticide residues on foods, and as dipsticks for water testing.

5.2 Methods

5.2.1 Materials

Chromatography paper (0.19 mm thickness) was purchased from Fisher and used for the substrate; silver nitrate, sodium citrate, ethanol, and glycerol were obtained from Sigma-Aldrich. R6G was purchased from Exciton. Malathion, heroin and cocaine samples were obtained from Cerilliant. All chemicals were handled according to their respective MSDS.

5.2.2 Substrate printing

A low-cost commercial piezo-based EPSON inkjet Workforce 30 printer was used to print the SERS-active substrates onto untreated chromatography paper, as described previously.[92] To form the ink, silver colloid prepared by the method of Lee and Meisel[80] was concentrated 100X by centrifugation; glycerol and ethanol were added (40% and 10% by volume respectively) to optimize the surface tension and viscosity for optimal printing. The ink was added into re-usable cartridges and printed 10 times onto the desired regions of the paper (Figure 5.1A). In the printing process, nanoparticles in the ink aggregate, forming clusters in the cellulose matrix, which are responsible for the SERS enhancement of the substrate. After printing silver nanoparticles onto the paper, individual dipsticks were cut out of the sheet. The entire

paper strip can be utilized for sample collection, while the end of the dipstick or swab containing the silver nanoparticles acts as the SERS detection region.

5.2.3 SERS measurements

Heroin and cocaine were dissolved in methanol, while R6G and malathion were dissolved in water and diluted to various concentrations for use as test samples. For the dipstick experiments, 5 μL of sample was added to the sample collection zone in a controlled approach to mimic the uptake of analyte onto the paper. For the surface swab experiments, 5 μL of sample was spotted arbitrarily over the surface of a microscope glass slide. After the sample had dried, the SERS-active paper was soaked with methanol (acetonitrile in the case of malathion) and wiped gently but firmly over the glass slide (Figure 5.1B), while ensuring that the entire swab was in contact with the surface during the swab. In both cases, after the dipstick or swab had dried, it was placed into a vial (Figure 5.1C) containing 2 mL of methanol or acetonitrile; the methanol or acetonitrile is quickly wicked up into the dipstick or swab toward the detection tip. After 20 minutes of run time, the dipstick or swab was allowed to dry and the detection zone was scanned to determine the strongest SERS signal. This was repeated for five separate trials, giving a total of five SERS measurements for each analyte concentration. A 785 nm laser (17 mW) was used for excitation, a QE65000 (Ocean Optics) portable spectrometer was used for detection, and a fiber optic probe (InPhotonics) was used for delivery of laser light and collection of Raman-scattered photons (Figure 5.1D). We have chosen to use 785 nm for two important reasons: (i) we have observed that longer wavelengths induce lower autofluorescence background from the paper substrate compared to shorter

wavelengths, (ii) 785 nm lasers are widely available as small portable diodes, and portability is imperative to the benefits of our analytical technique. A 1-second CCD exposure was used, and the SERS signal was averaged across five signal acquisitions. To determine the signal intensity, the height of the most prominent peak from the Raman bands was calculated (1508 cm^{-1} for R6G, 508 cm^{-1} for malathion, 1005 cm^{-1} for cocaine and 626 cm^{-1} for heroin). Background contributions were accounted for by manually subtracting the SERS signal obtained from blank samples. The limit of detection for each analyte was calculated by dividing 3 standard deviations of the blank samples by the slope of the linear line fit at low concentrations.

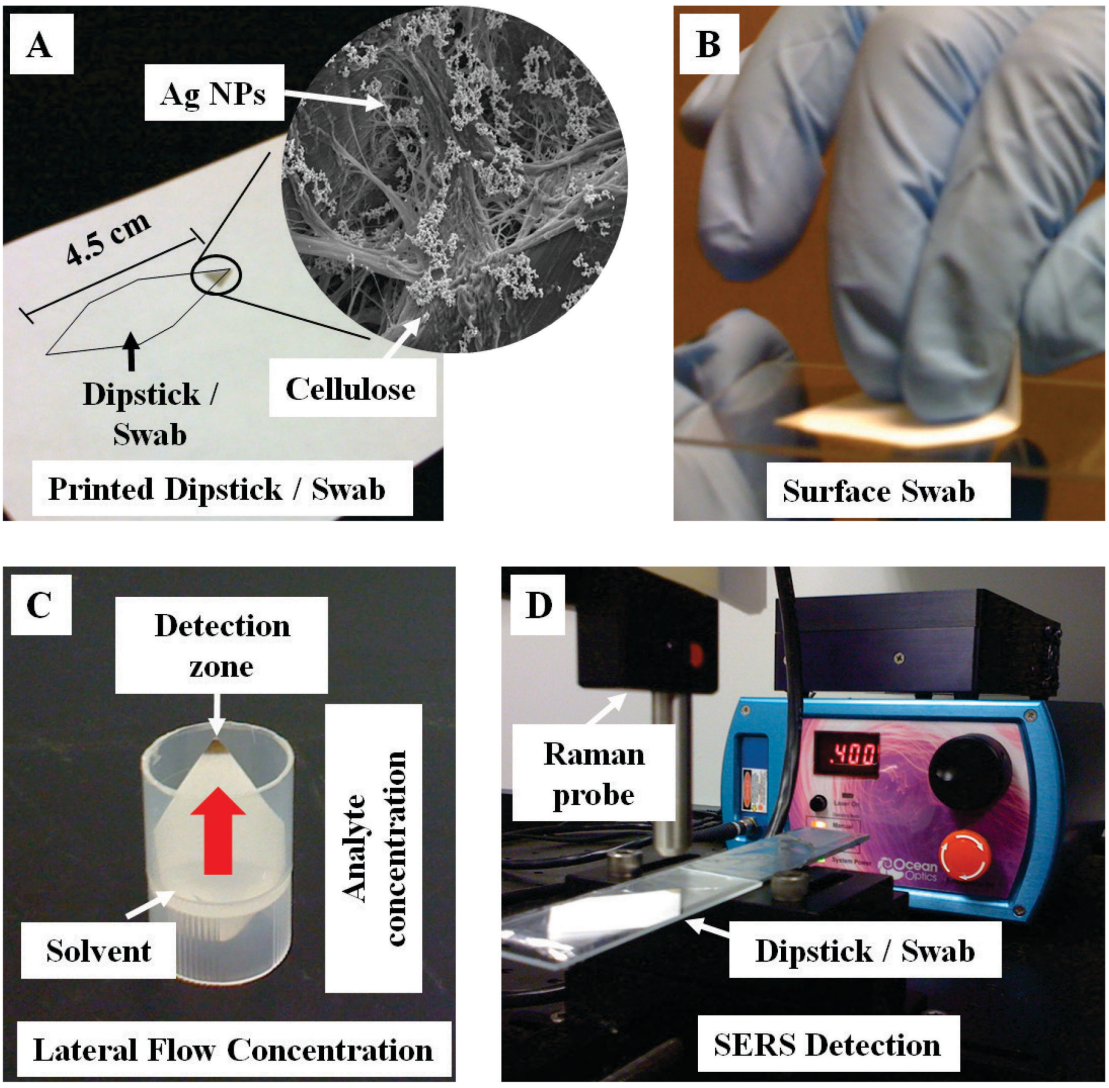

Figure 5.1 (A) Silver nanoparticles are printed onto paper to form a dipstick or swab (inset: SEM of silver nanoparticles on paper). (B) Swabbing a surface with the SERS-active swab. (C) Lateral flow concentration by placing the dipstick or swab in a volatile solvent. (D) SERS detection with a portable spectrometer using a fiber optic Raman probe.

5.3 Results and Discussion

5.3.1 Detection performance

To assess the detection performance of the paper SERS dipstick, we applied various concentrations of R6G directly to the bulk region of the dipstick followed by lateral-flow concentration. Figure 5.2(A) shows the SERS spectrum from 1.2 ng of R6G, while Figure 5.2(B) shows the SERS signal intensity at 1508 cm^{-1} at varying amounts of R6G. Two important aspects can be gleaned from this figure – (i) the fit of the data to the Langmuir isotherm is almost perfect (R^2 = 0.99951), and (ii) the SERS signal has fairly low variability from dipstick to dipstick. While randomly aggregated silver nanoparticles are often thought to result in poor variability and repeatability, in our system the laser spot size (and thus the scattering collection region) of the fiber optic probe is approximately 130 μm in diameter, and as a result we can deduce from the SEM micrograph in Figure 3.5(A) in Chapter 3 that hundreds of nanoparticle aggregates contribute to the SERS signal. Averaging over a large number of nanoparticles reduces the variation in plasmonic enhancement. The resulting low variability implies that it is possible not only to use the dipsticks to identify the presence of the analyte, but also to quantify the amount of analytes in the sample. Based on the obtained data, the limit of detection for R6G was calculated to be 95 fg. The background signal from the printed paper SERS substrate is compared with the SERS signal of 120 femtograms of R6G in Figure 5.3. The R6G signal can clearly be distinguished from the background.

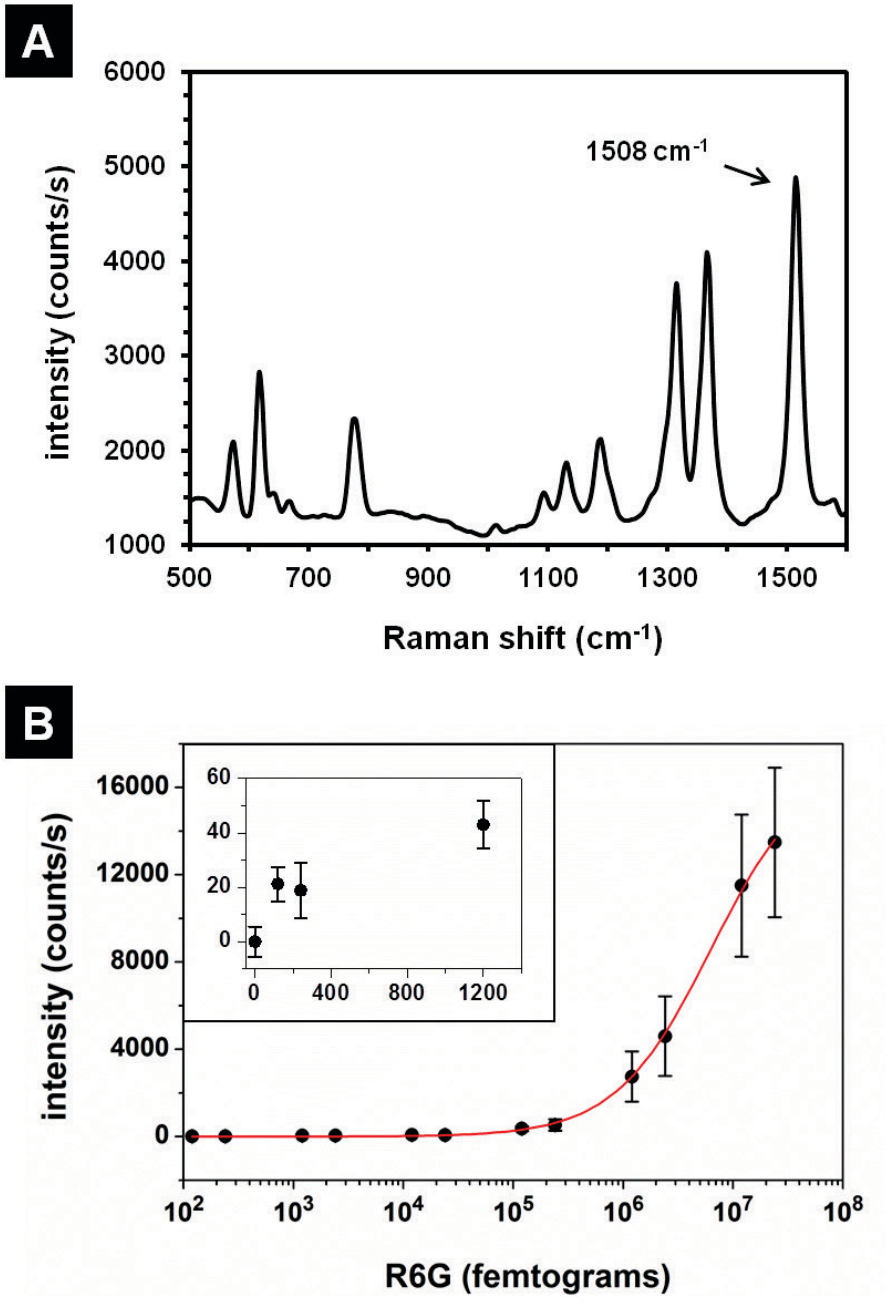

Figure 5.2 SERS measurements after applying R6G to the bulk region of the dipstick and then performing lateral flow concentration. (a) SERS spectrum of 1.2 ng R6G showing the 1508 cm^{-1} peak used to quantify the data. (b) Concentration curve of R6G signal intensity at 1508 cm^{-1}. Data is fitted using the Langmuir equation. (Inset: SERS signal at femtogram levels.)

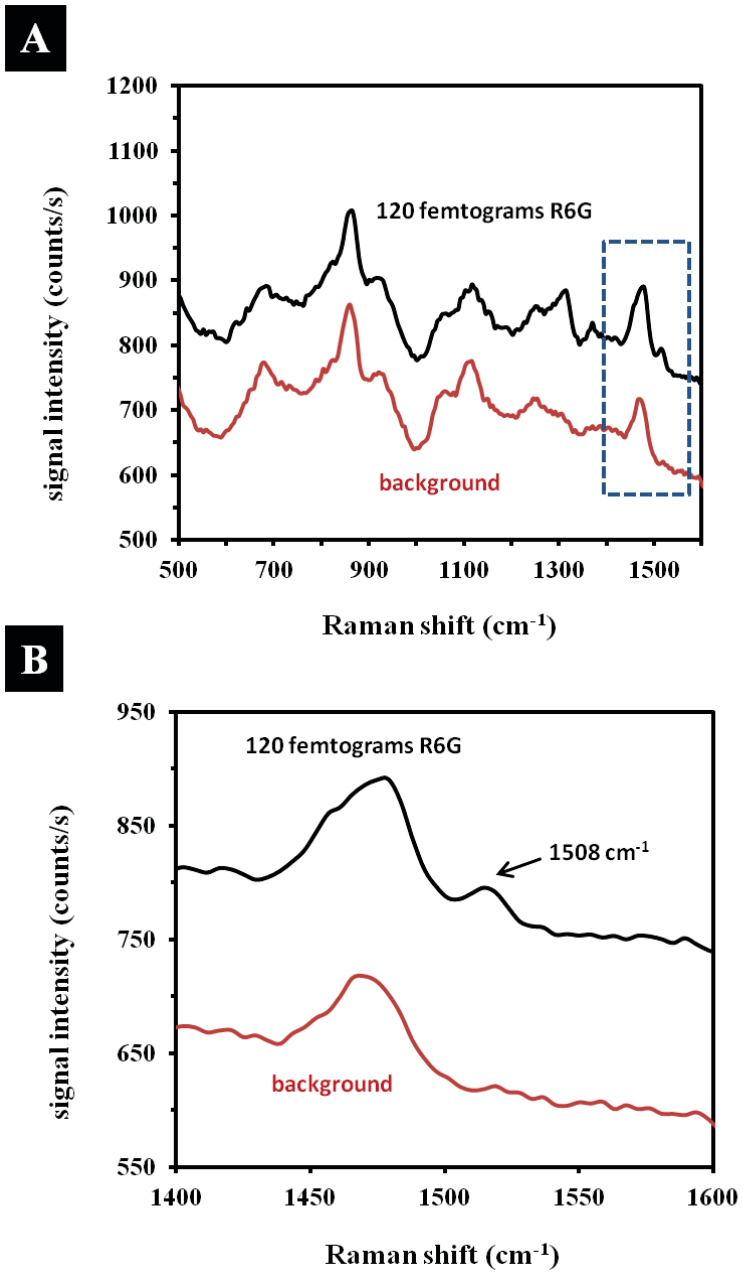

Figure 5.3 (A) Comparison of the SERS signal from 120 femtograms of R6G with the background signal of the paper SERS substrate. (B) Magnified view of selected portion of the SERS spectra showing the 1508 cm^{-1} peak. Note: The background spectrum has been shifted for clarity.

5.3.2 Application as surface swabs

To evaluate the applicability of these printed paper SERS substrates as surface swabs to collect analyte molecules from a surface prior to SERS detection, 5 µL of 5 µM R6G solution (12 ng) was pipetted onto a glass slide, dried, and swabbed using the SERS-active paper followed by lateral flow concentration. Figure 5.4 shows the resulting SERS signal intensity compared with equal amounts of R6G applied directly to the dipstick. After 5 trials, we observed an average efficiency of 35% in analyte collection by swabbing as compared to the direct application of the sample to the paper. This reduction can be attributed to the affinity of the analyte for the cellulose substrate and also the solvent used to soak the swab prior to swabbing. In addition to this, the thoroughness of the swabbing process has a significant influence on the efficiency at which the analyte is collected.

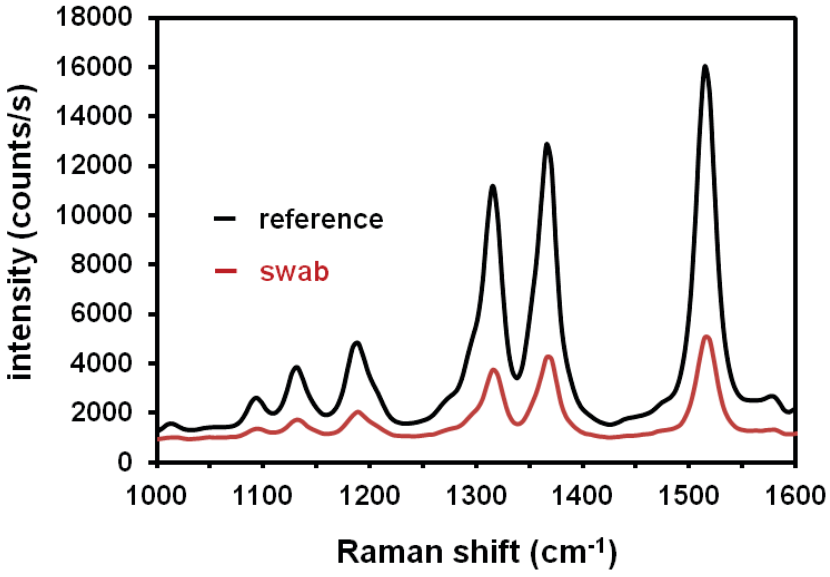

Figure 5.4 Comparison of the SERS intensity by swabbing a surface containing 12 ng of R6G versus a reference of 12 ng of R6G deposited directly onto the dipstick. Lateral flow concentration was performed after analyte collection in both cases.

5.3.3 Lateral flow concentration

To illustrate the advantages of the lateral flow concentration step, we used the printed paper SERS substrates to swab glass slides after depositing 5 μL of 10 μM R6G (24 ng). Figure 5.5 shows the SERS signal before and after performing the lateral-flow concentration. Before the lateral-flow concentration step, the SERS spectrum of R6G is barely visible, but after lateral concentration, the SERS signal intensity increases by 24X on average (5 trials), indicating the concentration of R6G onto the silver region. Because the calibration curve is non-linear, this 24X improvement in the SERS signal actually translates to 2 orders of magnitude improvement to the detection limit in terms of mass. We observed that the choice of solvent used for the lateral flow concentration can have an effect on the concentration enhancement. We hypothesize that this is due to the solubility of the analyte in the solvent and hence the mobility of the analyte along the paper strip. With judicious selection of a suitable solvent for a given analyte, we expect that it is possible to further improve the concentration enhancement and hence detection limits of these dipsticks and swabs. This optimization will be investigated further in future work.

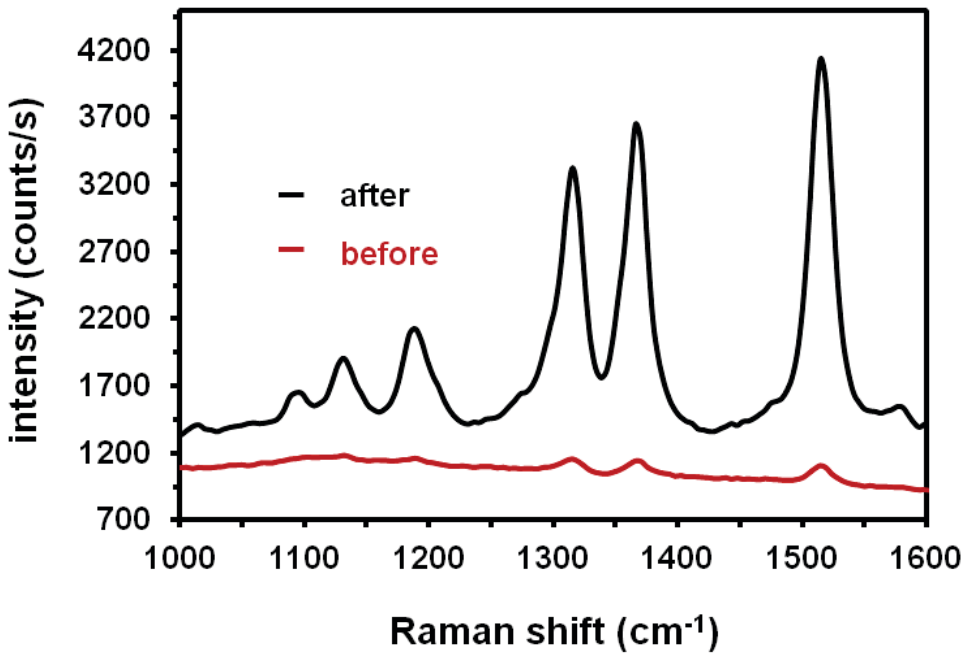

Figure 5.5 SERS signals from swabbing a glass slide containing 24 ng of R6G before and after performing the lateral flow concentration. The SERS signal strength is improved by 24X due to the lateral flow concentration. (Note: SERS spectra are shifted for clarity)

5.3.4 Applications for pesticide and narcotic detection

To illustrate the use of the paper SERS dipstick for a practical application, we detected the pesticide malathion in water. Malathion is one of the most commonly used organophosphate insecticides for pest control in the United States. As a result, malathion and malathion breakdown products can be found as contaminants in ground water and in/on foods.[194,195] Figure 5.6(A) shows the SERS spectrum from 307.5 ng of malathion, while Figure 5.6(B) shows the SERS signal intensity at 508 cm^{-1} at varying amounts of malathion. Again, the data fits extremely well to a Langmuir isotherm ($R^2 = 0.982$) with fairly low variability from dipstick to dipstick. The data yields a calculated detection limit of 413 pg of malathion in water.

To further demonstrate the real-world application of these SERS-active paper substrates as swabs, we applied them for the detection of two illegal narcotics – heroin and cocaine. Figure 5.7(A) shows the SERS spectrum obtained by wiping a microscope glass slide containing 5 μg of cocaine, while Figure 5.7(B) shows the associated calibration curve obtained by adding varying amounts of cocaine to the SERS-active paper fitted to the Langmuir equation ($R^2 = 0.963$). Likewise, the SERS spectrum obtained by swabbing a glass slide seeded with 5 μg of heroin is shown in Figure 5.8(A), while Figure 5.8(B) shows the associated heroin calibration curve fitted to the Langmuir equation ($R^2 = 0.932$). The calculated limits of detection for cocaine and heroin are 15 ng and 9 ng respectively.

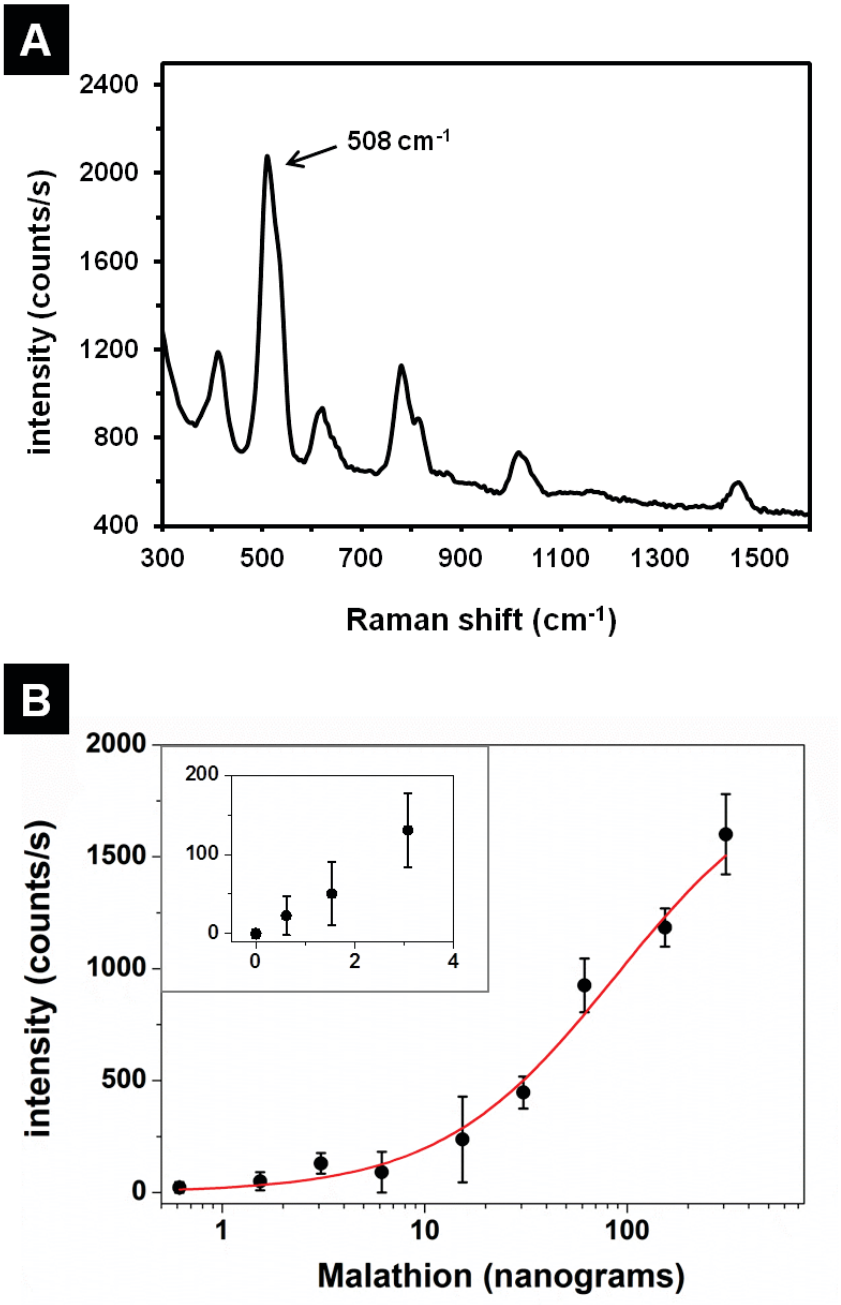

Figure 5.6 SERS measurements after applying malathion to the bulk region of the dipstick and then performing lateral flow concentration. (a) SERS spectrum of 307.5 ng malathion showing the 508 cm^{-1} peak used to quantify the data. (b) Concentration curve of SERS intensity at 508 cm^{-1}. Data is fitted using the Langmuir equation. (Inset: SERS at low nanogram levels.)

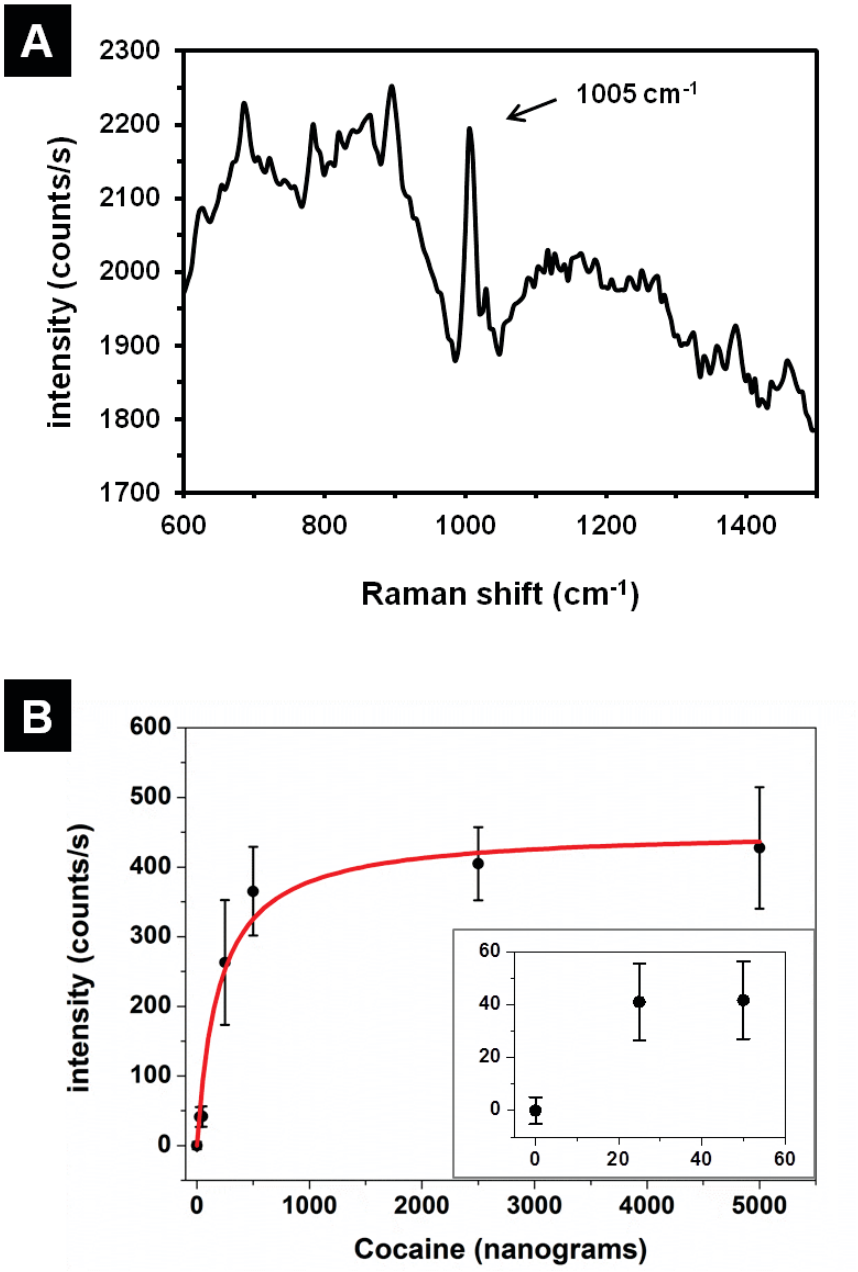

Figure 5.7 (A) SERS spectrum obtained after wiping a surface containing 5 µg of cocaine and performing lateral flow concentration. (B) Cocaine calibration curve obtained by measuring the intensity of the 1005 cm^{-1} peak. (Inset: SERS signal at low nanogram levels.)

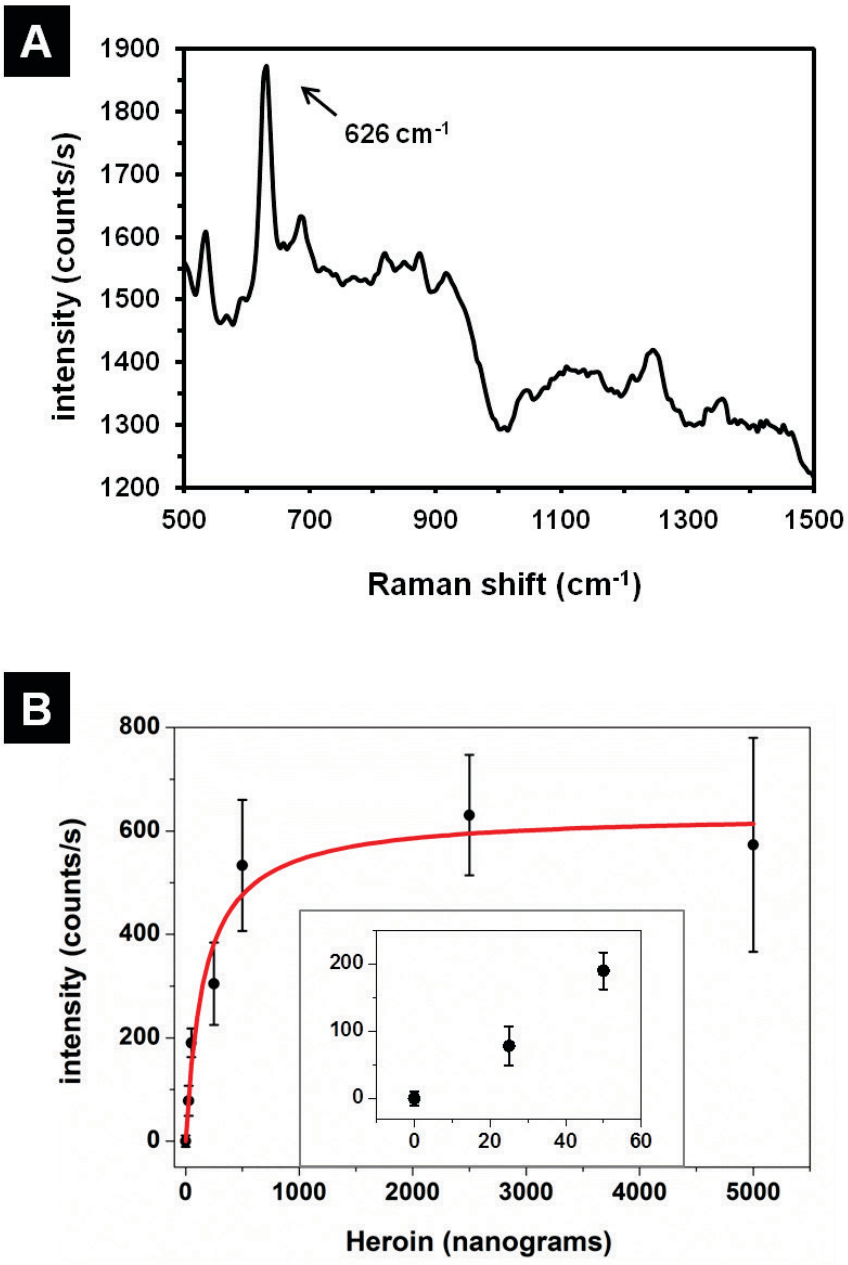

Figure 5.8 (A) SERS spectrum obtained after wiping a surface containing 5 µg of heroin and performing lateral flow concentration. (B) Heroin calibration curve obtained by measuring the intensity of the 626 cm^{-1} peak. (Inset: SERS signal at low nanogram levels.)

5.4 Conclusion

We have demonstrated an extraordinarily simple, low-cost analytical technique using a paper dipstick or swab with lateral-flow concentration and SERS detection on an inkjet-printed plasmonic substrate. These paper SERS devices are extremely simple to fabricate and to use as compared to conventional SERS substrates and traditional microfluidic devices. Utilizing the lateral flow concentration, we achieved detection limits as low as 95 fg of R6G, 413 pg of malathion, 15 ng of cocaine, and 9 ng of heroin. Although these detection limits are already comparable to many rigid SERS substrates fabricated through much more complex techniques, we can identify optimizations to our substrates that can improve the detection limit even further. First, the paper porosity and thickness, as well as the selection of the solvent can be optimized for improved concentration of the target analyte. Second, we hypothesize that it is possible to attain improved detection limits by tuning the plasmonic resonance of the nanostructures to match the 785 nm laser excitation wavelength. We project that the paper-based SERS device may be capable of detecting as low as 1 fg of R6G, even while using a portable spectrometer system. Ultimately, these inexpensive and highly sensitive SERS paper devices may have immediate applications for on-site trace chemical analysis in liquid samples or on surfaces, including the detection of illegal drugs by law enforcement agencies and the detection of pesticide contaminants on foods.

Chapter 6 : Chromatographic Separation and Detection of Multiple Analytes from Complex Samples Using Paper SERS[7]

6.1 Introduction

Recent years have seen an explosion in the investigation of SERS for a wide variety of applications, such as forensics, homeland security, food safety, and medical diagnostics.[196–201] One of the hypothetical advantages of using SERS as a detection modality is its ability to specifically differentiate a target analyte from non-targeted background molecules in complex real-world samples, and to detect multiple targets with a single scan.[23,202–205] However, identification of a targeted analyte in a complex sample may be challenging due to the interaction of molecules within the sample and interference by highly fluorescent molecules in the sample. Furthermore, multiple analytes may not be easy to detect simultaneously due to dominance of analytes with large Raman cross sections and overlapping of spectral signatures of analytes. The use of long-wavelength laser excitation sources can help reduce the problem of high sample fluorescence, but at the expense of a lower Raman signal.[206,207] Techniques such as pulsed excitation,[208,209] laser gating,[210–212] wavelength modulation[213,214] and shifted excitation[215] have been employed to mitigate situations in which highly fluorescent interferents are present, but these techniques require expensive and elaborate equipment. In addition, statistical techniques such as principal component

[7] This chapter is adapted from: Wei W. Yu and Ian M. White, *Chromatographic Separation and Detection of Target Analytes from Complex Samples Using Inkjet Printed SERS Substrates*, Analyst, 138, 3679–3686 (2013). Reproduced by permission of The Royal Society of Chemistry.

analysis (PCA), independent component analysis (ICA), hierarchical cluster analysis (HCA), and multivariate analysis have been used to resolve the spectrum into multiple components in order to detect the presence of multiple analytes.[23,216–219] These methods have proven effective, but to achieve good identification, some knowledge is required of the type of analytes in the sample and a large library of possible combinations of analyte Raman signatures is necessary. This may well be impossible when real-world samples are considered.

One potential solution is to separate the target analyte from the complex sample before analysis. Detection of analytes by SERS following extraction or chromatographic separation have been demonstrated,[220–225] but here the separation and detection steps are treated disjointly, in that separation is first performed, then SERS-active nanostructures are added to the analyte to facilitate detection. Others have achieved combined separation and SERS detection with good results using silica TLC plates or membranes with silver nanostructures deposited onto the support using the Brashear process and vapor deposition.[226,227] However, the use of silica TLC plates adds substantial cost to the substrate, while the slow deposition processes employed limit large scale production of the substrates.

Paper is an inexpensive and widely available material that has a long history of use as an extraction and separation medium. In this work, we extend the capabilities of inkjet printed SERS substrates by demonstrating that it is possible to use these SERS substrates to chromatographically separate target analytes from complex samples, allowing for the definite and unambiguous identification of individual analytes from the sample. This eliminates the difficulties that arise when

background components in the sample interfere with detection or when multiple analytes cannot be simultaneously distinguished. It also eliminates the need for multivariate statistical analysis. This is achieved by combining SERS with a well-established chromatography technique - paper chromatography, which is fast, inexpensive and does not require any bulky or complex equipment. Printed SERS substrates on paper and membranes with their inherent abilities for analyte separation and concentration combine the simplicity of capillary-action fluidic sensors with the sensitivity of SERS, turning ordinary pieces of nanoparticles-laden paper or membrane into a powerful analytical platform.

6.2 Methods

6.2.1 Materials

Fisher chromatography paper (0.19 mm thickness) and Millipore hydrophilic polyvinylidene fluoride (PVDF) membranes (0.22 μm) were purchased from Thermo-Fisher Scientific and used as the supports for the substrates. Silver nitrate, sodium citrate, acetone, ammonium acetate, acetic acid, malachite green oxalate, methylene blue, melamine, IR780 dye, hydrochloric acid and dextran (MW: 500k) were obtained from Sigma-Aldrich. Rhodamine 590 Chloride (R6G) was purchased from Exciton. Heroin was obtained from Cerilliant. All chemicals were used as received. Safety precautions were taken in the handling of all chemicals according to their respective MSDS. Malachite green, methylene blue and R6G samples were prepared in DI water at various concentrations and mixed at a ratio of 1:1:1. Commercial powdered infant

formula (Enfamil) was prepared at the recommended ratio of 1:7 (powder: liquid) with 1% HCl; appropriate amounts of melamine were then added to this stock solution to prepare samples of different concentrations. IR 780 and heroin were mixed at various ratios and dissolved in acetonitrile. Refillable ink cartridges were purchased from Alpha D Development and used without modification.

6.2.2 Silver nanoparticle synthesis

Silver nanoparticles were synthesized by reduction of silver nitrate using trisodium citrate as a reducing agent according to the method of Lee and Meisel.[80] Briefly, 90 mg silver nitrate was added to 500 mL of ultrapure water (18.2 MΩ), which was then brought to a boil in a flask under vigorous stirring. 100 mg of sodium citrate was added and the solution was left to boil for an additional 10 minutes. After the solution turned greenish brown, which indicated the formation of silver colloid, it was then removed from heat.

6.2.3 Ink formulation and printing

To form the silver ink, nanoparticle colloids were centrifuged at 6,000*g* to concentrate the nanoparticles by 100X in volume. The concentrated colloid was then mixed at a ratio of 1:1 with a 10 mg/mL dextran solution in water. The ink was then injected into refillable printing cartridges. An inkjet printer (Epson Workforce 30) was used to print the nanoparticles onto the chromatography paper or PVDF membrane as in Chapter 3. An open source vector graphics editor, Inkscape, was used to define the shapes to print. To increase the nanoparticle concentration in the substrate, the printing was repeated five times for paper and 10 times for PVDF. After

drying in air, excess unbound nanoparticles were removed from the paper or membrane by performing a pre-rinse with the mobile phase (dilute HCl was used in the case of PVDF membranes).

6.2.4 Chromatographic separation

To perform chromatographic separation of a sample, a pipette is used to place a small drop of the sample onto the printed SERS substrate. After drying, the substrate is placed upright inside a sealed jar that has been pre-saturated with the mobile phase while making sure that there is no contact with the sides of the jar. The mobile phase solvents differ depending on the sample and target components being separated. The level of the mobile phase is adjusted so that the meniscus is 1 cm below that of the position of the applied droplet. As the solvent is wicked up the chromatographic strip, the components of the sample are separated on the strip. The run time varies from 1 – 10 minutes depending on the mobile phase used. After performing the separation, the solvent front is marked using a pencil and the chromatogram is air-dried. To achieve separation of closely related species, 2D chromatographic separation is employed (Figure 6.1). This is done by rotating the strip by 90 degrees (after drying) and then performing another separation step using a second mobile phase. In addition, separated components may be concentrated by lateral flow concentration (Figure 6.1). This is done by cutting out the region containing the analyte of interest and dipping it into a volatile solvent.[93]

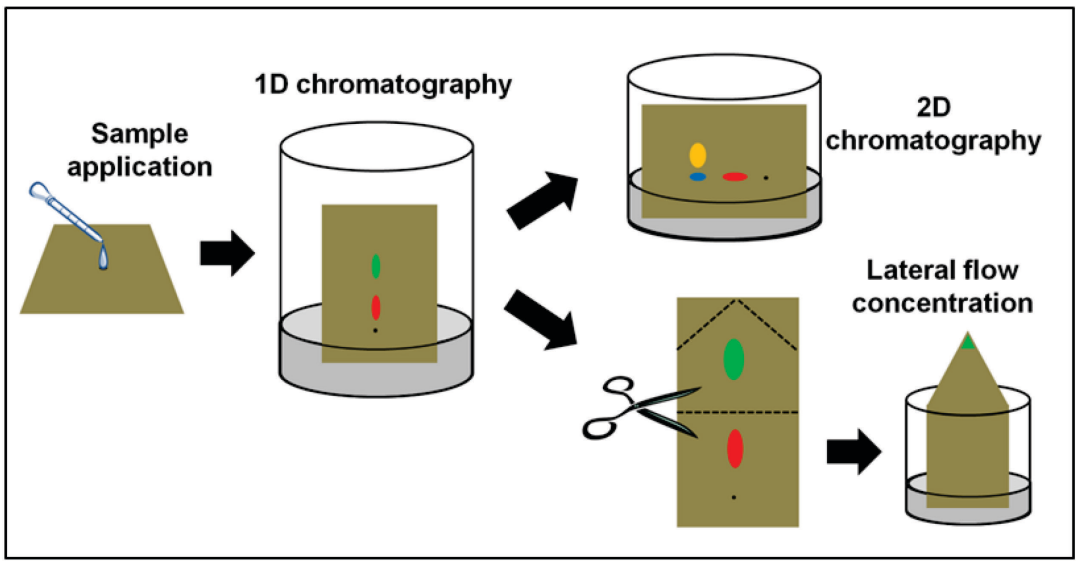

Figure 6.1 Schematics of the chromatographic separation and lateral concentration steps on paper SERS substrates.

6.2.5 SERS measurements

SERS measurements are performed using a 785 nm laser diode (Ocean Optics), a QE65000 (Ocean Optics) portable spectrometer, and a fiber optic probe (InPhotonics). A laser power of 17 mW was used to interrogate the samples on paper (8 mW for PVDF), and a 1-second CCD exposure was used for collecting the SERS spectra. The position of the target analytes on the chromatogram and their SERS spectra were recorded. SERS signals were averaged across 15 signal acquisitions from three separate trials and the variability in the signal was determined from the standard deviation. Background contributions from the substrates were accounted for by manually subtracting the SERS signals obtained from blank samples. To determine the signal intensity, the height of the most prominent peak from the Raman bands was calculated. This was repeated for three separate trials to determine their repeatability.

The limit of detection reported is the lowest concentration of analyte for which the Raman signature is easily visible. The retention factor (R_f) values of the analytes are calculated based on the positions of maximum SERS signals.

6.3 Results and Discussion

6.3.1 Detection of multiple analytes using paper SERS chromatography

Paper chromatography has been well established as a quick, easy, and inexpensive way to separate and analyze components in a mixture. Just like other chromatography techniques, the principle of the separation of analytes is based on the different affinity of analytes for the stationary phase and their solubility in the mobile phase. Identification of the different components is based on the retention factor (R_f), which is the ratio of the distance traveled by the analyte to the distance traveled by the mobile phase, or by extracting the analyte from the chromatogram for further analysis.[228,229] While useful for analyte separation, paper chromatography and in general thin-layer chromatography (TLC) is limited as an analytical technique because of the need for the analytes to be visible, or to be made visible by chemical means. The combination of SERS with paper chromatography removes this drawback by allowing analyte detection on the chromatogram without any chemical modifications, while also providing the added benefit of concentration and quantification of analytes without extraction.

The concept of paper SERS chromatography is demonstrated in Figure 6.2 using a mixture of 3 dyes consisting of 1 mM R6G, 1 mM methylene blue and 1 mM malachite green. From Figure 6.2(A) it is evident that without separation, the SERS

signature of the dye mixture is dominated by the SERS spectrum of methylene blue, as the SERS signatures of malachite green and R6G are not discernible. After a 4 minute chromatographic separation step using a mobile phase of (50% acetone: 50% 0.1 M ammonium acetate), the separation of methylene blue from malachite green and R6G is clearly visible in Figure 6.2(B). However, it is also evident that the malachite green was not successfully separated from R6G. By rotating the chromatogram 90 degrees and performing an additional 10 minute separation step using 0.1 M ammonium acetate as the mobile phase, it was possible to resolve the malachite green and R6G into separate bands, as shown in Figure 6.2(C). The distinct SERS spectra of the separated bands match closely with those of the reference spectra of the respective dyes. A slight cross contribution from each dye is visible due to residual retention of the dyes on the nanoparticles or the paper during the separation steps (Figure 6.3), but these do not interfere with the identification of the analytes as in the initial condition. Note that a high concentration (1 mM) of each dye was used in this case in order to illustrate visually the separation of the dye components.

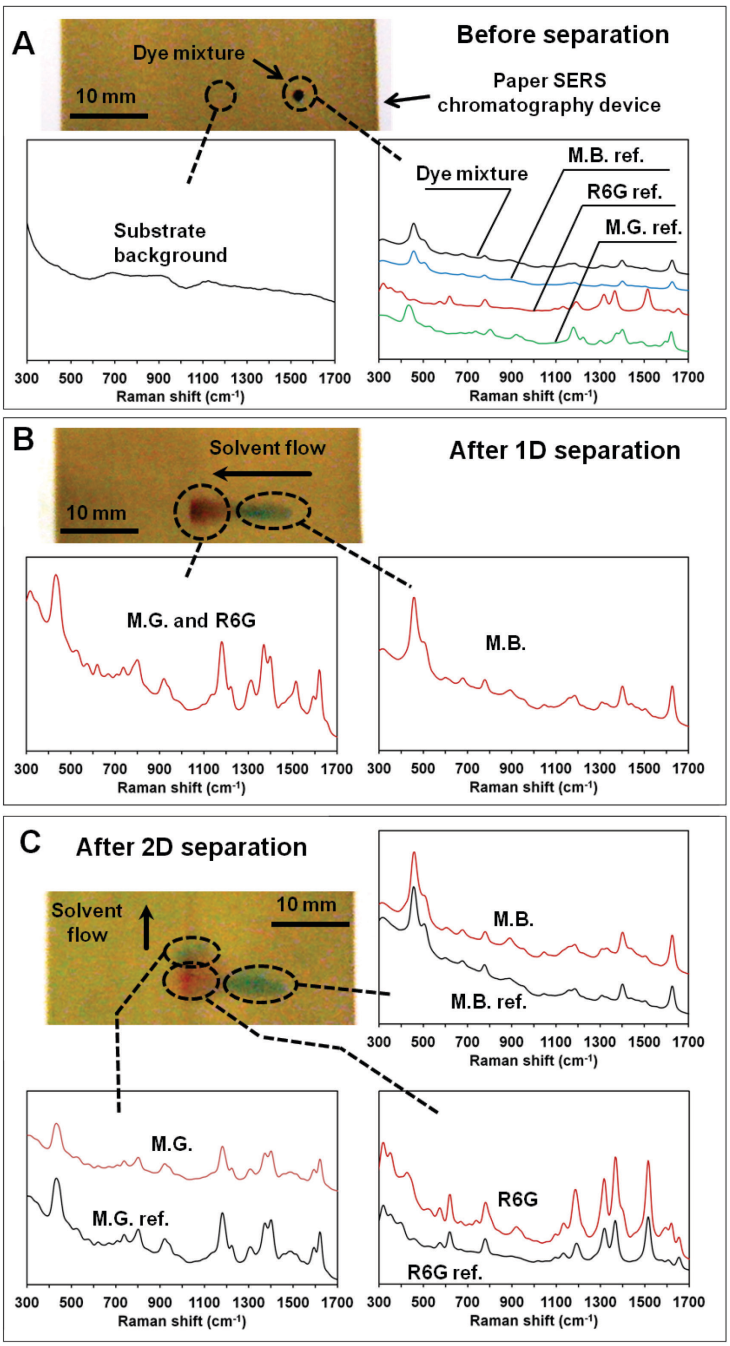

Figure 6.2 (A) SERS of a mixture of dyes on the paper substrate showing that the signal is dominated by methylene blue (MB). (B) After 1D separation, MB is clearly separated visually and confirmed by SERS, but the malachite green (MG) and R6G are not resolved. (C) After an additional 2D separation step, all 3 dyes are clearly separated from each other. A comparison of the SERS spectrum of each separated dye to the respective reference spectrum shows minimal cross contamination. SERS spectra have been shifted and rescaled for clarity.

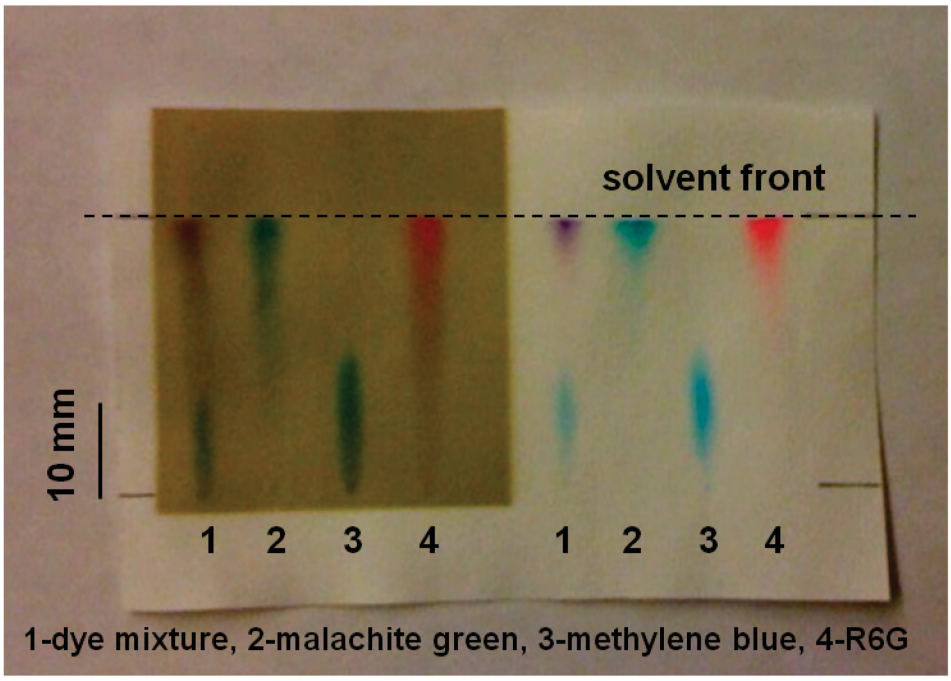

Figure 6.3 Comparison of chromatographic separation of individual dyes and dye mixture using paper and a printed paper SERS substrate. Note that there is no difference in the retention factor (R_f) for the dyes, but there is visibly more tailing of the dyes on the paper SERS chromatogram. This is due to the adhesion of the dyes to the silver nanoparticles.

6.3.2 Separation and detection from complex samples

One of the difficulties in applying SERS for the detection of a trace amount of a target in a complex sample (e.g., food, beverages, urine, blood, etc.) is the presence of large amount of proteins, ions, salts and other materials that can interact with the nanostructures and interfere with the SERS activity. Removal of such interferents often requires lengthy and labor intensive sample clean up steps, which ultimately reduces the efficiency of SERS detection. We demonstrate that paper SERS substrates

can also be used to chromatographically separate a target from a complex matrix without the need for additional sample clean-up steps.

As a practical example, we illustrate this by the separation and detection of melamine from infant formula. Infant formula is highly rich in proteins and other components, making it a complex sample to analyze. An examination of its ingredients reveals over 50 different compounds, such as proteins, lipids, vitamins, minerals and sugars. Adulteration of infant formula with melamine, a chemical that contains a high percentage of nitrogen, to make the infant formula appear to have higher protein content was a major problem in China in 2008 and led to the death of several infants.[230] Due to the complex matrix, many of the traditional and new techniques of detecting melamine in infant formula have relied on laborious and time consuming cleanup steps.[231–235] Others have utilized SERS towards this problem with good result,[78,96,236–239] but often the burden of labor and/or cost is shifted from sample cleanup to fabricating complex SERS substrates. Here we demonstrate the utilization of inkjet printed PVDF SERS membranes for a single step separation and detection of melamine in infant formula. PVDF membranes are used in this case instead of paper due to the high binding affinity of proteins to PVDF.

As shown in Figure 6.4(A), the SERS signature of 100 ppm melamine in a 0.2 μL droplet of infant formula on the SERS-active PVDF substrate is hardly visible due to the fouling of the nanoparticles by the abundant proteins, lipids and other molecules (region I). Interestingly, even before performing a separation, the potential benefit of separation is apparent; the hydrophilic membrane wicks the liquid sample outward (into region II), but larger solids and proteins do not move. In this outer

ring, a small SERS signal for melamine can be observed (Figure 6.4A). After performing the chromatography using a mobile phase of 0.1% acetic acid for 1 minute, melamine is separated in the chromatogram (region III); a clear SERS signature of melamine is apparent, and very little background can be seen. The melamine is located near the solvent front due to its good solubility in the dilute acid, while the larger protein molecules are localized where the sample was applied. Other non-target molecules from the sample are smeared over the surface on the membrane as indicated by the grey regions in the micrograph in Figure 6.4(A). A SERS chromatogram of the separation is shown in Figure 6.4(B), showing the location of melamine after performing the separation.

Using this technique, it was possible to detect as low as 5 ppm melamine in infant formula as shown in Figure 6.5, with a linear response over 2 orders of magnitude. However, without separation, the detection limit of melamine in infant formula is 100 ppm using the printed substrate; thus by performing a simple separation we are able to achieve greater than one order of magnitude improvement to the detection. The detection limit of a pure melamine sample on the PVDF SERS substrate on the other hand was 100 ppb (see Figure 6.6); hence detection is still better in a purified sample as compared to a chromatographically-separated sample. We suspect that this may be due to: (i) sequestration of some of the melamine (through binding to proteins or lipids), and/or (ii) fouling of the nanoparticles surfaces (which reduces their SERS activity) by some of the small molecules which remain unseparated from melamine.

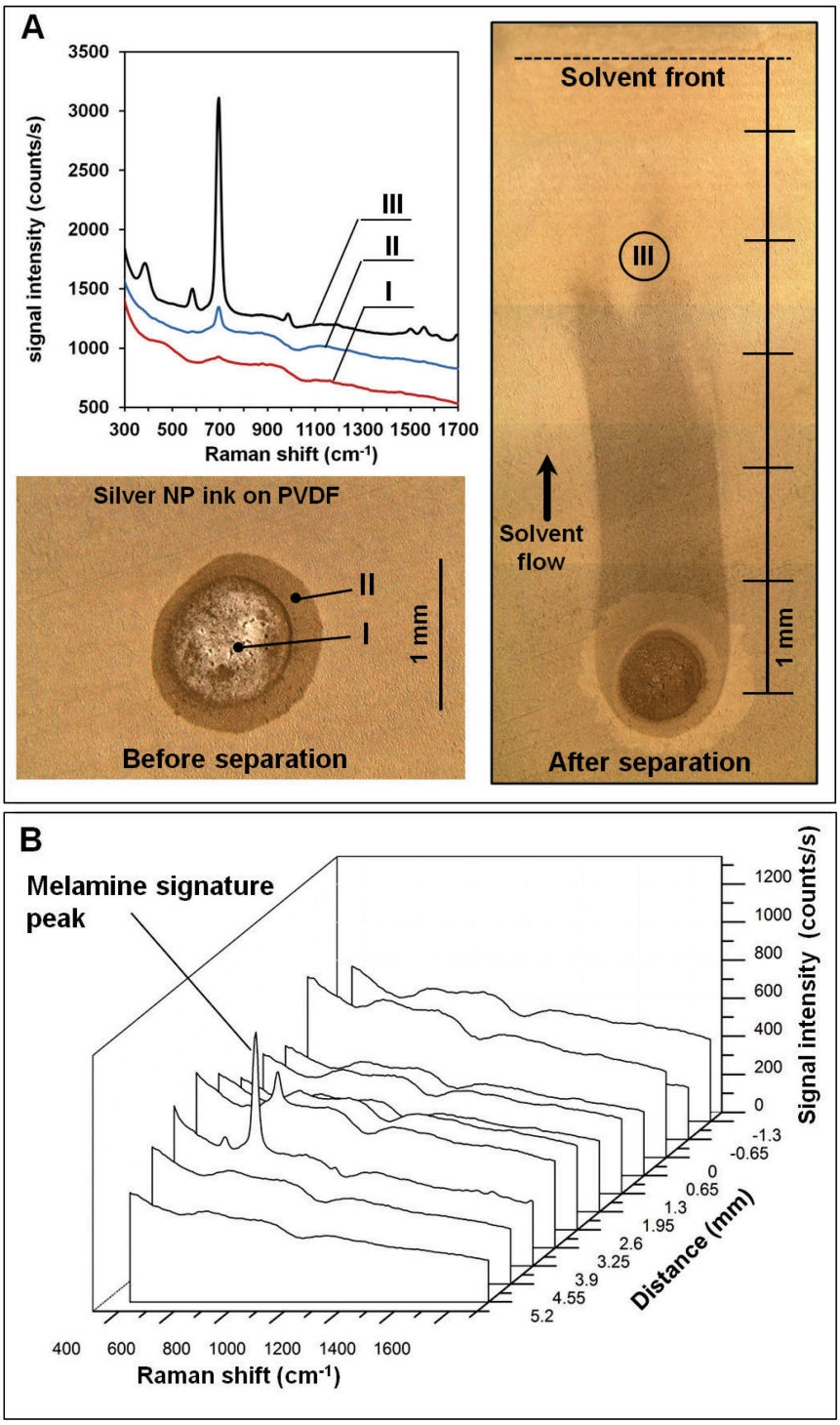

Figure 6.4 (A) Infant formula laced with melamine (100 ppm) on PVDF membrane before and after chromatographic separation. SERS of regions I, II and III shows the dramatic improvement of the 695 cm^{-1} peak of melamine after performing the separation. (B) SERS chromatogram showing the location of melamine on the PVDF membrane. (NP = nanoparticle)

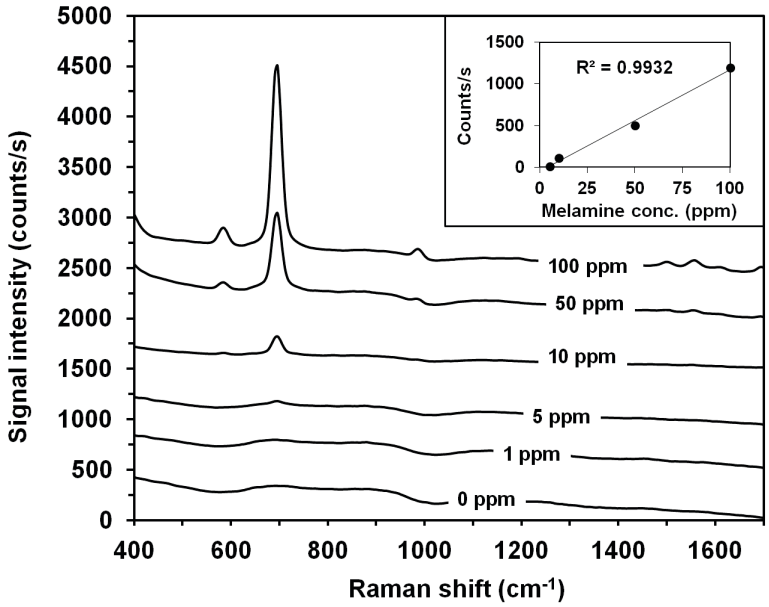

Figure 6.5 Variation of SERS signal intensity with melamine concentration. 695 cm^{-1} peak of melamine is visible even at 5 ppm in infant formula. Inset: Plot of signal intensity against concentration shows a good linear fit (R^2 = 0.9932).

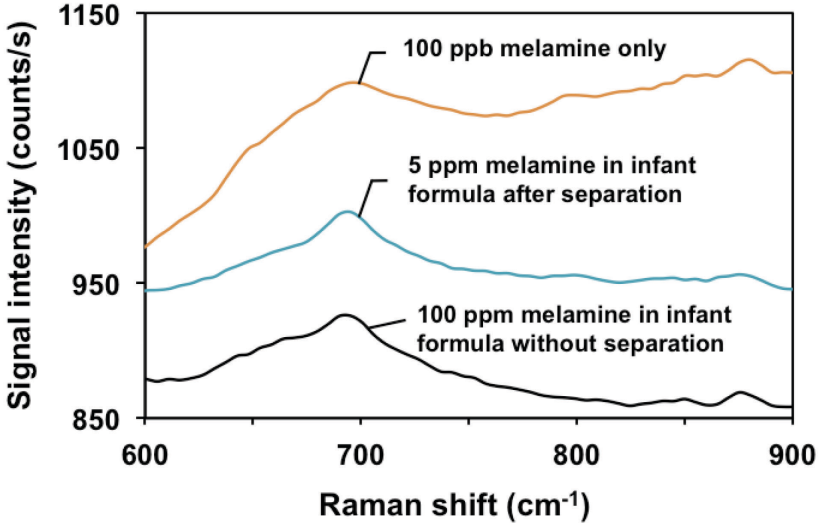

Figure 6.6 Detection limit of melamine using printed PVDF SERS membranes: 100 ppb melamine in 1% HCl only (top), 5 ppm melamine in infant formula after performing chromatographic separation (middle), and 100 ppm melamine in infant formula without any separation.

6.3.3 Separation, concentration, and detection of analytes

Often real world samples are contaminated intentionally or inadvertently by the presence of highly fluorescent materials which hinder the detection of the real target by SERS. As a practical example, one of the hurdles in the detection and quantification of illicit narcotics in "street" drugs is the presence of contaminants and cutting agents such as flour, milk powder, sugars, baking powder, caffeine, and other materials. Depending on the type of contaminants and cutting agents used, it may be extremely difficult and even impossible to identify the presence of the narcotic by Raman spectroscopy or even by a conventional SERS measurement.[212,240,241]

To appreciate the utility of paper SERS substrates, we demonstrate the detection and quantification of trace quantities of heroin in a sample adulterated with the infrared dye IR780, which is highly fluorescent in the excitation wavelength of the laser (785 nm). As shown in Figure 6.7(A), the fluorescence from the sample containing 1 μg of heroin mixed with 1 μg of IR780 is so high that the spectrometer CCD is saturated, making it impossible to observe any SERS signal from the heroin or from the dye itself. After performing a chromatographic separation with the paper SERS substrate for 5 minutes using 0.1% acetic acid as mobile phase, separate regions containing the fluorescent dye and heroin are distinctly visible in the SERS chromatogram, as shown in Figure 6.7(B). A comparison of the heroin SERS spectrum from the paper to a reference spectrum of pure heroin shows no contamination from the IR780 dye. The SERS chromatogram presented in Figure 6.7(C) demonstrates that the heroin is clearly separated away from the fluorescent dye.

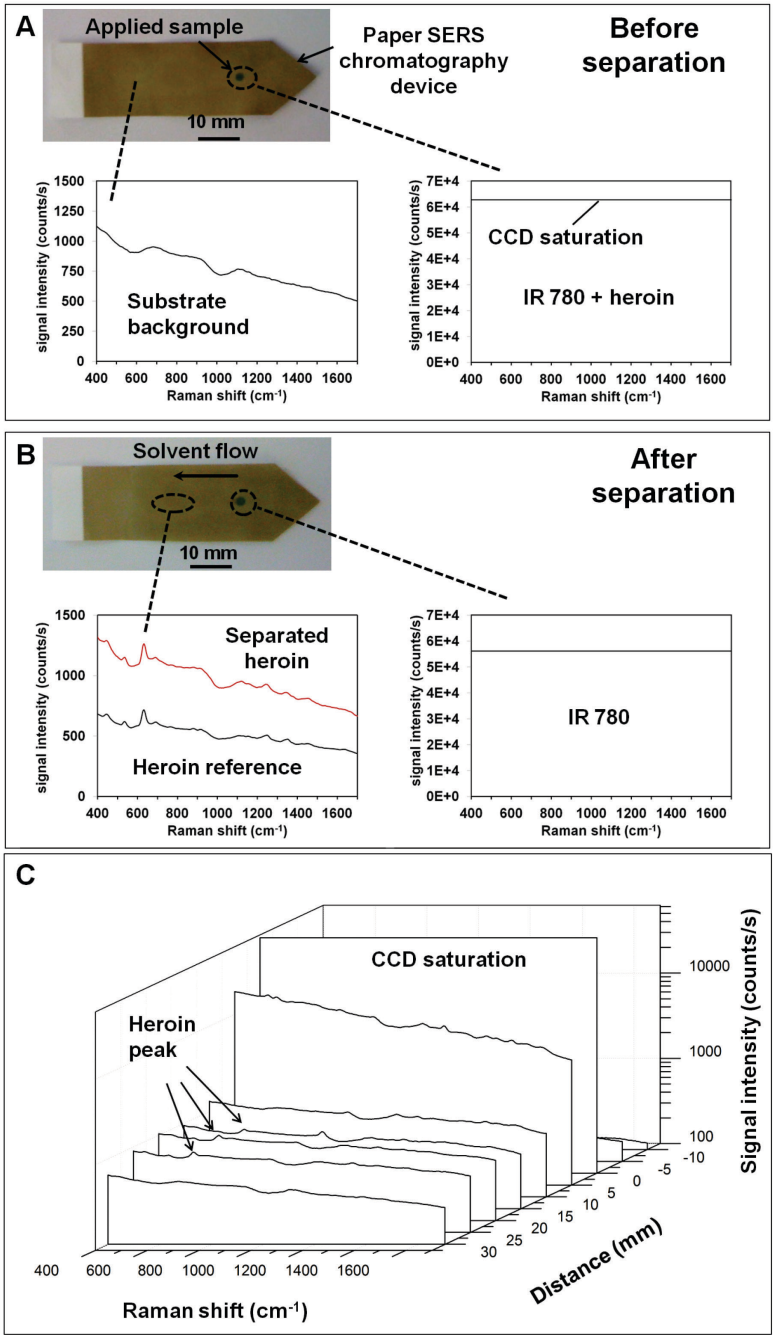

Figure 6.7 Separation of a mixture of IR780 and heroin using paper SERS chromatography. (A) Before separation, a sample of 1 µg IR780 and 1 µg heroin causes the spectrometer to be saturated even at 1s integration time due to the fluorescence from the dye. After separation, the heroin spectrum is clearly visible and separated from IR780. (B) A comparison of the heroin spectrum to a reference heroin spectrum shows that there is no contamination from the dye. (C) SERS Chromatogram showing the distribution of analytes on the paper SERS substrate.

While good separation and detection is achieved using paper SERS chromatography, the presence of a heroin 'tail' is evident from the SERS chromatogram (Figure 6.7C). This 'tailing' of the analyte, due to the smearing of the analyte over the paper, attenuates the detection limit and causes signal variability. Previously, we have demonstrated that a simple lateral flow technique can be used to concentrate analytes that are distributed over the paper surface into a small region. The same technique can be applied here by cutting out the region containing the target analyte of interest and performing a lateral flow concentration assay.

Prior to cutting, the paper strip was scanned with SERS to confirm the separation of heroin from the dye. The portion containing the heroin was cut from the strip and shaped into a dipstick as shown in Figure 6.8. The dipstick was then dipped into a solvent mix of 19:1 methanol: acetic acid (0.8M) for 15 minutes. Figure 6.8 shows the improvement to the SERS signal after the lateral flow concentration from three separate trials, showing that the separation and concentration is repeatable.

Furthermore, Figure 6.9 shows that when the amount of heroin is kept constant at 1 μg, the SERS intensity also remains fairly constant even as the amount of IR780 varies. This serves as further confirmation that the heroin is well separated from the IR 780. From Figure 6.9, an average of 5X improvement in the SERS signal can be obtained by performing a lateral flow concentration step. As we had noted in our previous works,[91,93] and as is indicated in Figure 6.10, the change in SERS intensity does not scale linearly with concentration, and thus a 5X improvement in signal intensity actually translates to an improvement of more than an order of magnitude in terms of the detection limit concentration.

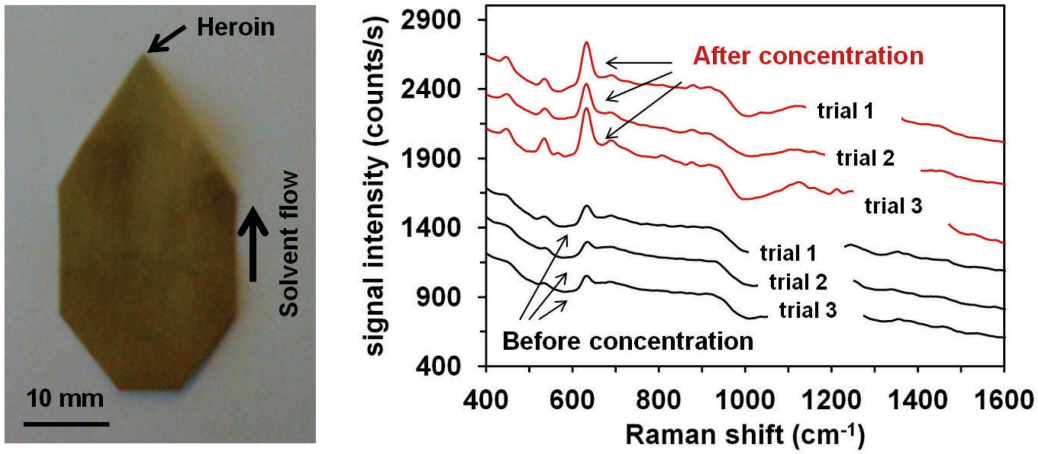

Figure 6.8 The section of the paper substrate containing heroin is cut from the chromatogram and undergoes a lateral flow concentration step. The SERS spectra on the right show the SERS signal intensity from three separate trials before and after the lateral flow concentration.

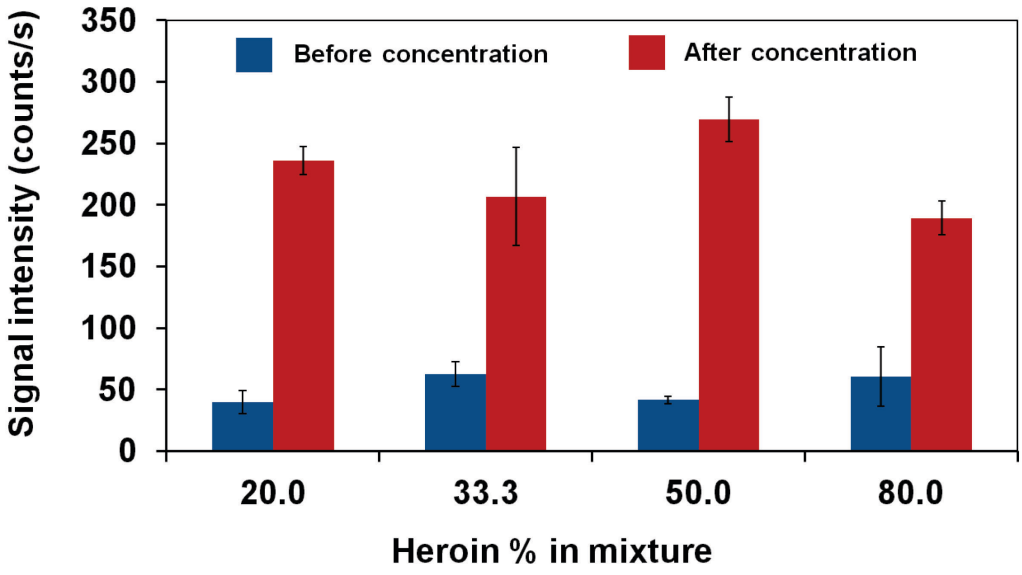

Figure 6.9 Comparison of SERS signal intensity at the 632 cm^{-1} peak before and after lateral flow concentration at different percentages of heroin in the mixture. The amount of heroin is kept constant at 1 µg while the amount of IR780 is varied. Error bars represent the standard deviation from three separate trials.

Moreover, the combination of paper SERS chromatography and lateral flow concentration is quantitative, as shown in Figure 6.10. The amount of heroin in the sample is varied while keeping the amount of IR780 constant at 0.5 µg. The resulting SERS intensity at 632 cm^{-1} can be fitted using the Langmuir isotherm (R^2 = 0.98). A detection limit of 25 ng of heroin in 0.5 µg of IR780 was attained.

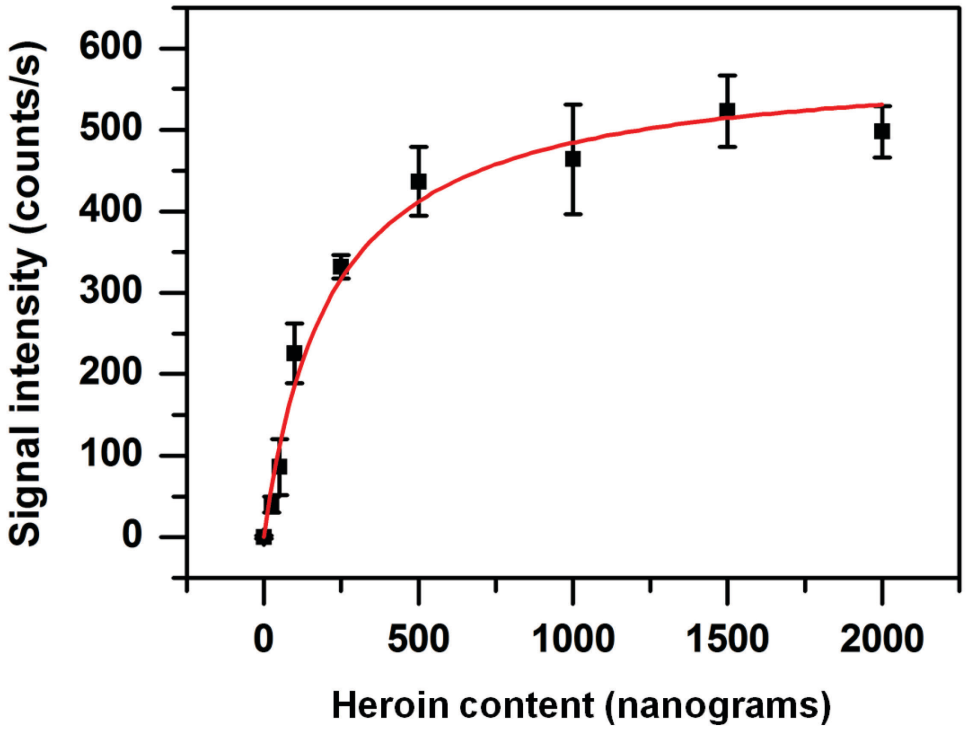

Figure 6.10 SERS signal intensity at 632 cm^{-1} with varying amounts of heroin while keeping the amount of IR780 constant at 0.5 µg. Error bars represent the standard deviation from three separate trials. Data is fitted to a Langmuir isotherm.

6.4 Conclusion

Printed SERS substrates combined with paper chromatography is an inexpensive, highly sensitive analytical technique for detection and quantification of multiple analytes from complex real-world samples. The technique is simple and easy to perform and does not require any sophisticated and expensive equipment. Compared to traditional analytical techniques such as high-performance liquid chromatography (HPLC) and mass spectrometry (MS), paper SERS chromatography detects the presence of target analytes without any sample processing while eliminating complicated and laborious clean up and analyte extraction steps. In addition, unlike other SERS techniques for multi-analyte detection, the analytes are well separated in the chromatogram, eliminating the need for multivariate analysis of the SERS spectra. We have demonstrated that paper SERS chromatography combined with lateral flow concentration is not only qualitative, but can also be quantitative. Detection of melamine in highly proteinaceous samples and detection of highly fluorescent samples are also demonstrated, with a detection limit of 5 ppm of melamine in infant formula and a detection limit of 25 ng of heroin mixed with a highly fluorescent material. The sensitivity and resolution of paper SERS chromatography can be further improved by optimizing the sample spot size to minimize tailing of the analytes, optimizing the mobile phase solvent to achieve better separation, and the astute selection of substrate membrane for the sample type. Unlike other conventional SERS substrates, printed SERS substrates, with their inherent ability to separate and concentrate analytes, are more than mere substrates; they are analytical systems in their own right.

Chapter 7 : Conclusion

7.1 Summary of findings

In this work, we have demonstrated the feasibility of creating highly SERS active substrates by inkjet printing nanostructures onto filter paper and membranes. The paper SERS substrates exhibit good enhancement properties with EF ranging from 10^5 – 10^7. Substrate fabrication is as simple as printing out a document. The resulting substrates are extremely versatile. Their use as arrays, swabs, dipsticks and filters was validated. In addition, the application of these substrates for separating and concentrating analytes was achieved. Real world applications of paper SERS substrates for the detection and quantification of pesticides, food contaminants, and narcotics were demonstrated.

In chapter 3, modification of the cellulose to be hydrophobic using a sizing agent - hexadecenyl succinic anhydride - allowed the paper substrate to behave like conventional substrates in that it prevented the spreading of analytes. However, like conventional solid state substrates, relying on analyte drying onto the surface as the concentration method introduced variability in addition to that arising from the random aggregation of the inkjet printed nanoparticles. Averaging of the SERS signal over several measurements within a printed region and over several substrates helped to reduce the effects of variability, and good predictability/trend over a large concentration range was observed. In effect, we are able to achieve comparable performance of solid state substrates while adding simplicity of fabrication and also the ability to fabricated custom or standard arrays.

In chapter 4, the use of paper and membranes as filters to extract analyte from liquid samples was established. In particular SERS substrate fabrication by filtration was demonstrated to be possible without the use of any complex equipment. The effect of colloidal loading, salt concentration and sample volume were studied. The resulting substrates showed good enhancement with EF of 10^6 and low signal variability. The ability of the technique to extract and quantify pesticides and food contaminant from liquid samples was demonstrated. In addition, it was shown that the choice of membranes used can lead to improvements in the analyte extraction. These results show that paper SERS substrates, in addition to being simple to fabricate, are also capable of extracting analyte from a sample, a feature which is absent from conventional SERS substrates.

In chapter 5, the practicality of inkjet printed substrates utilizing the hydrophilic and absorptive properties of paper was shown in the form of swabs to collect analyte from surfaces, and as dipsticks for analyte collection from liquid samples. The collected analytes can be concentrated using a lateral flow concentration assay, which results in up to 2 orders of magnitude improvement to the detection limit. The simplicity, effectiveness and convenience of these printed substrates have great implications on the accessibility of SERS as a point of sample analysis technique.

In chapter 6, taking advantage of the properties of the paper and membrane, chromatographical separation of analytes from complex mixtures using the printed SERS substrates was demonstrated. Appropriate selection of the substrate material and mobile phase helped to reduce the effect of interferents and fluorescent

background. In addition, it was shown that the separated components can be re-concentrated by lateral flow to improve the detection limit. The use of SERS as the detection modality greatly improved the detection capabilities of conventional paper chromatography, while the use of flexible porous materials enhanced the effectiveness of SERS substrates for practical applications. The separation and detection of melamine from a highly complex sample was attained, as well as the separation, detection and quantification of heroin from a highly fluorescent mixture. The findings from Chapter 5 and 6 takes full advantage of fluidic handling capabilities of inkjet printed SERS substrates for sample collection, processing and analysis. Paper SERS now resemble more of an analytical platform rather than just a simple SERS substrate.

7.2 Contributions to the field

A major focus of SERS research is in the development of novel and highly SERS active substrates. While attaining the highest enhancement factors possible is an important goal, we feel that a much more pressing need is to develop SERS substrates which are simple for the user to apply to real-world situation. The evidence to support this belief is that there already exist SERS substrates that have enhancement factors of 10^8 and more, sufficiently sensitive for down to single molecule detection capability, but SERS as a technique has remained largely confined to the laboratory, despite its high sensitivity and ability to out-gun more conventional analytical techniques such as HPLC and mass spectrometry.

Others share this belief and approach this problem through the integration of SERS with microfluidic device.[35,242–246] While there have been reports of impressive

results, the use of PDMS and plastic microfluidic devices only add to the complexity and cost of SERS analysis. Our innovative approach to solving this problem is the first ever demonstration of printed SERS substrates on paper and other porous membranes using a commercial inkjet printer. Our inkjet printed SERS concept is an advancement over conventional solid state SERS substrates in simplicity, cost and ease of use, and possesses unique sample processing capabilities due to the inherent properties of paper. This work has the potential to liberate SERS from the confines of the laboratory and enables high sensitivity chemical and biological analysis at the point of sample for a very low cost.

Since the initial publication of our work, several other groups have realized the value of paper SERS substrates and the advantages of substrate fabrication by printing, and have made their own contributions to the field.[88–90,135,247–253] In addition, several commercial enterprises have expressed interest in paper SERS substrates for commercial real-world applications. Our group continues to innovate on inkjet printed paper SERS sensor with the goal towards point of care medical diagnostics.

7.3 Applications and potential impact of paper SERS analytical devices

The vision for paper SERS substrates is that by virtue of their simplicity and low cost, will become widely adopted for a host of applications, ranging from trace chemical detection to environmental and food monitoring, and even biomedical diagnostics. The potential impact of paper SERS sensors is immense. This technology has the ability to revolutionize the field of chemical analysis and biosensing. Inkjet printed SERS devices have been proven to be capable of sample separation, analyte concentration and multiplexed detection of multiple analytes in a variety of easy to

use formats. Fabrication of paper SERS sensors can be accomplished very simply without the need for complicated micro/nanofabrication and at a fraction of the cost of current sensing technologies. Coupled with miniature portable SERS detection systems and computer software for automated detection and quantification of analytes, untrained users will be able to perform complex assays with ease.

7.4 Outlook and future work

In this work, we have demonstrated the fabrication and application of inkjet printed paper SERS, but further modification and improvements to the substrates are always possible. Below we describe some of the potential future avenues to improve paper SERS in terms of stability, reproducibility and functionality.

7.4.1 Improving stability / shelf-life

One of the advantages of inkjet printed SERS substrates is the ability to be fabricated on demand; this removes the oxidation-induced shelf-life problem that plagues conventional SERS substrates. Practically, having preprinted substrates on hand can be convenient. Depending on the type of metal nanoparticle used, initial tests indicate that the SERS active life-time of paper SERS substrate after printing can vary from days (for silver) to weeks (for gold), depending on storage conditions such as humidity, temperature and oxygen concentration. A more systematic study of effects of each of these parameters on the lifetime of paper SERS substrates are proposed for future works. The use of foil packs with humectants and oxygen scavengers can be used to control the storage conditions.

In addition to controlling external conditions, an alternate approach is to modify the surfaces of the nanostructures to form a barrier to prevent oxidation. One

potential method is to deposit a thin nanometer layer of silica onto the nanoparticle surface during synthesis. Nanoparticle-silica (core-shell) types of structures have been studied previously,[254] but we are not aware of any systematic study of the effectiveness of the shells on preventing oxidation of the underlying metal core. It is expected however, that the presence of the thin barrier will reduce the SERS intensity, so there is a tradeoff for higher stability.

It may also be possible to protect the nanoparticles from oxidation through the choice of chemicals used in the ink formulation. Qu et al.[90] observed that the use of sodium carboxymethylcellulose (CMC) as a viscous agent in screen printing ink help to prolong the shelf-life of silver nanoparticles. They hypothesized that this is as a result of CMC preventing the exposure of the Ag nanoparticles to the atmosphere. However, a protective barrier from oxidation will also likely be an impediment to the adsorption of analyte onto the nanoparticle surface; hence this strategy will need to be evaluated thoroughly.

7.4.2 Monitoring substrate quality using internal markers

In general, with any type of SERS substrate fabrication by conventional methods, the quality of the substrate in terms of SERS-activity is largely unknown until the substrate is tested with the analyte. This means that prior testing and calibration is necessary before sample analysis. For real-world applications, especially in point of sample application, this can be a major inconvenience. One approach to circumvent this is to employ internal markers in the substrate – this can be achieved by conjugating a low concentration of a SERS active molecule to the paper matrix or to the surface of the nanoparticles. By looking at the signal intensity

of this marker, the quality of the paper SERS substrates can be monitored. For practical reasons, such an internal marker must be tightly bound to the substrate, as its mobility can interfere with fluidic applications of the paper SERS substrates. In addition, the marker should be chosen such that its SERS signature does not overlap those of the target analytes.

7.4.3 Controlling aggregation and substrate variability

One of the most frequently asked questions with the introduction of a new SERS substrate is its reproducibility. In part, this arises from the nature of hotspot formation, and the interaction of analyte and hotspots on the substrate. This is especially true of substrate relying on random hotspot generation. While the averaging techniques discussed in Chapter 2 can address this variability to a certain extent, a way to direct or control the hotspot formation on the paper surface would be helpful. To this end, we introduce two approaches that may be promising.

Approach 1: Employ nanostars instead of relying on aggregation of nanospheres for hotspots. Individual nanostars have been observed to be highly SERS active due to the presence of many sharp branches.[83,255–259] To avoid random aggregation of the nanostars after printing, it will be necessary to keep them dispersed through the use of capping agents in the ink formulation.

Approach 2: Control the extent of aggregation of nanospheres through the use of linker molecules and capping agents. The formation of nanoparticle dimers and larger clusters have been demonstrated by several research groups using different linker molecules.[260–263]

7.4.4 Surface functionalization

SERS detection relies on the adsorption of analyte onto the nanoparticles. For analyte that has no or low affinity to the nanoparticle surface (either by charge or chemical bonding), detection is not optimized. For large biological molecules such as proteins and nucleic acids, this is a significant problem as these molecules will have difficulty in adhering to the nanoparticles. Furthermore, because of the large number of different chemical bonds within biological molecules, and the random orientation of molecules, identification of biological analyte by SERS can be exceptionally difficult; one way of circumventing this obstacle is to employ the use of labeled biorecognition elements such as antibodies, enzymes and aptamers. This allows for the generation of a specific signal upon binding which enables the detection of target biomolecules.

One technique which we believe to hold exceptional promise is the use of labeled nucleic acid based aptamers to specifically capture the biological analytes and provide a uniquely identifiable SERS signature.[264–272] The use of nucleic acid aptamers is a paradigm shift from traditional immunoassays which have relied heavily on fluorophore labeled and enzyme labeled antibodies as biorecognition elements. The synthesis of these antibodies requires either live animal hosts or hybridoma cell lines, and very small quantities are produced at a time, making this process very time consuming and expensive.[273] Nucleic acid aptamers on the other hand, are short artificial DNA and RNA sequences selectively chosen by their extremely strong binding affinity to their targets through a process called Systematic Evolution of Ligands by Exponential Enrichment (SELEX). The binding affinity of aptamers for their targets is comparable and can even be better than antibodies, and

are not just limited to protein targets.[270,274–276] Once identified, these nucleic acid sequences can be synthesized very simply in a short time period and on large scale in a test tube using basic nucleic acid components. Aptamers are also much more resistant to degradation compared to antibodies and enzymes and can be made to bind to targets under diverse conditions. Additionally, chemical modifications such as 2'-fluorine substituted pyrimidines can be made to protect them from nuclease cleavage.[275,276] The deliberate use of these modified nucleic acid based aptamers instead of widely available, but difficult to synthesize antibodies and enzymes in this role have potential to enhance the stability and shelf life of the paper SERS biosensors. By using multiple aptamers with affinity for different antigen targets, it is possible to detect multiple analytes within a single assay.

The innovative combination of SERS and labeled aptamers have the potential to make paper SERS sensing much more sensitive and specific compared to existing approaches of sensing on paper. With this development it is possible that in the future we will see SERS becoming more widespread, not only for the identification of trace chemical species such as pesticides, explosives, drugs, and metabolites, but also for larger biological molecules such as proteins, RNA, and DNA, and even whole viruses and bacteria. This would transform these inexpensive paper SERS substrates into biosensors for the detection of pathogens and diseases.

Bibliography

1. Ghallab, Y. H. & Badawy, W. *Lab-on-a-chip: techniques, circuits, and biomedical applications*. (Artech House: 2010).

2. Whitesides, G. M. The origins and the future of microfluidics. *Nature* **442**, 368–373 (2006).

3. Burns, M. A. *et al.* An integrated nanoliter DNA analysis device. *Science* **282**, 484–487 (1998).

4. Martinez, A. W., Phillips, S. T., Butte, M. J. & Whitesides, G. M. Patterned paper as a platform for inexpensive, low-volume, portable bioassays. *Angewandte Chemie (International ed. in English)* **46**, 1318–1320 (2007).

5. Martinez, A. W., Phillips, S. T., Whitesides, G. M. & Carrilho, E. Diagnostics for the developing world: microfluidic paper-based analytical devices. *Analytical Chemistry* **82**, 3–10 (2010).

6. Ellerbee, A. K. *et al.* Quantifying colorimetric assays in paper-based microfluidic devices by measuring the transmission of light through paper. *Analytical Chemistry* **81**, 8447–8452 (2009).

7. Osborn, J. L. *et al.* Microfluidics without pumps: reinventing the T-sensor and H-filter in paper networks. *Lab on a Chip* **10**, 2659–2665 (2010).

8. Fu, E., Lutz, B., Kauffman, P. & Yager, P. Controlled reagent transport in disposable 2D paper networks. *Lab on a Chip* **10**, 918–920 (2010).

9. Fu, E., Kauffman, P., Lutz, B. & Yager, P. Chemical signal amplification in two-dimensional paper networks. *Sensors and Actuators B: Chemical* **149**, 325–328 (2010).

10. Fu, E. *et al.* Two-dimensional paper network format that enables simple multistep assays for use in low-resource settings in the context of malaria antigen detection. *Analytical Chemistry* **84**, 4574–9 (2012).

11. Dungchai, W., Chailapakul, O. & Henry, C. S. Electrochemical detection for paper-based microfluidics. *Analytical Chemistry* **81**, 5821–5826 (2009).

12. Apilux, A. *et al.* Lab-on-paper with dual electrochemical/colorimetric detection for simultaneous determination of gold and iron. *Analytical Chemistry* **82**, 1727–1732 (2010).

13. Khan, M. S. *et al.* Biosurface engineering through ink jet printing. *Colloids and Surfaces B: Biointerfaces* **75**, 441–447 (2010).

14. Li, X., Tian, J. & Shen, W. Progress in patterned paper sizing for fabrication of paper-based microfluidic sensors. *Cellulose* **17**, 649–659 (2010).

15. Abe, K., Suzuki, K. & Citterio, D. Inkjet-printed microfluidic multianalyte chemical sensing paper. *Analytical Chemistry* **80**, 6928–6934 (2008).

16. Abe, K., Kotera, K., Suzuki, K. & Citterio, D. Inkjet-printed paperfluidic immuno-chemical sensing device. *Analytical and Bioanalytical Chemistry* **398**, 885–893 (2010).

17. Hossain, S. M. Z., Luckham, R. E., McFadden, M. J. & Brennan, J. D. Reagentless bidirectional lateral flow bioactive paper sensors for detection of pesticides in beverage and food samples. *Analytical Chemistry* **81**, 9055–9064 (2009).

18. Hossain, S. M. Z. *et al.* Development of a bioactive paper sensor for detection of neurotoxins using piezoelectric inkjet printing of sol-gel-derived bioinks. *Analytical Chemistry* **81**, 5474–5483 (2009).

19. Ali, M. M. *et al.* Detection of DNA using bioactive paper strips. *Chemical Communications* 6640–6642 (2009). DOI:10.1039/b911559e

20. Nie, S. & Emory, S. R. Probing single molecules and single nanoparticles by surface-enhanced Raman scattering . *Science* **275** , 1102–1106 (1997).

21. Kneipp, K. *et al.* Single molecule detection using surface-enhanced Raman scattering (SERS). *Physical Review Letters* **78**, 1667–1670 (1997).

22. Yu, C. & Irudayaraj, J. Multiplex biosensor using gold nanorods. *Analytical Chemistry* **79**, 572–579 (2007).

23. Faulds, K., Jarvis, R., Smith, W. E., Graham, D. & Goodacre, R. Multiplexed detection of six labelled oligonucleotides using surface enhanced resonance Raman scattering (SERRS). *Analyst* **133**, 1505–1512 (2008).

24. Long, D. A. *The Raman effect: a unified treatment of the theory of Raman scattering by molecules*. (John Wiley & Sons: 2002).

25. Aroca, R. *Surface-enhanced vibrational spectroscopy*. (Wiley: 2006).

26. Le Ru, E. & Etchegoin, P. *Principles of surface-enhanced Raman spectroscopy: and related plasmonic effects*. (Elsevier Science: 2008).

27. Marcelli, A., Cricenti, A., Kwiatek, W. M. & Petibois, C. Biological applications of synchrotron radiation infrared spectromicroscopy. *Biotechnology Advances* **30**, 1390–1404 (2012).

28. Fleischmann, M., Hendra, P. J. & McQuillan, A. J. Raman spectra of pyridine adsorbed at a silver electrode. *Chemical Physics Letters* **26**, 163–166 (1974).

29. Jeanmaire, D. L. & Duyne, R. P. Van Surface raman spectroelectrochemistry: Part I. Heterocyclic, aromatic, and aliphatic amines adsorbed on the anodized silver electrode. *Journal of Electroanalytical Chemistry and Interfacial Electrochemistry* **84**, 1–20 (1977).

30. Albrecht, M. G. & Creighton, J. A. Anomalously intense Raman spectra of pyridine at a silver electrode. *Journal of the American Chemical Society* **99**, 5215–5217 (1977).

31. Tian, Z. Q. Surface-enhanced Raman spectroscopy: advancements and applications. *Journal of Raman Spectroscopy* **36**, 466–470 (2005).

32. Haynes, C. L., Yonzon, C. R., Zhang, X. & Van Duyne, R. P. Surface-enhanced Raman sensors: early history and the development of sensors for quantitative biowarfare agent and glucose detection. *Journal of Raman Spectroscopy* **36**, 471–484 (2005).

33. Moskovits, M. Surface-enhanced Raman spectroscopy: a brief retrospective. *Journal of Raman Spectroscopy* **36**, 485–496 (2005).

34. Jayawardhana, S., Mazzolini, A. P. & Stoddart, P. R. Trace level detection of water contamination by SERS. *AIP Conference Proceedings 1267*, 1063-1064 (2010). DOI:10.1063/1.3482296

35. Lee, D. *et al.* Quantitative analysis of methyl parathion pesticides in a polydimethylsiloxane microfluidic channel using confocal surface-enhanced Raman spectroscopy. *Applied Spectroscopy* **60**, 373–377 (2006).

36. Wang, X. T., Shi, W. S., She, G. W., Mu, L. X. & Lee, S. T. High-performance surface-enhanced Raman scattering sensors based on Ag nanoparticles-coated Si nanowire arrays for quantitative detection of pesticides. *Applied Physics Letters* **96**, 053104 (2010).

37. Dasary, S. S. R., Singh, A. K., Senapati, D., Yu, H. & Ray, P. C. Gold nanoparticle based label-free SERS probe for ultrasensitive and selective detection of trinitrotoluene. *Journal of the American Chemical Society* **131**, 13806–13812 (2009).

38. Wang, Y., Li, Y.-S., Zhang, Z. & An, D. Surface-enhanced Raman scattering of some water insoluble drugs in silver hydrosols. *Spectrochimica Acta Part A: Molecular and biomolecular spectroscopy* **59**, 589–594 (2003).

39. Chen, J. *et al.* A new aptameric biosensor for cocaine based on surface-enhanced Raman scattering spectroscopy. *Chemistry* **14**, 8374–8382 (2008).

40. Dou, X., Yamaguchi, Y., Yamamoto, H., Doi, S. & Ozaki, Y. NIR SERS detection of immune reaction on gold colloid particles without bound/free antigen separation. *Journal of Raman Spectroscopy* **29**, 739–742 (1998).

41. Wang, Y. *et al.* SERS opens a new way in aptasensor for protein recognition with high sensitivity and selectivity. *Chemical Communications* 5220–5222 (2007). DOI:10.1039/b709492b

42. Fabris, L., Dante, M., Nguyen, T.-Q., Tok, J. B.-H. & Bazan, G. C. SERS Aptatags: new responsive metallic nanostructures for heterogeneous protein detection by surface enhanced Raman spectroscopy. *Advanced Functional Materials* **18**, 2518–2525 (2008).

43. Cho, H., Lee, B., Liu, G. L., Agarwal, A. & Lee, L. P. Label-free and highly sensitive biomolecular detection using SERS and electrokinetic preconcentration. *Lab on a Chip* **9**, 3360–3363 (2009).

44. Sun, L. *et al.* Ethanol-induced formation of silver nanoparticle aggregates for highly active SERS substrates and application in DNA detection. *Journal of Physical Chemistry C* **112**, 1415–1422 (2008).

45. Bhabra, G. *et al.* Nanoparticles can cause DNA damage across a cellular barrier. *Nature Nanotechnology* **4**, 876–883 (2009).

46. Yuan, W., Ho, H. P., Lee, R. K. Y. & Kong, S. K. Surface-enhanced Raman scattering biosensor for DNA detection on nanoparticle island substrates. *Applied Optics* **48**, 4329–4337 (2009).

47. Barhoumi, A., Zhang, D., Tam, F. & Halas, N. J. Surface-enhanced Raman spectroscopy of DNA. *Journal of the American Chemical Society* **130**, 5523–5529 (2008).

48. Yakes, B. J., Lipert, R. J., Bannantine, J. P. & Porter, M. D. Detection of Mycobacterium avium subsp. paratuberculosis by a sonicate immunoassay based on surface-enhanced Raman scattering. *Clinical and Vaccine Immunology* **15**, 227–234 (2008).

49. Huh, Y. S., Chung, A. J. & Erickson, D. Surface enhanced Raman spectroscopy and its application to molecular and cellular analysis. *Microfluidics and Nanofluidics* **6**, 285–297 (2009).

50. Grubisha, D. S., Lipert, R. J., Park, H.-Y., Driskell, J. & Porter, M. D. Femtomolar detection of prostate-specific antigen: an immunoassay based on surface-enhanced Raman scattering and immunogold labels. *Analytical Chemistry* **75**, 5936–5943 (2003).

51. Lu, W. *et al.* Gold nano-popcorn-based targeted diagnosis, nanotherapy treatment, and in situ monitoring of photothermal therapy response of prostate cancer cells using surface-enhanced Raman spectroscopy. *Journal of the American Chemical Society* **132**, 18103–18114 (2010).

52. Hutter, E. & Fendler, J. H. Exploitation of localized surface plasmon resonance. *Advanced Materials* **16**, 1685–1706 (2004).

53. Stiles, P. L., Dieringer, J. a., Shah, N. C. & Van Duyne, R. P. Surface-enhanced Raman spectroscopy. *Annual Review of Analytical Chemistry* **1**, 601–626 (2008).

54. Campion, A. & Kambhampati, P. Surface-enhanced Raman scattering. *Chemical Society Reviews* **27**, 241 (1998).

55. Kovacs, G. J., Loutfy, R. O., Vincett, P. S., Jennings, C. & Aroca, R. Distance dependence of SERS enhancement factor from Langmuir-Blodgett monolayers on metal island films: evidence for the electromagnetic mechanism. *Langmuir* **2**, 689–694 (1986).

56. Weaver, M. J., Zou, S. & Chan, H. Y. H. Peer reviewed: the new interfacial ubiquity of surface-enhanced Raman spectroscopy. *Analytical Chemistry* **72**, 38 A–47 A (2000).

57. Kennedy, B. J., Spaeth, S., Dickey, M. & Carron, K. T. Determination of the distance dependence and experimental effects for modified SERS substrates based on self-assembled monolayers formed using alkanethiols. *The Journal of Physical Chemistry B* **103**, 3640–3646 (1999).

58. Ekinci, Y., Solak, H. H. & Loffler, J. F. Plasmon resonances of aluminum nanoparticles and nanorods. *Journal of Applied Physics* **104**, 083107 (2008).

59. Kim, K., Kim, K. L., Lee, H. B. & Shin, K. S. Surface-enhanced Raman scattering on aggregates of platinum nanoparticles with definite size. *The Journal of Physical Chemistry C* **114**, 18679–18685 (2010).

60. Muniz-Miranda, M., Gellini, C. & Giorgetti, E. Surface-enhanced Raman scattering from copper nanoparticles obtained by laser ablation. *The Journal of Physical Chemistry C* **115**, 5021–5027 (2011).

61. Wang, Y. & Asefa, T. Poly(allylamine)-stabilized colloidal copper nanoparticles: synthesis, morphology, and their surface-enhanced Raman scattering properties. *Langmuir* **26**, 7469–7474 (2010).

62. Sigle, D. O., Perkins, E., Baumberg, J. J. & Mahajan, S. Reproducible deep-UV SERRS on aluminum nanovoids. *The Journal of Physical Chemistry Letters* **4**, 1449–1452 (2013).

63. Cobley, C. M. & Xia, Y. Engineering the properties of metal nanostructures via galvanic replacement reactions. *Materials Science & Engineering. R: Reports* **70**, 44–62 (2010).

64. Khlebtsov, N. G. T-matrix method in plasmonics: an overview. *Journal of Quantitative Spectroscopy and Radiative Transfer* **123**, 184–217 (2013).

65. Li, W., Camargo, P. H. C., Lu, X. & Xia, Y. Dimers of silver nanospheres: facile synthesis and their use as hot spots for surface-enhanced Raman scattering. *Nano Letters* **9**, 485–490 (2009).

66. Meyer, M. W. & Smith, E. A. Optimization of silver nanoparticles for surface enhanced Raman spectroscopy of structurally diverse analytes using visible and near-infrared excitation. *Analyst* **136**, 3542–3549 (2011).

67. Bell, S. E. J. & McCourt, M. R. SERS enhancement by aggregated Au colloids: effect of particle size. *Physical Chemistry Chemical Physics* **11**, 7455–7462 (2009).

68. Liao, P. F. Lightning rod effect in surface enhanced Raman scattering. *The Journal of Chemical Physics* **76**, 751 (1982).

69. McMahon, J. M. *et al.* Gold nanoparticle dimer plasmonics: finite element method calculations of the electromagnetic enhancement to surface-enhanced Raman spectroscopy. *Analytical and Bioanalytical Chemistry* **394**, 1819–1825 (2009).

70. Tuschel, D. D., Pemberton, J. E. & Cook, J. E. SERS and SEM of roughened silver electrode surfaces formed by controlled oxidation-reduction in aqueous chloride media. *Langmuir* **2**, 380–388 (1986).

71. Abdelsalam, M. E. *et al.* Electrochemical SERS at a structured gold surface. *Electrochemistry Communications* **7**, 740–744 (2005).

72. Liu, Y.-C., Wang, C.-C. & Tsai, C.-E. Effects of electrolytes used in roughening gold substrates by oxidation–reduction cycles on surface-enhanced Raman scattering. *Electrochemistry Communications* **7**, 1345–1350 (2005).

73. Jiao, L. *et al.* In situ electrochemical SERS studies on electrodeposition of aniline on 4-ATP/Au surface. *Journal of Solid State Electrochemistry* **10**, 886–893 (2005).

74. Compton, R. G. *New techniques for the study of electrodes and their reactions*. **29**, (Elsevier Science: 1989).

75. Sarkar, A. & Manthiram, A. Synthesis of Pt@Cu core−shell nanoparticles by galvanic displacement of Cu by Pt^{4+} ions and their application as electrocatalysts for oxygen reduction reaction in fuel cells. *The Journal of Physical Chemistry C* **114**, 4725–4732 (2010).

76. Sun, Y., Wiley, B., Li, Z.-Y. & Xia, Y. Synthesis and optical properties of nanorattles and multiple-walled nanoshells/nanotubes made of metal alloys. *Journal of the American Chemical Society* **126**, 9399–9406 (2004).

77. Hangarter, C. M., Lee, Y.-I., Hernandez, S. C., Choa, Y.-H. & Myung, N. V Nanopeapods by galvanic displacement reaction. *Angewandte Chemie (International ed. in English)* **49**, 7081–7085 (2010).

78. Betz, J. F., Cheng, Y. & Rubloff, G. W. Direct SERS detection of contaminants in a complex mixture: rapid, single step screening for melamine in liquid infant formula. *Analyst* **137**, 826–828 (2012).

79. Gutés, A., Carraro, C. & Maboudian, R. Silver dendrites from galvanic displacement on commercial aluminum foil as an effective SERS substrate. *Journal of the American Chemical Society* **132**, 1476–1477 (2010).

80. Lee, P. C. & Meisel, D. Adsorption and surface-enhanced Raman of dyes on silver and gold sols. *The Journal of Physical Chemistry* **86**, 3391–3395 (1982).

81. Jana, N. R., Gearheart, L. & Murphy, C. J. Wet chemical synthesis of high aspect ratio cylindrical gold nanorods. *The Journal of Physical Chemistry B* **105**, 4065–4067 (2001).

82. Jana, N. R., Gearheart, L. & Murphy, C. J. Seed-mediated growth approach for shape-controlled synthesis of spheroidal and rod-like gold nanoparticles using a surfactant template. *Advanced Materials* **13**, 1389–1393 (2001).

83. Yuan, H. *et al.* Gold nanostars: surfactant-free synthesis, 3D modelling, and two-photon photoluminescence imaging. *Nanotechnology* **23**, 75102 (2012).

84. Sun, Y. & Xia, Y. Shape-controlled synthesis of gold and silver nanoparticles. *Science* **298**, 2176–2179 (2002).

85. Xia, X. *et al.* Silver nanocrystals with concave surfaces and their optical and surface-enhanced Raman scattering properties. *Angewandte Chemie (International ed. in English)* **50**, 12542–12546 (2011).

86. Jana, N. R., Gearheart, L. & Murphy, C. J. Wet chemical synthesis of silver nanorods and nanowires of controllable aspect ratio. *Chemical Communications* 617–618 (2001).

87. Kho, K. W., Shen, Z. X., Zeng, H. C., Soo, K. C. & Olivo, M. Deposition method for preparing SERS-active gold nanoparticle substrates. *Analytical Chemistry* **77**, 7462–7471 (2005).

88. Lee, C. H., Tian, L. & Singamaneni, S. Paper-based SERS swab for rapid trace detection on real-world surfaces. *ACS Applied Materials & Interfaces* **2**, 3429–3435 (2010).

89. Lee, C. H., Hankus, M. E., Tian, L., Pellegrino, P. M. & Singamaneni, S. Highly sensitive surface enhanced Raman scattering substrates based on filter paper loaded with plasmonic nanostructures. *Analytical Chemistry* **83**, 8953–8958 (2011).

90. Qu, L.-L. *et al.* Batch fabrication of disposable screen printed SERS arrays. *Lab on a Chip* **12**, 876–881 (2012).

91. Yu, W. W. & White, I. M. A simple filter based approach to surface enhanced Raman spectroscopy for trace chemical detection. *Analyst* **137**, 1168–1173 (2012).

92. Yu, W. W. & White, I. M. Inkjet printed surface enhanced Raman spectroscopy array on cellulose paper. *Analytical Chemistry* **82**, 9626–9630 (2010).

93. Yu, W. W. & White, I. M. Inkjet-printed paper-based SERS dipsticks and swabs for trace chemical detection. *Analyst* **138**, 1020–1025 (2013).

94. Yu, W. W. & White, I. M. Chromatographic separation and detection of target analytes from complex samples using inkjet printed SERS substrates. *Analyst* **138**, 3679–3686 (2013).

95. Chaney, S. B., Shanmukh, S., Dluhy, R. A. & Zhao, Y.-P. Aligned silver nanorod arrays produce high sensitivity surface-enhanced Raman spectroscopy substrates. *Applied Physics Letters* **87**, 031908 (2005).

96. Zhang, X.-F. *et al.* Detection of melamine in liquid milk using surface-enhanced Raman scattering spectroscopy. *Journal of Raman Spectroscopy* **41**, 1655–1660 (2010).

97. Tao, A. *et al.* Langmuir−Blodgett silver nanowire monolayers for molecular sensing using surface-enhanced Raman spectroscopy. *Nano Letters* **3**, 1229–1233 (2003).

98. Im, H., Bantz, K. C., Lindquist, N. C., Haynes, C. L. & Oh, S.-H. Vertically oriented sub-10-nm plasmonic nanogap arrays. *Nano Letters* **10**, 2231–2236 (2010).

99. Alvarez-Puebla, R., Cui, B., Bravo-Vasquez, J.-P., Veres, T. & Fenniri, H. Nanoimprinted SERS-active substrates with tunable surface plasmon resonances. *Journal of Physical Chemistry C* **111**, 6720–6723 (2007).

100. Wu, W., Hu, M., Ou, F. S., Li, Z. & Williams, R. S. Cones fabricated by 3D nanoimprint lithography for highly sensitive surface enhanced Raman spectroscopy. *Nanotechnology* **21**, 255502 (2010).

101. Li, K., Cui, B., Clime, L. & Veres, T. Fabrication of SERS active substrates by nanoimprint lithography. *MRS Proceedings* **1054**, 1054–FF01–03 (2011).

102. Cui, B., Cortot, Y. & Veres, T. Polyimide nanostructures fabricated by nanoimprint lithography and its applications. *Microelectronic Engineering* **83**, 906–909 (2006).

103. Lee, S.-W. *et al.* Highly sensitive biosensing using arrays of plasmonic Au nanodisks realized by nanoimprint lithography. *ACS Nano* **5**, 897–904 (2011).

104. Lucas, B. D., Kim, J.-S., Chin, C. & Guo, L. J. Nanoimprint lithography based approach for the fabrication of large-area, uniformly-oriented plasmonic arrays. *Advanced Materials* **20**, 1129–1134 (2008).

105. Choi, C. J., Xu, Z., Wu, H.-Y., Liu, G. L. & Cunningham, B. T. Surface-enhanced Raman nanodomes. *Nanotechnology* **21**, 415301 (2010).

106. Hulteen, J. C. & Van Duyne, R. P. Nanosphere lithography: a materials general fabrication process for periodic particle array surfaces. *Journal of Vacuum Science & Technology A: Vacuum, Surfaces, and Films* **13**, 1553 (1995).

107. Dieringer, J. A. *et al.* Introductory lecture: surface enhanced Raman spectroscopy: new materials, concepts, characterization tools, and applications. *Faraday Discussions* **132**, 9 (2006).

108. Jensen, T. R., Malinsky, M. D., Haynes, C. L. & Van Duyne, R. P. Nanosphere lithography: tunable localized surface plasmon resonance spectra of silver nanoparticles. *The Journal of Physical Chemistry B* **104**, 10549–10556 (2000).

109. Camden, J. P., Dieringer, J. A., Zhao, J. & Van Duyne, R. P. Controlled plasmonic nanostructures for surface-enhanced spectroscopy and sensing. *Accounts of chemical research* **41**, 1653–1661 (2008).

110. Haynes, C. L. & Van Duyne, R. P. Nanosphere lithography: a versatile nanofabrication tool for studies of size-dependent nanoparticle optics. *The Journal of Physical Chemistry B* **105**, 5599–5611 (2001).

111. McFarland, A. D., Young, M. A., Dieringer, J. A. & Van Duyne, R. P. Wavelength-scanned surface-enhanced Raman excitation spectroscopy. *The Journal of Physical Chemistry. B* **109**, 11279–85 (2005).

112. Kleinman, S. L., Frontiera, R. R., Henry, A.-I., Dieringer, J. A. & Van Duyne, R. P. Creating, characterizing, and controlling chemistry with SERS hot spots. *Physical Chemistry Chemical Physics* **15**, 21–36 (2013).

113. Banholzer, M. J., Millstone, J. E., Qin, L. & Mirkin, C. A. Rationally designed nanostructures for surface-enhanced Raman spectroscopy. *Chemical Society Reviews* **37**, 885–897 (2008).

114. Fan, M., Andrade, G. F. S. & Brolo, A. G. A review on the fabrication of substrates for surface enhanced Raman spectroscopy and their applications in analytical chemistry. *Analytica Chimica Acta* **693**, 7–25 (2011).

115. Lin, X.-M., Cui, Y., Xu, Y.-H., Ren, B. & Tian, Z.-Q. Surface-enhanced Raman spectroscopy: substrate-related issues. *Analytical and Bioanalytical Chemistry* **394**, 1729–1745 (2009).

116. Whitney, A. V *et al.* Localized surface plasmon resonance nanosensor: a high-resolution distance-dependence study using atomic layer deposition. *The Journal of Physical Chemistry. B* **109**, 20522–20528 (2005).

117. Zhao, Y.-P., Chaney, S. B., Shanmukh, S. & Dluhy, R. A. Polarized surface enhanced Raman and absorbance spectra of aligned silver nanorod arrays. *The Journal of Physical Chemistry. B* **110**, 3153–7 (2006).

118. Orendorff, C. J., Gearheart, L., Jana, N. R. & Murphy, C. J. Aspect ratio dependence on surface enhanced Raman scattering using silver and gold nanorod substrates. *Physical Chemistry Chemical Physics* **8**, 165–170 (2006).

119. Khoury, C. G. & Vo-Dinh, T. Gold nanostars for surface-enhanced Raman scattering: synthesis, characterization and optimization. *Journal of Physical Chemistry C* **112**, 18849–18859 (2008).

120. Garcia-Leis, A., Garcia-Ramos, J. V. & Sanchez-Cortes, S. Silver nanostars with high SERS performance. *The Journal of Physical Chemistry C* **117**, 7791–7795 (2013).

121. Wu, H.-L. *et al.* A comparative study of gold nanocubes, octahedra, and rhombic dodecahedra as highly sensitive SERS substrates. *Inorganic chemistry* **50**, 8106–8111 (2011).

122. Costa, J. C. S. *et al.* High performance gold nanorods and silver nanocubes in surface-enhanced Raman spectroscopy of pesticides. *Physical Chemistry Chemical Physics* **11**, 7491–7498 (2009).

123. Kodiyath, R. *et al.* Assemblies of silver nanocubes for highly sensitive SERS chemical vapor detection. *Journal of Materials Chemistry A* **1**, 2777 (2013).

124. Van Duyne, R. P., Hulteen, J. C. & Treichel, D. A. Atomic force microscopy and surface-enhanced Raman spectroscopy. I. Ag island films and Ag film over polymer nanosphere surfaces supported on glass. *The Journal of Chemical Physics* **99**, 2101 (1993).

125. Sockalingum, G. D., Beljebbar, A., Morjani, H., Angiboust, J. F. & Manfait, M. Characterization of island films as surface-enhanced Raman spectroscopy substrates for detecting low antitumor drug concentrations at single cell level. *Biospectroscopy* **4**, S71–S78 (1998).

126. Schlegel, V. L. & Cotton, T. M. Silver-island films as substrates for enhanced Raman scattering: effect of deposition rate on intensity. *Analytical Chemistry* **63**, 241–247 (1991).

127. Weitz, D. A., Garoff, S. & Gramila, T. J. Excitation spectra of surface-enhanced Raman scattering on silver-island films. *Optics Letters* **7**, 168–170 (1982).

128. Aroca, R. & Martin, F. Tuning metal island films for maximum surface-enhanced Raman scattering. *Journal of Raman Spectroscopy* **16**, 156–162 (1985).

129. Jennings, C. A., Kovacs, G. J. & Aroca, R. Near-infrared surface-enhanced Raman scattering from metal island films. *The Journal of Physical Chemistry* **96**, 1340–1343 (1992).

130. Ofir, A., Kaganovskii, Y. & Rosenbluh, M. SERS of ultra-thin Rhodamine 6G layers on Ag nanocrystals. *Conference on Lasers and Electro-Optics* JTuD31 (2006).

131. Mabbott, S., Eckmann, A., Casiraghi, C. & Goodacre, R. 2p or not 2p: tuppence-based SERS for the detection of illicit materials. *Analyst* **138**, 118–122 (2013).

132. Sun, X., Lin, L., Li, Z., Zhang, Z. & Feng, J. Novel Ag–Cu substrates for surface-enhanced Raman scattering. *Materials Letters* **63**, 2306–2308 (2009).

133. Ruan, C., Wang, W. & Gu, B. Single-molecule detection of thionine on aggregated gold nanoparticles by surface enhanced Raman scattering. *Journal of Raman Spectroscopy* **38**, 568–573 (2007).

134. Schwartzberg, A. M. *et al.* Unique gold nanoparticle aggregates as a highly active surface-enhanced Raman scattering substrate. *The Journal of Physical Chemistry B* **108**, 19191–19197 (2004).

135. Abbas, A. *et al.* Multifunctional analytical platform on a paper strip: separation, preconcentration, and subattomolar detection. *Analytical Chemistry* **85**, 3977–3983 (2013).

136. Yue, W. *et al.* Electron-beam lithography of gold nanostructures for surface-enhanced Raman scattering. *Journal of Micromechanics and Microengineering* **22**, 125007 (2012).

137. Félidj, N. *et al.* Gold particle interaction in regular arrays probed by surface enhanced Raman scattering. *The Journal of Chemical Physics* **120**, 7141–7146 (2004).

138. Félidj, N. *et al.* Controlling the optical response of regular arrays of gold particles for surface-enhanced Raman scattering. *Physical Review B* **65**, 075419 (2002).

139. Yu, Q., Guan, P., Qin, D., Golden, G. & Wallace, P. M. Inverted size-dependence of surface-enhanced Raman scattering on gold nanohole and nanodisk arrays. *Nano Letters* **8**, 1923–1928 (2008).

140. Gunnarsson, L. *et al.* Interparticle coupling effects in nanofabricated substrates for surface-enhanced Raman scattering. *Applied Physics Letters* **78**, 802 (2001).

141. Ward, D. R. *et al.* Electromigrated nanoscale gaps for surface-enhanced Raman spectroscopy. *Nano Letters* **7**, 1396–1400 (2007).

142. Tessier, P. M. *et al.* Assembly of gold nanostructured films templated by colloidal crystals and use in surface-enhanced Raman spectroscopy. *Proc. SPIE 4577, Vibrational Spectroscopy-based Sensor Systems* (2002).

143. Wang, H., Levin, C. S. & Halas, N. J. Nanosphere arrays with controlled sub-10-nm gaps as surface-enhanced Raman spectroscopy substrates. *Journal of the American Chemical Society* **127**, 14992–14993 (2005).

144. Fang, Y., Seong, N.-H. & Dlott, D. D. Measurement of the distribution of site enhancements in surface-enhanced Raman scattering. *Science* **321**, 388–392 (2008).

145. Stuart, D. A. *et al.* Glucose sensing using near-infrared surface-enhanced Raman spectroscopy: gold surfaces, 10-day stability, and improved accuracy. *Analytical Chemistry* **77**, 4013–4019 (2005).

146. Zhang, X., Young, M. A., Lyandres, O. & Van Duyne, R. P. Rapid detection of an anthrax biomarker by surface-enhanced Raman spectroscopy. *Journal of the American Chemical Society* **127**, 4484–9 (2005).

147. Zhang, X., Zhao, J., Whitney, A. V, Elam, J. W. & Van Duyne, R. P. Ultrastable substrates for surface-enhanced Raman spectroscopy: Al_2O_3 overlayers fabricated by atomic layer deposition yield improved anthrax biomarker detection. *Journal of the American Chemical Society* **128**, 10304–10309 (2006).

148. Leverette, C. L. *et al.* Aligned silver nanorod arrays as substrates for surface-enhanced infrared absorption spectroscopy. *Applied Spectroscopy* **60**, 906–913 (2006).

149. Liu, Y.-J., Chu, H. Y. & Zhao, Y.-P. Silver nanorod array substrates fabricated by oblique angle deposition: morphological, optical, and SERS characterizations. *The Journal of Physical Chemistry C* **114**, 8176–8183 (2010).

150. Driskell, J. D. *et al.* The use of aligned silver nanorod arrays prepared by oblique angle deposition as surface enhanced Raman scattering substrates. *Journal of Physical Chemistry C* **112**, 895–901 (2008).

151. Song, C. *et al.* Gold-modified silver nanorod arrays: growth dynamics and improved SERS properties. *Journal of Materials Chemistry* **22**, 1150 (2012).

152. Hu, M. *et al.* Gold nanofingers for molecule trapping and detection. *Journal of the American Chemical Society* **132**, 12820–12822 (2010).

153. Ou, F. S. *et al.* Hot-spot engineering in polygonal nanofinger assemblies for surface enhanced Raman spectroscopy. *Nano Letters* **11**, 2538–2542 (2011).

154. Félidj, N. *et al.* Enhanced substrate-induced coupling in two-dimensional gold nanoparticle arrays. *Physical Review B* **66**, 245407 (2002).

155. Hildebrandt, P. & Stockburger, M. Surface-enhanced resonance Raman spectroscopy of Rhodamine 6G adsorbed on colloidal silver. *The Journal of Physical Chemistry* **88**, 5935–5944 (1984).

156. Cai, W. B. *et al.* Investigation of surface-enhanced Raman scattering from platinum electrodes using a confocal Raman microscope: dependence of surface roughening pretreatment. *Surface Science* **406**, 9–22 (1998).

157. Su, K.-H. *et al.* Raman enhancement factor of a single tunable nanoplasmonic resonator. *The Journal of Physical Chemistry. B* **110**, 3964–8 (2006).

158. LeRu, E. C., Meyer, M. & Etchegoin, P. G. Surface enhanced Raman scattering enhancement factors: a comprehensive study. *Journal of Physical Chemistry C* **111**, 13794–13803 (2007).

159. Erol, M. *et al.* SERS not to be taken for granted in the presence of oxygen. *Journal of the American Chemical Society* **131**, 7480–7481 (2009).

160. Qi, H., Alexson, D., Glembocki, O. & Prokes, S. M. The effect of size and size distribution on the oxidation kinetics and plasmonics of nanoscale Ag particles. *Nanotechnology* **21**, 215706 (2010).

161. Betz, J., Yu, W., Cheng, Y., White, I. & Rubloff, G. Simple SERS substrates: powerful, portable, and full of potential. *in preparation*

162. Shin, K. & Chung, H. Wide area coverage Raman spectroscopy for reliable quantitative analysis and its applications. *Analyst* 3335–3346 (2013). DOI:10.1039/c3an36843b

163. Bell, S. E. J. *et al.* Development of sampling methods for Raman analysis of solid dosage forms of therapeutic and illicit drugs. *Journal of Raman Spectroscopy* **35**, 409–417 (2004).

164. Yeo, B.-S., Schmid, T., Zhang, W. & Zenobi, R. A strategy to prevent signal losses, analyte decomposition, and fluctuating carbon contamination bands in surface-enhanced Raman spectroscopy. *Applied Spectroscopy* **62**, 708–713 (2008).

165. Abell, J. L., Garren, J. M. & Zhao, Y. Dynamic rastering surface-enhanced Raman scattering (SERS) measurements on silver nanorod substrates. *Applied Spectroscopy* **65**, 734–740 (2011).

166. Laserna, J. J., Campiglia, a D. & Winefordner, J. D. Mixture analysis and quantitative determination of nitrogen-containing organic molecules by surface-enhanced Raman spectrometry. *Analytical Chemistry* **61**, 1697–1701 (1989).

167. Vo-Dinh, T., Hiromoto, M. Y. K., Begun, G. M. & Moody, R. L. Surface-enhanced Raman spectrometry for trace organic analysis. *Analytical Chemistry* **56**, 1667–1670 (1984).

168. Cabalín, L. M. & Laserna, J. J. Fast spatially resolved surface-enhanced Raman spectrometry on a silver coated filter paper using charge-coupled device detection. *Analytica Chimica Acta* **310**, 337–345 (1995).

169. Wu, D. & Fang, Y. The adsorption behavior of p-hydroxybenzoic acid on a silver-coated filter paper by surface enhanced Raman scattering. *Journal of Colloid and Interface Science* **265**, 234–238 (2003).

170. Yano, T., Ohtani, H., Tsuge, S. & Obokata, T. Determination of neutral sizing agents in paper by pyrolysis - gas chromatography. *Analyst* **117**, 849 (1992).

171. Ek, M., Gellerstedt, G. & Henriksson, G. *Paper Chemistry and Technology*. **3**, (de Gruyter: 2009).

172. Munro, C. H., Smith, W. E., Garner, M., Clarkson, J. & White, P. C. Characterization of the surface of a citrate-reduced colloid optimized for use as a substrate for surface-enhanced resonance Raman scattering. *Langmuir* **11**, 3712–3720 (1995).

173. Pelton, R. Bioactive paper provides a low-cost platform for diagnostics. *Trends in Analytical Chemistry* **28**, 925–942 (2009).

174. Deegan, R. D. *et al.* Capillary flow as the cause of ring stains from dried liquid drops. *Nature* **389**, 827–829 (1997).

175. Wu, H.-Y., Choi, C. J. & Cunningham, B. T. Plasmonic nanogap-enhanced Raman scattering using a resonant nanodome array. *Small* **8**, 2878–2885 (2012).

176. Hankus, M. E., Stratis-Cullum, D. N. & Pellegrino, P. M. Surface enhanced Raman scattering (SERS)-based next generation commercially available substrate: physical characterization and biological application. *Proc. SPIE 8099, Biosensing and Nanomedicine IV* 80990N–80990N (2011).

177. Yang, A. H. J. *et al.* Direct Manipulation of nanoparticles and DNA in sub-wavelength optical nanochannels. *Conference on Lasers and Electro-Optics/International Quantum Electronics Conference* CTuU4 (2009).

178. Esmonde-White, K. A., Le Clair, S. V, Roessler, B. J. & Morris, M. D. Effect of conformation and drop properties on surface-enhanced Raman spectroscopy of dried biopolymer drops. *Applied Spectroscopy* **62**, 503–511 (2008).

179. *FDA issues health information advisory on infant formula*. (2008). <http://www.fda.gov/NewsEvents/Newsroom/PressAnnouncements/2008/ucm116947.htm>

180. White, I. M., Yazdi, S. H. & Yu, W. W. Optofluidic SERS: synergizing photonics and microfluidics for chemical and biological analysis. *Microfluidics and Nanofluidics* DOI: 10.1007/s10404–012–0962–2 (2012).

181. Lim, C., Hong, J., Chung, B. G., DeMello, A. J. & Choo, J. Optofluidic platforms based on surface-enhanced Raman scattering. *Analyst* **135**, 837–844 (2010).

182. Yin, Y., Qiu, T., Zhang, W. & Chu, P. K. Recent developments in optofluidic-surface-enhanced Raman scattering systems: design, assembly, and advantages. *Journal of Materials Research* **26**, 170–185 (2011).

183. Chen, L. & Choo, J. Recent advances in surface-enhanced Raman scattering detection technology for microfluidic chips. *Electrophoresis* **29**, 1815–1828 (2008).

184. Orendorff, C. J., Gole, A., Sau, T. K. & Murphy, C. J. Surface-enhanced Raman spectroscopy of self-assembled monolayers: sandwich architecture and nanoparticle shape dependence. *Analytical Chemistry* **77**, 3261–3266 (2005).

185. Liz-Marzán, L. M. Tailoring surface plasmons through the morphology and assembly of metal nanoparticles. *Langmuir* **22**, 32–41 (2006).

186. Kuncicky, D. M., Prevo, B. G. & Velev, O. D. Controlled assembly of SERS substrates templated by colloidal crystal films. *Journal of Materials Chemistry* **16**, 1207 (2006).

187. Jung, H. Y., Park, Y.-K., Park, S. & Kim, S. K. Surface enhanced Raman scattering from layered assemblies of close-packed gold nanoparticles. *Analytica Chimica Acta* **602**, 236–243 (2007).

188. Liberman, V. *et al.* A nanoparticle convective directed assembly process for the fabrication of periodic surface enhanced Raman spectroscopy substrates. *Advanced Materials* **22**, 4298–4302 (2010).

189. Lu, Y., Liu, G. L. & Lee, L. P. High-density silver nanoparticle film with temperature-controllable interparticle spacing for a tunable surface enhanced Raman scattering substrate. *Nano Letters* **5**, 5–9 (2005).

190. Gupta, R. & Weimer, W. A. High enhancement factor gold films for surface enhanced Raman spectroscopy. *Chemical Physics Letters* **374**, 302–306 (2003).

191. Abu Hatab, N. A., Oran, J. M. & Sepaniak, M. J. Surface-enhanced Raman spectroscopy substrates created via electron beam lithography and nanotransfer printing. *ACS Nano* **2**, 377–385 (2008).

192. Chattopadhyay, S., Lo, H.-C., Hsu, C.-H., Chen, L.-C. & Chen, K.-H. Surface-enhanced Raman spectroscopy using self-assembled silver nanoparticles on silicon nanotips. *Chemistry of Materials* **17**, 553–559 (2005).

193. Yang, Y., Shi, J., Tanaka, T. & Nogami, M. Self-assembled silver nanochains for surface-enhanced Raman scattering. *Langmuir* **23**, 12042–12047 (2007).

194. Newhart, K. *Environmental fate of malathion*. 1–20 (2006). <http://www.cdpr.ca.gov/docs/emon/pubs/fatememo/efate_malathion.pdf>

195. U.S. Department of Health and Human Services *Toxicological profile for malathion*. 1–327 (2003). <http://www.atsdr.cdc.gov/ToxProfiles/tp154.pdf>

196. Bantz, K. C. *et al.* Recent progress in SERS biosensing. *Physical Chemistry Chemical Physics* **13**, 11551–11567 (2011).

197. Kneipp, K., Kneipp, H., Itzkan, I., Dasari, R. R. & Feld, M. S. Surface-enhanced Raman scattering and biophysics. *Journal of Physics: Condensed Matter* **14**, R597 (2002).

198. Cialla, D. *et al.* Surface-enhanced Raman spectroscopy (SERS): progress and trends. *Analytical and Bioanalytical Chemistry* **403**, 27–54 (2012).

199. Baker, G. A. & Moore, D. S. Progress in plasmonic engineering of surface-enhanced Raman-scattering substrates toward ultra-trace analysis. *Analytical and Bioanalytical Chemistry* **382**, 1751–1770 (2005).

200. Golightly, R. S., Doering, W. E. & Natan, M. J. Surface-enhanced Raman spectroscopy and homeland security: a perfect match? *ACS Nano* **3**, 2859–2869 (2009).

201. Larmour, I. A. & Graham, D. Surface enhanced optical spectroscopies for bioanalysis. *Analyst* **136**, 3831–3853 (2011).

202. Yazdi, S. H. & White, I. M. Multiplexed detection of aquaculture fungicides using a pump-free optofluidic SERS microsystem. *Analyst* **138**, 100–103 (2013).

203. MacAskill, A., Crawford, D., Graham, D. & Faulds, K. DNA sequence detection using surface-enhanced resonance Raman spectroscopy in a homogeneous multiplexed assay. *Analytical Chemistry* **81**, 8134–8140 (2009).

204. Cao, Y. C., Jin, R. & Mirkin, C. A. Nanoparticles with Raman spectroscopic fingerprints for DNA and RNA detection. *Science* **297**, 1536–1540 (2002).

205. Dougan, J. & Faulds, K. Surface enhanced Raman scattering for multiplexed detection. *Analyst* **137**, 545–554 (2012).

206. Chalmers, J. M., Edwards, H. G. M. & Hargreaves, M. D. *Infrared and Raman spectroscopy in forensic science*. (Wiley: 2012).

207. Chase, D. B. Fourier transform Raman spectroscopy. *Journal of the American Chemical Society* **108**, 7485–7488 (1986).

208. Yaney, P. P. The pulsed laser and gated detection in Raman spectroscopy - a survey of the spectra of common substances including studies of adsorbed benzene. *Journal of Raman Spectroscopy* **5**, 219–241 (1976).

209. Van Duyne, R. P., Jeanmaire, D. L. & Shriver, D. F. Mode-locked laser Raman spectroscopy. New technique for the rejection of interfering background luminescence signals. *Analytical Chemistry* **46**, 213–222 (1974).

210. Matousek, P., Towrie, M., Stanley, A. & Parker, A. W. Efficient rejection of fluorescence from Raman spectra using picosecond Kerr gating. *Applied Spectroscopy* **53**, 1485–1489 (1999).

211. Matousek, P. *et al.* Fluorescence suppression in resonance Raman spectroscopy using a high-performance picosecond Kerr gate. *Journal of Raman Spectroscopy* **32**, 983–988 (2001).

212. Littleford, R. E. *et al.* Raman spectroscopy of street samples of cocaine obtained using Kerr gated fluorescence rejection. *Analyst* **129**, 505–506 (2004).

213. De Luca, A. C., Mazilu, M., Riches, A., Herrington, C. S. & Dholakia, K. Online fluorescence suppression in modulated Raman spectroscopy. *Analytical Chemistry* **82**, 738–745 (2010).

214. Praveen, B. B., Steuwe, C., Mazilu, M., Dholakia, K. & Mahajan, S. Wavelength modulated surface enhanced (resonance) Raman scattering for background-free detection. *Analyst* **138**, 2816–2820 (2013).

215. Shreve, A. P., Cherepy, N. J. & Mathies, R. A. Effective rejection of fluorescence interference in Raman spectroscopy using a shifted excitation difference technique. *Applied Spectroscopy* **46**, 707–711 (1992).

216. Driskell, J. D. *et al.* Rapid microRNA (miRNA) detection and classification via surface-enhanced Raman spectroscopy (SERS). *Biosensors and Bioelectronics* **24**, 917–922 (2008).

217. Jarvis, R. M. & Goodacre, R. Discrimination of bacteria using surface-enhanced Raman spectroscopy. *Analytical Chemistry* **76**, 40–47 (2004).

218. Pearman, W. F. & Fountain, A. W. Classification of chemical and biological warfare agent simulants by surface-enhanced Raman spectroscopy and multivariate statistical techniques. *Applied Spectroscopy* **60**, 356–365 (2006).

219. Shanmukh, S. *et al.* Identification and classification of respiratory syncytial virus (RSV) strains by surface-enhanced Raman spectroscopy and multivariate statistical techniques. *Analytical and Bioanalytical Chemistry* **390**, 1551–1555 (2008).

220. Trachta, G., Schwarze, B., Sägmüller, B., Brehm, G. & Schneider, S. Combination of high-performance liquid chromatography and SERS detection applied to the analysis of drugs in human blood and urine. *Journal of Molecular Structure* **693**, 175–185 (2004).

221. Horvath, E., Kátay, G., Tyihák, E., Kristóf, J. & Redey, A. Critical evaluation of experimental conditions influencing the surface-enhanced Raman spectroscopic (SERS) detection of substances separated by layer liquid chromatographic techniques. *Chromatographia* **51**, 297–301 (2000).

222. Geiman, I., Leona, M. & Lombardi, J. R. Application of Raman spectroscopy and surface-enhanced Raman scattering to the analysis of synthetic dyes found in ballpoint pen inks. *Journal of Forensic Sciences* **54**, 947–952 (2009).

223. Brosseau, C. L. *et al.* Ad-hoc surface-enhanced Raman spectroscopy methodologies for the detection of artist dyestuffs: thin layer chromatography-surface enhanced Raman spectroscopy and in situ on the fiber analysis. *Analytical Chemistry* **81**, 3056–3062 (2009).

224. Somsen, G. W., Coulter, S. K., Gooijer, C., Velthorst, N. H. & Brinkman, U. A. Coupling of column liquid chromatography and surface-enhanced resonance Raman spectroscopy via a thin-layer chromatographic plate. *Analytica Chimica Acta* **349**, 189–197 (1997).

225. Sägmüller, B., Schwarze, B., Brehm, G., Trachta, G. & Schneider, S. Identification of illicit drugs by a combination of liquid chromatography and

surface-enhanced Raman scattering spectroscopy. *Journal of Molecular Structure* **661**, 279–290 (2003).

226. Chen, J., Abell, J., Huang, Y. & Zhao, Y. On-chip ultra-thin layer chromatography and surface enhanced Raman spectroscopy. *Lab on a Chip* **12**, 3096–3102 (2012).

227. Szabo, N. J. & Winefordner, J. D. Evaluation of a solid-phase extraction membrane as a surface-enhanced Raman substrate. *Applied Spectroscopy* **52**, 500–512 (1998).

228. Scott, R. P. W. *Techniques and practice of chromatography*. **70**, (CRC: 1995).

229. Wall, P. E. *Thin-layer chromatography: a modern practical approach*. (Royal Society of Chemistry: 2005).

230. Ingelfinger, J. R. Melamine and the global implications of food contamination. *New England Journal of Medicine* **359**, 2745–2748 (2008).

231. Kim, B. *et al.* Determination of melamine in pet food by enzyme immunoassay, high-performance liquid chromatography with diode array detection, and ultra-performance liquid chromatography with tandem mass spectrometry. *Journal of AOAC International* **91**, 408–413 (2008).

232. Garber, E. A. E. Detection of melamine using commercial enzyme-linked immunosorbent assay technology. *Journal of Food Protection* **71**, 590–594 (2008).

233. Ehling, S., Tefera, S. & Ho, I. P. High-performance liquid chromatographic method for the simultaneous detection of the adulteration of cereal flours with melamine and related triazine by-products ammeline, ammelide, and cyanuric acid. *Food Additives and Contaminants* **24**, 1319–1325 (2007).

234. Lin, M. A review of traditional and novel detection techniques for melamine and its analogues in foods and animal feed. *Frontiers of Chemical Engineering in China* **3**, 427–435 (2009).

235. Sun, F. *et al.* Analytical methods and recent developments in the detection of melamine. *Trends in Analytical Chemistry* **29**, 1239–1249 (2010).

236. Lin, M. *et al.* Detection of melamine in gluten, chicken feed, and processed foods using surface enhanced Raman spectroscopy and HPLC. *Journal of Food Science* **73**, T129–T134 (2008).

237. Kim, A., Barcelo, S. J., Williams, R. S. & Li, Z. Melamine sensing in milk products by using surface enhanced Raman scattering. *Analytical Chemistry* **84**, 9303–9309 (2012).

238. Lee, S. Y., Ganbold, E.-O., Choo, J. & Joo, S.-W. Detection of melamine in powdered milk using surface-enhanced Raman scattering with no pretreatment. *Analytical Letters* **43**, 2135–2141 (2010).

239. Chen, L. *et al.* ZnO/Au composite nanoarrays as substrates for surface-enhanced Raman scattering detection. *The Journal of Physical Chemistry C* **114**, 93–100 (2010).

240. Hargreaves, M. D. *et al.* Analysis of seized drugs using portable Raman spectroscopy in an airport environment – a proof of principle study. *Journal of Raman Spectroscopy* **39**, 873–880 (2008).

241. Ryder, A. G., O'Connor, G. M. & Glynn, T. J. Identifications and quantitative measurements of narcotics in solid mixtures using near-IR Raman spectroscopy and multivariate analysis. *Journal of Forensic Sciences* **44**, 1013–1019 (1999).

242. Park, T. *et al.* Highly sensitive signal detection of duplex dye-labelled DNA oligonucleotides in a PDMS microfluidic chip: confocal surface-enhanced Raman spectroscopic study. *Lab on a Chip* **5**, 437–442 (2005).

243. Wilson, R., A Bowden, S., Parnell, J. & M Cooper, J. Signal enhancement of surface enhanced Raman scattering and surface enhanced resonance Raman scattering using in situ colloidal synthesis in microfluidics. *Analytical Chemistry* **82**, 2119–2123 (2010).

244. Chou, I.-H. *et al.* Nanofluidic biosensing for beta-amyloid detection using surface enhanced Raman spectroscopy. *Nano Letters* **8**, 1729–1735 (2008).

245. Yang, X. *et al.* High-sensitivity molecular sensing using hollow-core photonic crystal fiber and surface-enhanced Raman scattering. *Journal of the Optical Society of America A* **27**, 977 (2010).

246. Measor, P. *et al.* On-chip surface-enhanced Raman scattering detection using integrated liquid-core waveguides. *Applied Physics Letters* **90**, 211107 (2007).

247. Ngo, Y. H., Li, D., Simon, G. P. & Garnier, G. Effect of cationic polyacrylamides on the aggregation and SERS performance of gold nanoparticles-treated paper. *Journal of Colloid and Interface Science* **392**, 237–246 (2013).

248. Ngo, Y. H., Li, D., Simon, G. P. & Garnier, G. Gold nanoparticle-paper as a three-dimensional surface enhanced Raman scattering substrate. *Langmuir* **28**, 8782–8790 (2012).

249. Liu, X., Zong, C., Ai, K., He, W. & Lu, L. Engineering natural materials as surface-enhanced Raman spectroscopy substrates for in situ molecular sensing. *Applied Materials & Interfaces* **4**, 6599–6608 (2012).

250. Chen, Y. *et al.* A paper-based surface-enhanced resonance Raman spectroscopic (SERRS) immunoassay using magnetic separation and enzyme-catalyzed reaction. *Analyst* **138**, 2624–2631 (2013).

251. Li, B., Zhang, W., Chen, L. & Lin, B. A fast and low-cost spray method for prototyping and depositing SERS arrays on microfluidic paper-based device. *Electrophoresis* (2013). DOI:10.1002/elps.201300138

252. Eshkeiti, A. *et al.* Detection of heavy metal compounds using a novel inkjet printed surface enhanced Raman spectroscopy (SERS) substrate. *Sensors and Actuators B: Chemical* **171-172**, 705–711 (2012).

253. Fierro-Mercado, P. M. & Hernández-Rivera, S. P. Highly sensitive filter paper substrate for SERS trace explosives detection. *International Journal of Spectroscopy* **2012**, (2012).

254. Liz-Marzán, L. M., Giersig, M. & Mulvaney, P. Synthesis of nanosized gold−silica core−shell particles. *Langmuir* **12**, 4329–4335 (1996).

255. Guerrero-Martínez, A., Barbosa, S., Pastoriza-Santos, I. & Liz-Marzán, L. M. Nanostars shine bright for you: colloidal synthesis, properties and applications of branched metallic nanoparticles. *Current Opinion in Colloid & Interface Science* **16**, 118–127 (2011).

256. Wu, H.-L., Chen, C.-H. & Huang, M. H. Seed-mediated synthesis of branched gold nanocrystals derived from the side growth of pentagonal bipyramids and the formation of gold nanostars. *Chemistry of Materials* **21**, 110–114 (2009).

257. Hrelescu, C., Sau, T. K., Rogach, A. L., Jackel, F. & Feldmann, J. Single gold nanostars enhance Raman scattering. *Applied Physics Letters* **94**, 153113 (2009).

258. Nalbant Esenturk, E. & Hight Walker, a. R. Surface-enhanced Raman scattering spectroscopy via gold nanostars. *Journal of Raman Spectroscopy* **40**, 86–91 (2009).

259. Song, H., Wei, Q., Ong, Q. K. & Wei, A. Plasmon-resonant nanoparticles and synthesis and magnetomotive imaging. *ACS Nano* **4**, 5163–5173 (2010).

260. Cheng, Y., Wang, M., Borghs, G. & Chen, H. Gold nanoparticle dimers for plasmon sensing. *Langmuir* **27**, 7884–7891 (2011).

261. Busson, M. P. *et al.* Optical and topological characterization of gold nanoparticle dimers linked by a single DNA double strand. *Nano Letters* **11**, 5060–5065 (2011).

262. Yim, T.-J., Wang, Y. & Zhang, X. Synthesis of a gold nanoparticle dimer plasmonic resonator through two-phase-mediated functionalization. *Nanotechnology* **19**, 435605 (2008).

263. Indrasekara, A. S. D. S. *et al.* Dimeric gold nanoparticle assemblies as tags for SERS-based cancer detection. *Advanced Healthcare Materials* (2013). DOI:10.1002/adhm.201200370

264. Cao, X. *et al.* Combining use of a panel of ssDNA aptamers in the detection of Staphylococcus aureus. *Nucleic Acids Research* **37**, 4621–4628 (2009).

265. Su, S., Nutiu, R., Filipe, C. D. M., Li, Y. & Pelton, R. Adsorption and covalent coupling of ATP-binding DNA aptamers onto cellulose. *Langmuir* **23**, 1300–1302 (2007).

266. Potyrailo, R. a., Conrad, R. C., Ellington, A. D. & Hieftje, G. M. Adapting selected nucleic acid ligands (aptamers) to biosensors. *Analytical Chemistry* **70**, 3419–3425 (1998).

267. Ozaki, H., Nishihira, A., Wakabayashi, M., Kuwahara, M. & Sawai, H. Biomolecular sensor based on fluorescence-labeled aptamer. *Bioorganic & Medicinal Chemistry Letters* **16**, 4381–4384 (2006).

268. Cao, Z., Suljak, S. W. & Tan, W. Molecular beacon aptamers for protein monitoring in real-time and in homogeneous solutions. *Current Proteomics* **2**, 31–40 (2005).

269. Nguyen, T., Hilton, J. P. & Lin, Q. Emerging applications of aptamers to micro- and nanoscale biosensing. *Microfluidics and Nanofluidics* **6**, 347–362 (2009).

270. Tombelli, S., Minunni, M. & Mascini, M. Aptamers-based assays for diagnostics, environmental and food analysis. *Biomolecular Engineering* **24**, 191–200 (2007).

271. Cho, H. *et al.* Aptamer-based SERRS sensor for thrombin detection. *Nano Letters* **8**, 4386–4390 (2008).

272. Chiu, T.-C. & Huang, C.-C. Aptamer-functionalized nano-biosensors. *Sensors* **9**, 10356–10388 (2009).

273. Alberts, B. *et al. Molecular biology of the cell*. (Garland Science: 2007).

274. Ellington, A. D. & Szostak, J. In vitro selection of RNA molecules that bind specific ligands. *Nature* **346**, 818–822 (1990).

275. Ray, P. & White, R. R. Aptamers for targeted drug delivery. *Pharmaceuticals* **3**, 1761–1778 (2010).

276. Jayasena, S. D. Aptamers: an emerging class of molecules that rival antibodies in diagnostics. *Clinical Chemistry* **45**, 1628–1650 (1999).